Response of the Elemental Chemistry of Carbonate Phases to Secular Change in Ocean Chemistry

by

Franciszek Józef Hasiuk

A dissertation submitted in partial fulfillment
of the requirements for the degree of
Doctor of Philosophy
(Geology)
in The University of Michigan
2008

Doctoral Committee:
Professor Kyger C Lohmann, Chair
Professor Tomasz Konrad Baumiller
Professor Joel David Blum
Professor George Wesley Kling II
Associate Professor Christopher James Poulsen

The road to understanding the Earth is paved with limestone.

Dedication

I would like to dedicate this dissertation to the following people:

- My wife, Britta, who has provided constant love and support during my undergraduate and graduate careers
- My daughter, Lena, who has encouraged the timely completion of my graduate studies.
- My mother, the university librarian, for bringing me up in a world of books, knowledge and scholarly inquiry.
- My father, the first Dr. Hasiuk, for encouraging my love of science and the outdoors.
- My grandfather, the veterinarian, for showing me how much fun scientific research can be.
- All of the other good teachers I have had throughout my life.
- My officemates, Matt Wasson, Liz Smith, Maria Marcano, Jim Hnat, and Sasha Abrajevitch, who have helped me on numerous occasions with research and teaching.
- My committee members, Tom Baumiller, Joel Blum, George Kling, and Chris Poulsen, who have diligently helped me develop as a scientist.
- Bruce Wilkinson, iconoclast.
- And of course, my advisor and mentor during my time as graduate student, **Kacey Lohmann**, who allowed me the freedom and the guidance to become the scientist I am today.

Acknowledgements

Lora Wingate provided substantial help with analyses performed in the University of Michigan's Stable Isotope Laboratory.

Ted Huston provided substantial help with analyses performed in the University of Michigan's Keck Environmental Geochemistry Laboratory

Funding for analyses in this dissertation were provided by the Scott Turner Research Grant Program (Department of Geological Sciences, University of Michigan) and National Science Foundation Grant OPP-0125589.

Chapter 2 of this dissertation was published in the Journal of Sedimentary Research:

Hasiuk, F. J. and Lohmann, K. C, 2008, Mississippian paleocean chemistry from biotic and abiotic carbonate, Muleshoe Mound, Lake Valley Formation, New Mexico, U.S.A., Journal of Sedimentary Research, v. 78, p. 147–160.

Table of Contents

List of Figures

List of Tables

List of Equations

List of Appendices

List of Abbreviations

Abbreviation	*Description*
X/Ca_C	Ratio of element *X* to Ca in the crystal structure of calcite, where element *X* is often Mg, Sr, Fe, or Mn
X/Ca_{sw}	Ratio of element *X* to Ca, both being dissolved constituents in a solution, where element *X* is often Mg, Sr, Fe, or Mn
δ_C	$\delta^{18}O$ of calcite (in ‰ relative to PDB)
δ_C*	Species "offset," which accounts for non-equilibrium $\delta^{18}O$ compositions in biotic carbonates.
δ_W	$\delta^{18}O$ of seawater (in ‰ relative to SMOW)
δ_W*	Difference between δ_W measured against the SMOW and PDB scales, equal to –0.27‰ (Hut, 1987)
Δ_W	Difference in $\delta^{18}O$ between surface and deep seawater (in ‰ relative to SMOW)
T	Temperature (in °C)

Abstract

Calcium carbonate is the dominant inorganic mineral precipitate of the global ocean and by no coincidence, it is also the most abundant mineral produced by life. Secular variation in the paleontologic, stratigraphic, petrographic, and geochemical character of limestones argues that the physicochemical conditions under which it has precipitated from seawater have not been constant over geologic time. A major aspect of this variation has been the modality in the primary mineralogy between times of dominantly low-Mg calcite and times of aragonite and high-Mg calcite. Because these minerals have different chemical characteristics, they respond differently during diagenesis and thus affect the evolution of important limestone attributes such as porosity and permeability. Seawater Mg/Ca likely controls this modality.

To estimate seawater Mg/Ca from calcite Mg/Ca it has been customary to assume a linear relationship between these two quantities. However, experiments where biotic and abiotic calcites were precipitated in the laboratory suggest that this relationship is a power function. This power function, a “partition power function” , accounts for the observation that partition coefficients tend to decrease at high solution Mg/Ca because of interference with the growing calcite crystal surface by Mg. This method more accurately estimates paleoseawater Mg/Ca from ancient calcite phases.

Partition power functions can be used to model the change in the Mg/Ca of calcite phases in response to secular variation in seawater Mg/Ca. The smaller range and average

value of Mg/Ca in carbonate phases precipitated during times of low seawater Mg/Ca implies that during such times, there existed a reduced driving force for diagenesis because of the paucity of metastable high-Mg calcite.

Calcite Mg/Ca has also been used as a thermometer of paleoceans. When applied to recent geologic history, this exercise is elementary because change in seawater Mg/Ca has been negligible. By combining a partition power function with a modern temperature calibration to produce "Mg-T partition functions," secular variation in seawater Mg/Ca can be accounted for accurately for strata older than 5 Ma. In this way, reasonable paleotemperatures and seawater $\delta^{18}O$ values can be obtained while using a model of seawater Mg/Ca in accordance with geochemical proxy data.

Chapter 1: Introduction

Carbonate rocks, limestones, have long been studied in terms of their chemistry to serve as proxies of past environments. As direct chemical precipitates of fluids at the Earth's surface and within its sedimentary shell, this approach seems quite valid. However, because of the high degree of solubility of carbonate minerals in aqueous solutions, post-depositional diagenetic alteration is the rule, rather than the exception. Within this context, understanding the spatial and temporal variability in the fluids responsible for diagenetic alteration is a prerequisite for unraveling the primary chemistry and subsequent alteration history of any carbonate stratum.

Until relatively recently, little attention was paid to possible temporal variation in the solution from which biotic and abiotic marine carbonates precipitate, that is, seawater. With uniformitarianism's edict that the present is the key to the past, the null hypothesis for carbonate geologists has been that the chemistry of ancient oceans has always been similar to that of the modern. This notion began to be challenged in the 1970s and 1980s (Mackenzie and Pigott, 1981; Milliken, 1977) culminating with Sandberg (1983)when it was argued that there existed modality in the primary mineralogy of ooids, detrital grains coated in marine carbonate cement. It was noticed that during certain times during the Phanerozoic the primary mineralogy of the carbonate comprising ooids was aragonite (like today), yet at other times it was calcite. These intervals in time came to be known as "aragonite seas" and "calcite seas." This variation was initially suggested to follow

atmospheric pCO_2 (Mackenzie and Pigott, 1981; Sandberg, 1983), but now is suggested to arise from variation in oceanic Mg/Ca (Stanley and Hardie, 1998). In a broader context, it could be considered that Mg/Ca and pCO_2 are both proxies of the plate tectonic cycle, as high rates of seafloor spreading would cause both increased atmospheric pCO_2 through volcanic outgassing as well as lower oceanic Mg/Ca through more hydrothermal alteration of basalt.

This mineralogical variation has been suggested to be evident in the paleontological record as well. The dominance of certain taxa, which are either voluminous carbonate sediment producers or massive reef builders, is suggested to relate to their skeletal mineralogy (Stanley and Hardie, 1998). For example, during the "calcite seas" of the Cretaceous, calcitic rudistids were the major reef-building fauna, while today (an "aragonite seas") aragonitic scleractinian corals dominate. It has even been argued that the skeletal mineralogies of marine invertebrates were "locked in" at their time of origination (Porter, 2007).

This mineralogical modality has been documented in the other major group of seawater precipitates, the evaporites. Hardie (1996) noted variation in the type of evaporites that was synchronous with aragonite-calcite sea modality. Potassium-chloride type evaporites dominated during calcite seas, while magnesium-sulfate type evaporites dominated during aragonite seas. Analyses of fluid inclusions in evaporites offer a chance to analyze aliquots of ancient oceans (Horita et al., 1991; Lowenstein et al., 2001; Zimmermann et al., 2000). Despite the complex hydrology of evaporitic basins, the Mg/Ca ratios calculated from evaporite fluid inclusions show remarkably synchronous variation with calcite/aragonite sea modality.

The Mg/Ca of a marine carbonate phase offers a simpler approach to calculate paleoseawater Mg/Ca. This stems from the simplicity and chemical uniformity of open marine seawater from which carbonates precipitate as opposed to the complex, chemically variable nature of basins in which evaporites form. It is for this reason that Dickson (2002) analyzed the Mg content of fossil echinoderms. But to calculate paleoseawater Mg/Ca, Dickson recognized the difficulty in selecting an appropriate partition coefficient from the many that have been estimated from natural and experimental precipitates. In the end, Dickson selected a partition coefficient based on the average Mg/Ca of modern tropical echinoids despite acknowledging the likely impact of seawater Mg/Ca and temperature on the Mg/Ca of echinodermal calcite. It is the fundamental goal of this dissertation to expand upon the methods used to estimate paleoseawater elemental chemistry from marine calcite by accounting for the effects of seawater Mg/Ca and temperature on Mg partitioning into calcite. This objective is explored in four chapters.

In Chapter 2, a petrographic and geochemical study is performed on the early marine carbonate cements of Muleshoe Mound (Sacramento Mountains, Alamogordo, NM, USA) in an attempt to estimate Mississippian seawater Mg/Ca and Sr/Ca. During this investigation, it was recognized that the accepted way of calculating paleocean elemental ratios from carbonate material, by using partition coefficients calculated from modern analog materials, is not in agreement with recent experimental data which suggests partition coefficients change as a function of seawater Mg/Ca.

Chapter 3 delves more deeply into the theory behind the partitioning of Mg into calcite by examining how linear and power models describe this behavior. Power models

are shown to be more accurate in most circumstances and the difference in resulting estimates of secular variation in seawater Mg/Ca is discussed. Partition functions are also used to model the variation in primary Mg/Ca of biotic and abiotic marine carbonates. This highlighted the main difference geochemically between calcite and aragonite seas: there will be a larger range and higher average Mg/Ca during aragonite seas than during calcite seas. Because one of the main drivers of post-depositional alteration in carbonates is the stabilization of metastable minerals (e.g., high-Mg calcite), during calcite seas it should be expected that this impetus would be greatly reduced as aragonite would be less abundant and calcite would have a lower Mg/Ca. This reduced diagenetic potential has important implications on the porosity evolution and diagenetic pathways undertaken by carbonates formed during each of these end member mineralogic states.

Chapter 4 revises the current method for using the Mg/Ca of foraminiferal calcite as a paleocean thermometer. Previously, the equation for the Mg/Ca paleothermometer had only included a rough parameterization of the effect of changing seawater chemistry on foram Mg/Ca. By formulating a Mg-T partition function, a Mg/Ca paleothermometer based on empirical calibrations for both seawater temperature and Mg/Ca is applied to foraminiferal calcite Mg/Ca data both over the last 50 My as well as over a short time span (~2 My) across the Eocene-Oligocene boundary (at ~35 Ma). Paleotemperatures and δ_W trends are then calculated using two different models of Cenozoic Mg/Ca_{sw} (Hardie, 1996; Wilkinson and Algeo, 1989). Although the resulting paleotemperature trends are similar, the differences are significant when used to calculate Cenozoic δ_W trends such that major interpretive alternatives arise. For example, the Hardie model suggests

persistent continental glaciation throughout the entire Cenozoic, while the Wilkinson and Algeo model suggests glaciation only from 40-38 Ma and 15-0 Ma.

In Chapter 5:, the revised methodology for Mg/Ca paleothermometry used to reach the conclusions in Chapter 4 is discussed in greater detail. In addition, the difference between the Mg/Ca of planktonic and benthic foraminifera, respectively recording conditions in the surface and deep oceans are discussed. This study shows that a larger difference existed between surface and deep ocean $\delta^{18}O$ during the Eocene than exists today (~3.5‰ vs. 0.7‰, respectively). This could be caused by higher rates of evaporation during the warmer Eocene climate.

These chapters together advance the methodologies used for calculating paleoseawater Mg/Ca from calcite Mg/Ca as well as increase the accuracy of paleoseawater $\delta^{18}O$ estimates by improving the Mg/Ca paleothermometer. From this theoretical basis, the past 60 My of global climate is illuminated.

Chapter 2: Mississippian Paleocean Chemistry from Biotic and Abiotic Carbonate, Muleshoe Mound, Lake Valley Formation, New Mexico, USA

2.1 Abstract

It has been proposed that Phanerozoic variation in the Mg/Ca ratio of seawater has resulted in variation in the primary mineralogies of shallow-water carbonates between aragonite- and calcite-dominated "seas." To test this hypothesis, this study estimates the Mississippian oceanic Mg/Ca and Sr/Ca ratios from the composition of marine carbonate cements and crinoidal carbonate, both of which have been suggested to faithfully record seawater chemistry.

The Early Mississippian (Tournaisian–Visean) Muleshoe Mound (Lake Valley Fm, Alamogordo, NM, USA) lends itself well to this endeavor because it contains abundant crinoids and marine carbonate cement. Stable isotope and elemental analyses, as well as cathodoluminescence characteristics, elucidate the diagenetic history of the bioherm and identify the least diagenetically altered materials for reconstruction of paleoseawater chemistry. Isotopic analyses document two diagenetic trends, one meteoric and one burial, diverging from values similar to literature estimates of Mississippian marine calcite (–1.5‰ $\delta^{18}O$, +4.5‰ $\delta^{13}C$). The burial diagenetic trend follows from this origin to more negative oxygen values (–7‰ $\delta^{18}O$, +3‰ $\delta^{13}C$). The meteoric diagenetic trend is

defined by a meteoric calcite line at ~ –3‰ $\delta^{18}O$. Similarity of non-luminescent marine cement and non-luminescent crinoid isotopic and elemental compositions suggests that crinoidal carbonate was completely replaced by cement in the marine environment. Average elemental ratios for least altered marine cements are: Mg/Ca = 11 mmol/mol; Sr/Ca = 0.2 mmol/mol; Mn/Ca = 0.2 mmol/mol, and Fe/Ca = 0.4 mmol/mol.

Early Mississippian seawater is estimated to have had a Mg/Ca ratio of ~ 0.2–0.3 mol/mol. This Mg/Ca ratio is compatible with the Early Mississippian being an interval of "calcite sea" conditions and compares well with the Devonian estimate from marine cements, 0.5, though it is 5–10 times lower than estimates from mass balance modeling. The Sr/Ca for early Mississippian seawater was between 0.5 and 0.9 mmol/mol, which is much lower than previous estimates of ~ 6 mmol/mol from brachiopod calcite and argues for the development of a Sr sink (aragonite?) in the latest Devonian to earliest Mississippian.

2.2 Introduction

Just as current ocean chemistry has provided valuable insight into the nature of modern Earth systems, a robust geological perspective on ocean chemistry could illuminate not only the possible ranges of seawater composition but also the timescales and the magnitudes of processes responsible for those changes. Of the major chemical sediment components produced in the oceans today, calcium carbonate is the most voluminous and functions as the largest sink in the carbon cycle.

The dominant mineralogy of carbonate-rich sediments has been observed to change through geologic time. While aragonite and high-Mg calcite dominate the mineralogy of Holocene tropical shallow-water carbonate cements and skeletal debris, numerous studies

(e.g., Mackenzie and Pigott, 1981; Sandberg, 1983; Stanley and Hardie, 1998; Wilkinson et al., 1984) document ancient tropical shallow water carbonates composed originally of low-Mg calcite. Sandberg (1983) recognized an "aragonite-threshold" which in later literature became the boundary between "aragonite seas" and "calcite seas" (Milliken, 1977). In addition, dolomite is more abundant during calcite seas than during aragonite seas (Given and Wilkinson, 1987). Further evidence for secular variation in seawater chemistry has been reported from: evaporite mineralogies (Hardie, 1996), evaporite fluid inclusions (e.g. Horita et al., 2002; Kovalevich et al., 1998; Lowenstein et al., 2003; Lowenstein et al., 2001), geochemical modeling (e.g. Berner, 2004; Hardie, 1996; Wilkinson and Algeo, 1989), mineralogy of dominant reef building organisms (Stanley and Hardie, 1998), and the Mg content of fossils (Dickson, 2002; Ries, 2004). Atmospheric pCO_2 (Given and Wilkinson, 1987; Sandberg, 1983) and oceanic Mg/Ca (Sandberg, 1975; Stanley and Hardie, 1998), both controlled by tectonics, have been causally implicated in this mineralogical variation. However, the Mg/Ca hypothesis has been favored more recently because unreasonably high pCO_2 values would be required to effect "aragonite sea"–"calcite sea" transitions (Stanley and Hardie, 1998).

Marine abiotic carbonate cements offer another excellent method to evaluate past seawater chemistry because the elemental and isotopic compositions of abiotic carbonate reflect the physical and chemical characteristics of the fluid from which they precipitate. The major challenge in using marine cements is to characterize the influence of post-depositional diagenesis. These uncertainties, however, can be well constrained through petrography and coupled stable isotope and elemental analysis (e.g., Carpenter and Lohmann, 1992; Major and Wilber, 1991). At Muleshoe Mound (Mississippian Lake

Valley Fm, New Mexico), the diagenetic history of marine cements has been well studied (e.g., Frank et al., 1996; Lohmann and Meyers, 1977; Meyers, 1974; Meyers and Lohmann, 1985; Stanton et al., 2002; Wu and Chafetz, 2002). In addition to these cements, crinoid carbonate is available to test the recent suggestion that such material is a reliable proxy of Phanerozoic Mg/Ca variation (Dickson, 2002, 2004). Thus, a unique opportunity exists to test the worthiness of both phases as records of ancient seawater chemistry and, within this context, to expand and refine our understanding of the chemical characteristics of Mississippian seawater.

2.3 Geologic Setting

2.3.1 Paleoecology and Paleogeography

Numerous Waulsortian mud mounds, ranging in height from 5 to 100 meters, are well exposed in strata of the Lower Carboniferous (Mississippian) Lake Valley Formation, which crops out on the western escarpment of the Sacramento Mountains, near Alamogordo, New Mexico, USA (Figure 2-1). Muleshoe Mound, one of these largest bioherms in this locality at 100 m thick, is typical of a carbonate mud mound where growth was truncated by wave base with concomitant development of off-mound debris deposits (Kirkby et al., 1996; Schlager et al., 2003).

Muleshoe Mound developed on a south-facing homoclinal ramp (Ahr, 1989) at an equatorial latitude (~ 10°S, Webb et al., 2002). Similar settings today have mean annual temperatures of ~ 25°C with minor seasonal temperature fluctuations. Ahr et al. (1996) suggest initial mound accretion near the base of or below the photic zone, while later growth is argued to have occurred in only tens of meters of water (e.g., Kirkby et al., 1996). This is reflected in the division of Muleshoe Mound by early workers into two

growth stages: a lower stage initiated during Alamogordo Member time (Figure 2-2), characterized by a low, domical mound composed of micrite and a later marine cement-rich upper stage formed during Nunn and Tierra Blanca Member times, when the mound gained much of its topographic relief.

Kirkby and Hunt (1996) further delineate three phases of mound growth within the upper mound stage, each punctuated by a "mound crisis" of short duration when poorly oxygenated waters asphyxiated the biota before retreating shortly thereafter (as evidenced by only thin accumulations of argillaceous material at hiatal surfaces), followed by recolonization by encrusting organisms. Final cessation of mound growth is recorded in the dark lime muds of the Arcente Member, suggesting that oxygen-poor water smothered the mound long enough for the development of a thick, non-rigid substrate such that the biota common before Arcente deposition were unable to recolonize Muleshoe Mound. While marine cementation occurred synchronously with mound formation, it has been argued that meteoric diagenesis and cementation did not occur until late Mississippian subaerial exposure (Meyers, 1974).

2.3.2 Stratigraphy

The upper part of the accretionary core of Muleshoe Mound is largely bryozoan cementstone, containing abundant fenestrate bryozoan debris and radiaxial fibrous, syntaxial and blocky cements, common crinoid columnals and micrite, and occasional ostracod and other fossil debris. The lower part of the accretionary core is characterized by a micritic cementstone to crinoid-rich packstone. Off-mound flank beds are dominantly crinoidal grainstones with porosity filled by syntaxial and blocky cements.

Neptunian dikes crosscut the mound and are dominantly mudstones, with scattered pockets of crinoid and brachiopod packstone–grainstone.

2.3.3 Petrography

Radiaxial calcites, which isopachously coat much of the fossil debris, were chosen for this investigation because they have been interpreted to represent synsedimentary cementation in seawater of open-marine chemistry (Kendall et al., 1985; Lohmann and Meyers, 1977; Saller, 1986; Wilson and Dickson, 1996). These cements are currently a mixture of low-Mg calcite and microdolomite (Lohmann and Meyers, 1977), though this assemblage suggests an originally magnesian calcite mineralogy (Wilson and Dickson, 1996). Some syntaxial and blocky calcite cements were also sampled but were generally avoided because previous work (Frank and Lohmann, 1995; Meyers, 1974; Meyers and Lohmann, 1985) had showed them to originate predominantly during meteoric phreatic, mixed meteoric–marine phreatic, and/or burial diagenesis. Crinoid carbonate was also sampled for comparison with the marine cements.

Cathodoluminescence petrography was employed to qualitatively establish the degree of alteration of the various constituents. Non-luminescence was taken as indicative of a relatively unaltered phase while luminescence suggested alteration. Non-luminescent radiaxial calcites from the bryozoan cementstone were analyzed and considered to represent unaltered syndepositional marine cement. In addition, luminescent, variably luminescent, and non-luminescent crinoids were selected for geochemical analysis from all three of the main lithologies. These four phases (Figure 2-3) account for 150 of 175 paired isotopic and elemental analyses. The remaining analyses were carried out on luminescent radiaxial calcites, blocky cements, and micrite (Appendix 1).

2.4 Methods

Coarse sampling was performed using a dental drill to manually extract ~ 100 μg of powder from 0.5 mm^2 areas of micrite and crinoids. A Merchantek (New Wave) MicroMill computer-controlled drilling system was used to recover ~ 50 μg of powder from cements and crinoid calcites in petrographic thin sections that had been chosen based on luminescence character. Resultant powders were split for paired stable isotope and elemental analysis.

Splits for isotopic analysis were roasted *in vacuo* for one hour at 200°C to remove volatile contaminants and water. They were then reacted with anhydrous H_3PO_4 at 76 ± 2°C in a Kiel automated carbonate preparation device coupled directly to the inlet of a Finnigan MAT mass spectrometer at the University of Michigan's Stable Isotope Laboratory. ^{17}O-corrected data are adjusted for acid fractionation and source mixing by calibration to a best-fit regression line defined by NBS-18 and NBS-19 standards. Data are reported in ‰ variation relative to the V-PDB standard. Measured precision is better than 0.1‰ for both $\delta^{13}C$ and $\delta^{18}O$.

Splits for elemental analysis were dissolved with 1 ml 0.1N HNO_3. 1.6 ml of 0.1N HNO_3 was added to 0.4 ml of the dissolved split for analysis via Finnigan Element ICP-MS at the University of Michigan's Keck Environmental Geochemistry Laboratory. Samples were calibrated to run at a constant Ca concentration to correct for matrix effects. The Rutgers method for analyzing elemental ratios in calcium carbonates via ICP-MS was employed (Rosenthal et al., 1999).

2.5 Results

Elemental and isotopic results are summarized in a series of scatter plots in Figure 2-

4. A linear covariant trend dominates the $\delta^{13}C$–$\delta^{18}O$ plot (Figure 2-4A) and likely represents intergrowth of an early meteoric cement phase and a later burial cement within pre-existing marine cement. The burial diagenetic trend (Choquette and James, 1990) ranges from –1‰ to –7‰ $\delta^{18}O$ and from +5.5‰ to +3‰ $\delta^{13}C$.

The power of coupled stable isotope and elemental analyses lies in the ability to place elemental along diagenetic trends as defined by isotopic data. Because the main variation in the burial diagenetic trend at Muleshoe Mound is in $\delta^{18}O$, elemental data have been plotted against $\delta^{18}O$ in Figure 2-4 (B through E).

At $\delta^{18}O$ values more positive than –3.7‰, the Mg/Ca of both cement and crinoid calcite averages 11 mmol/mol Mg/Ca. At $\delta^{18}O$ more negative than –3.7‰, however, crinoid samples average 35 mmol/mol, while cements maintain 11 mmol/mol (Figure 2-4B). Sr/Ca data show no such pattern (Figure 2-4C) and, in fact, display little variation with respect to $\delta^{18}O$. Fe/Ca (Figure 2-4D) increases from an average of ~ 0.2 mmol/mol at the most positive $\delta^{18}O$ to ~ 2 mmol/mol at the most negative $\delta^{18}O$. Such an increase in Fe is commonly seen during burial diagenesis (Choquette and James, 1990). Mn/Ca (Figure 2-4E) is closely associated with luminescence. Non-luminescent phases cluster at very low Mn/Ca (~ 0.1 mmol/mol), while luminescent phases were generally above 0.5 mmol/mol. Fe contents were insufficient to quench luminescence.

A meteoric diagenetic trend is weakly defined by analyses with variable $\delta^{13}C$ and comparatively invariant $\delta^{18}O$ of approximately –3‰ (a “meteoric calcite line” sensu Lohmann, 1988). The three samples that were analyzed with the most negative $\delta^{13}C$ also have the highest Mn/Ca, as is common for meteoric precipitates, which reflects both Mn availability and reducing conditions common in this environment. Synsedimentary

marine diagenesis, on the other hand, is more often characterized by well-oxygenated water where Mn would exist as an oxide and thus be unavailable for incorporation into marine calcite. The meteoric calcite line for the Lake Valley Formation present at Muleshoe Mound has been better delineated at more northerly exposures in the Sacramento Mountains (Frank and Lohmann, 1995; Goldstein, 1990), where paleospeleothem calcite averaged –3‰ $\delta^{18}O$ and between +3‰ and –10‰ $\delta^{13}C$.

2.6 Discussion

2.6.1 Fidelity of the Muleshoe Record

While the original mineralogy of the Muleshoe Mound cement and crinoid carbonate has been interpreted as Mg-calcite, what exists today is a mixture of low-Mg calcite and microdolomite inclusions (Lohmann and Meyers, 1977; Meyers and Lohmann, 1978). Such diagenetic transitions are inherently prone to changes in elemental and isotopic chemistry, thus it is necessary to understand the extent to which the cements and crinoids at Muleshoe Mound have undergone alteration and the degree to which their original isotopic and elemental chemistries have been modified.

Calcites with a range of elemental and isotopic values are present at Muleshoe Mound because of various phases of diagenesis. Initial diagenesis occurred in contact with open-marine seawater and acted to create a less heterogeneous mixture of carbonate phases on the sea floor by dissolving the less stable (more magnesian) calcites and precipitating more stable (less magnesian) calcite. It should be noted, however, that during a calcite sea there exists a reduced mineralogical drive for diagenesis due to the mineralogical similarity among all carbonate phases—they are all low-Mg calcite. During this phase of diagenesis, the chemistry of biotic grains, which might diverge from abiotic values,

homogenize their chemistry to values in abiotic equilibrium with seawater through inorganic processes (Patterson and Walter 1994).

Diagenetic processes in carbonates generally produce phases with more negative $\delta^{18}O$ and $\delta^{13}C$. Therefore, it has become a metric to many (e.g., Kasting et al., 2006; Mii et al., 1999; Veizer et al., 1999) that samples of marine carbonate with the most positive $\delta^{18}O$ and $\delta^{13}C$ are the least altered. The convergence in some samples of the most positive ends of both meteoric and burial diagenetic trends at Muleshoe Mound with literature estimates of Mississippian marine carbonate (Brand, 1982; Frank et al., 1996; Lohmann and Walker, 1989; Meyers and Lohmann, 1985; Veizer et al., 1999) suggests retention of Mississippian marine calcite $\delta^{18}O$ values, and thus retention of $\delta^{13}C$, Mg/Ca and Sr/Ca.

A second phase of diagenesis, occurring in a marine phreatic or mixed meteoric–marine phreatic zone, also likely influenced Muleshoe Mound carbonate cements. This mode of diagenesis can be constrained by modeling the geochemical evolution of the diagenetic precipitate. The ratio between the abundance of an element or isotope in the dissolving phase (i.e., the "rock") and the diagenetic fluid (i.e., the "water") determines how quickly the composition of the diagenetic precipitate will reflect the original rock composition. For example, any carbonate rock has much more carbon than the water dissolving it, so relatively little rock must be dissolved before its carbon isotope composition dominates that of the water and any diagenetic precipitate in equilibrium thence. Oxygen, on the other hand, is much more abundant in the water than in the rock, so relatively large amounts of rock must be dissolved before the diagenetic precipitate obtains rock $\delta^{18}O$ values. Mg and Sr respond more like carbon than oxygen, inasmuch as

they are much more abundant in the rock than the water. From this we can conclude that if a diagenetic carbonate precipitate retains the original $\delta^{18}O$ value, it should also preserved the original $\delta^{13}C$, Mg/Ca, and Sr/Ca compositions.

Cicero and Lohmann (2001) provided a quantitative basis for the dissolution of metastable Mg-calcite and reprecipitation of a Mg-calcite during meteoric diagenesis based on the work of Lawrence et al. (1976). Applying their iterative model (Figure 2-5) to Muleshoe Mound, original rock $\delta^{13}C$ is preserved at R/W ratios of $10^{-2.5}$, Sr/Ca at R/W ratios of $10^{-1.5}$, Mg/Ca at R/W ratios of $10^{-0.5}$, and $\delta^{18}O$ at R/W ratios of $10^{0.5}$. Thus, once $\delta^{18}O$ values in the diagenetic precipitate reach original rock values, it can be supposed that Mg/Ca and Sr/Ca have reached original rock values as well.

In order to compute average Muleshoe Mound elemental data, samples with elemental or isotopic values that suggest diagenetic alteration and non-retention of original values were first removed from the dataset. Because Fe and Mn incorporate into calcite only in their reduced state, their presence indicates precipitation under reducing conditions and not open-marine conditions (e.g., Morrison and Brand, 1986). Thus samples with Mn/Ca or Fe/Ca > 1 mmol/mol were assumed to have not retained their original values (78 samples). Most samples with high Mn/Ca were from luminescent phases (12 samples), and most with high Fe/Ca (66 samples) were from burial phases with very negative $\delta^{18}O$ (Figure 2-4D). In addition, 18 samples with a burial signature ($\delta^{18}O < -3.7‰$) were discarded. The remaining 79 samples are assumed to reflect original marine carbonate elemental and isotopic compositions. These samples had the following average elemental and isotopic compositions: $\delta^{18}O = -2.5‰$ (range = –0.6 to –

3.6‰, SD = 0.6%), $\delta^{13}C$ = 4.6‰ (range = +3 to +5.2‰, SD = 0.4‰), Mg/Ca = 11 mmol/mol (range = 5.8–18.6, SD = 3.2); Sr/Ca = 0.2 mmol/mol (range = 0.1–0.4, SD = 0.1); Mn/Ca = 0.2 mmol/mol (range = 0–1.0, SD = 0.2), and Fe/Ca = 0.4 mmol/mol (range = 0.1–1.0, SD = 0.2).

2.6.2 Estimating Paleoseawater Mg/Ca

To estimate elemental ratios of paleoseawater from measured values derived from marine carbonate, it is common to employ a partition coefficient (*D*), which is the ratio of an elemental ratio in the fluid to that of a solid precipitate. For example, the equation describing the partition coefficient for Mg incorporation into calcite would look like this:

$$D_{Mg} = \frac{Mg/Ca_{Calcite}}{Mg/Ca_{Seawater}} \quad (2\text{-}1)$$

Laboratory experiments attempting to reproduce calcite precipitation from natural waters have yielded D_{Mg} = 0.017 (Mucci and Morse, 1983) to 0.12 (Katz, 1973), while Holocene marine cements from Enewetak Atoll yield an average D_{Mg} of 0.034 (Carpenter and Lohmann, 1992). To account for possible secular changes in seawater chemistry, we must use a partition power function, which describes how partition coefficients change with variations in Mg/Ca ratio of the precipitating fluid. Partition power functions have also been derived to describe how Mg incorporation varies as a function of temperature (e.g., Ries, 2004), and alkalinity (e.g., Russell et al., 2004). Two such partition power functions for abiotic calcite can be derived by fitting a power equation to published empirical data:

Füchtbauer and Hardie (1976) $$Mg/Ca_{Seawater} = 29.3\left(Mg/Ca_{Calcite}\right)^{1.11}, R^2 = 0.93 \quad (2\text{-}2)$$

Mucci and Morse (1983) $$Mg/Ca_{Seawater} = 162\left(Mg/Ca_{Calcite}\right)^{1.4}, R^2 = 0.94 \quad (2\text{-}3)$$

Applying these functions to the chemistry of Muleshoe abiotic carbonate with 11 mmol/mol Mg/Ca estimates a Mg/Ca ratio for Mississippian seawater of 0.19 mol/mol (Füchtbauer and Hardie, 1980) to 0.29 (Mucci and Morse, 1983). In this case, the correction provided by the partition power functions is small because Mg content of the precipitated carbonate is low. However, if the Mg/Ca of the precipitate had been large, using a partition power function would have resulted in a more substantial correction. For example, if a marine cement were found in the rock record with a Mg/Ca of 100 mmol/mol, using a D_{Mg} of 0.03 would yield a seawater Mg/Ca of 3.3, while the partition power function of Füchtbauer and Hardie (1980) yields a Mg/Ca of 2.3. Estimates provided here for Mississippian marine calcites are generally lower than previously estimated values (e.g., Dickson, 2004; Hardie, 1996), yet comparable to the 0.5 mol/mol obtained from Devonian marine calcite (Carpenter and Lohmann, 1992).

2.6.3 Estimating Paleoseawater Sr/Ca

Utilizing a similar approach, the Sr/Ca ratio of early Mississippian seawater can be calculated. Given the modern oceanic Sr/Ca of 8.8 mmol/mol, a D_{Sr} of 0.15 can be calculated from modern marine cement Sr contents (Carpenter and Lohmann, 1992) and a D_{Sr} of 0.3 can be calculated from average echinoderm Sr contents (Thompson, 1955). From empirical studies, D_{Sr} for abiotic calcite ranges from 0.02 to 0.39 (Mucci and Morse, 1983; Tesoriero and Pankow, 1996). The most reasonable D_{Sr} values come from Mucci and Morse (Mucci and Morse, 1983) with coefficients ranging from 0.22 to 0.39, where abiotic calcite was precipitated from natural seawater. Applying a range of partition coefficients (D_{Sr} = 0.22-0.39) to the unaltered carbonate from Muleshoe Mound (0.2 mmol/mol Sr/Ca) yields seawater Sr/Ca of 0.5 to 0.9 mmol/mol. This range of values

agrees with the Mississippian average Sr/Ca of ~ 6 mmol/mol derived from brachiopod skeletal calcite (Steuber and Veizer, 2002). If correct, this suggests that Mississippian oceanic Sr/Ca was ~ 10% of the modern value. The Devonian value of 14.6 mmol/mol obtained from carbonate cements (Carpenter et al., 1991), is line with the brachiopod estimate of 14.5 to 8 mmol/mol (Steuber and Veizer, 2002). If correct, this suggests that Mississippian oceanic Sr/Ca was ~ 10% of the modern value. The Devonian value of 14.6 mmol/mol (Carpenter et al., 1991), however, is ~ 25 times higher than Mississippian value and differs significantly from the brachiopod estimate of 1.3 mmol/mol (Steuber and Veizer, 2002).

Sr partition functions for the incorporation of Sr into calcite at different fluid Sr concentrations have been reported only for coccolith calcite (Langer et al., 2006), and this behavior was linear (i.e., constant D_{Sr}). However, the applicability of these coccolith partition functions is questionable, in that coccolith Mg partition power functions are quite variable (Stanley et al., 2005) and thus could suggest that coccolith calcite does not faithfully record of seawater elemental chemistry.

The coprecipitation behavior of Sr with Mg in calcite (Mucci and Morse, 1983) has been observed and at Muleshoe Mound is described thusly (all quantities are in mmol/mol):

(Abiotic cement, this study) $$Sr/Ca = 0.013(Mg/Ca) + 0.046,\ R^2 = 0.57 \quad (2\text{-}4)$$

Equations (2-5) and (2-6) are other examples from the literature (Carpenter and Lohmann, 1992):

Biotic (Recent) $$Sr/Ca = 0.0066(Mg/Ca) + 1.5,\ R^2 = 0.70 \quad (2\text{-}5)$$

Abiotic (Recent) $$Sr/Ca = 0.0066(Mg/Ca) + 0.11,\ R^2 = 0.79 \quad (2\text{-}6)$$

In these equations, the slope is the Sr/Mg ratio and the *y* intercept is the "biotic offset." Based on the similarity in slope and difference in *y* intercept between Equations (2-5) and (2-6), Carpenter and Lohmann (1992) suggest that biotic phases have a higher Sr content for a given Mg content due to a kinetic vital effect. As we can see, the y-intercept of Equation (2-4) is very near zero. Its Sr/Mg ratio is different from modern biotic and abiotic marine carbonate, but is consistent with the Phanerozoic variation in Sr/Mg reported by Cicero and Lohmann (2001), where marine carbonate tends to have higher Sr/Mg during calcite seas than during aragonite seas.

2.6.4 Crinoidal Calcite at Muleshoe Mound

Echinoderm calcite has been proposed to record variation in seawater Mg/Ca over the Phanerozoic (Dickson, 2002, 2004). To ascertain whether Muleshoe's crinoids accurately record Mississippian seawater Mg/Ca, we compare the isotopic and elemental compositions of modern echinoderms to those found at Muleshoe Mound.

The $\delta^{18}O$ of modern echinoids and ophiuroids range from +2 to –4‰ $\delta^{18}O$, crinoids and asteroids from 0 to –6‰, and aragonite and Mg-calcite cements from +4 to –4‰ (Figure 2-6A). Temperature is suggested to be the dominant control on $\delta^{18}O$ in echinoderms (Weber, 1968) and likely explains the ~ 6‰ variation within each taxonomic family of echinoderms and each mineralogy of marine cement. At Muleshoe Mound, the ranges of $\delta^{18}O$ for marine cements (–1.3 to –6‰) and crinoids (–1.5 to –5.2‰) overlap (Figure 2-6B).

In terms of $\delta^{13}C$, modern echinoderms are more negative than marine cements (marine cements: +3 to +4‰; echinoids and ophiuroids: 0‰; crinoids and asteroids: –6‰; Figure 2-6A). This suggests that the composition of echinoderm calcite, which is

isotopically more negative, may result from a low efficiency in expelling isotopically light respiratory CO_2 due to their small visceral mass (Weber, 1968) or perhaps incorporation of ingested, isotopically light organic matter (Ries 2007, personal communication). In contrast to these modern differences between the isotopic compositions of marine cements and crinoid calcite, Muleshoe Mound crinoids and cements exhibit nearly identical $\delta^{13}C$ and $\delta^{18}O$ values (Figure 2-6B).

In addition, modern biotic and abiotic calcite phases define distinct patterns in Sr–Mg space (Figure 2-7A). Sr and Mg in modern echinoderms (Carpenter and Lohmann, 1992; Weber, 1969) and marine cements (Carpenter et al., 1991) covary along trends with similar slopes but different *y*-intercepts (Figure 2-7A), an offset that Carpenter et al. (Carpenter et al., 1991) attributed to more rapid precipitation of biotic phases. This was likely the case during the Mississippian as well, because a difference in *y* intercepts exists between Muleshoe Mound marine cements and data from early Mississippian brachiopods of the Russian platform (Figure 7B, Mii et al., 1999). It is also evident from this plot that crinoids and marine cements from Muleshoe Mound overlap.

The similarity between elemental and isotopic compositions of marine cement and crinoidal carbonate suggests that crinoidal calcite in Muleshoe carbonates has been diagenetically altered—but that this early diagenesis has changed their primary composition to one identical to that of marine cement. If Muleshoe crinoids have been replaced by abiotic marine carbonate during early marine diagenesis, an interesting opportunity arises. In this study, 24 of 35 non-luminescent cements did not meet the criteria for preservation of original chemistry, in contrast to only 6 out of 34 non-luminescent crinoids. This implies that a “cement in crinoid clothing” may be likely to

escape subsequent diagenesis and thus would provide a more reliable record of past seawater chemistry. This reduction in diagenetic susceptibility could result from the unit crystal of the syntaxial infilling calcite cements, which formed upon replacement of the crinoid and which would possess a much smaller ratio of surface area to volume compared to fibrous marine cements.

2.6.5 Estimating Paleo–Crinoid Composition

It is reasonable from the previous discussion that crinoidal carbonate at Muleshoe Mound was likely replaced by marine carbonate during synsedimentary diagenesis, erasing any vestige of its primary composition and, in turn, inheriting the elemental and isotopic composition of the marine carbonate. Despite this, a rough estimate of the original Mg/Ca composition of the crinoids can be made by combining the range of early Mississippian seawater Mg/Ca values calculated above (0.19–0.29 mol/mol Mg/Ca) with the Mg partition power function for echinoid plate carbonate (the material most analogous to crinoid calcite for which a partition power function has been empirically derived):

$$Mg/Ca_{Crinoid} = 0.047\left(Mg/Ca_{Seawater}\right)^{0.67} \tag{2-7}$$

Thus, early Mississippian crinoids at Muleshoe Mound would have had a Mg/Ca ratio between 16 and 21 mmol/mol, much lower than the modern range of crinoid Mg contents (120–240 mmol/mol, Weber, 1969). It might follow that a lower Mg content would mean that Mississippian crinoid skeletal carbonate would possess a lower potential for diagenetic alteration; however, the complete replacement of the crinoid calcite, as suggested by Muleshoe crinoids, argues for the converse. Even with such low Mg

contents, crinoid carbonate must have been diagenetically reactive, which would have led to its alteration and replacement during marine diagenesis.

Crinoid Sr/Ca can be estimated from the crinoid Mg/Ca calculated above (16–21 mmol/mol), the Sr/Mg of Mississippian marine calcite (the slope of unaltered Muleshoe Mound calcite from Figure 2-7B, 0.012) as well as a value for the biotic Sr incorporation offset equivalent to the differences between intercepts of Equations (2-4) and (2-5), 1.4 mmol/mol).

$$Sr/Ca_{Crinoid} = (Sr/Mg) \times (Mg/Ca_{Crinoid}) + Biotic\ Offset \quad (2\text{-}8)$$

From this information, Mississippian crinoids most likely had a skeletal composition of 1.5 to 1.7 mmol/mol Sr/Ca. This is still below the average modern value, 2.6 mmol/mol, reported by Thompson and Chow (1955).

2.6.6 Mississippian Seawater

Marine cements at Muleshoe Mound suggest that Mississippian seawater had Mg/Ca between 0.19 and 0.29 mol/mol and a Sr/Ca between 0.5 and 0.9 mmol/mol, which are much different than the modern values of 5.1 and 8.8, respectively. It is necessary thus to reconcile these values within the framework of our current understanding of chemical fluxes to the oceans if we are to understand the implications for the chemistry of Mississippian seawater and the fluxes that supported it.

The processes by which Mg, Sr, and Ca are added or removed from seawater are essentially identical, though the concentrations, rates, and magnitudes of each flux differ. These cations are derived from the weathering of continental rock and the hydrothermal alteration of mid-ocean ridge basalts, while the formation of chemical sediments (e.g., carbonates, sulfates, halides) removes these cations from seawater. Other factors

moderating these fluxes include: climate, which varies the temperature and precipitation regime for continental weathering; mid-ocean ridge spreading rates, which alter the amount of fresh basalt available for cation exchange; and the latitudinal distribution of continental lithosphere, which controls the extent of shallow shelf available for production of carbonates and/or evaporites.

Numerous models exist to estimate Phanerozoic Mg/Ca variation in terms of these fluxes. The Spencer–Hardie mixing model (Demicco et al., 2005; Hardie, 1996; Spencer and Hardie, 1990) suggests that seawater chemistry is defined by the mixing of different proportions of river water and mid-ocean ridge hydrothermal brines. GEOCARBSULF (Berner, 2004) and MAGic (Arvidson et al., 2006) are dynamically coupled hydrosphere–atmosphere–lithosphere models of geochemical cycling that model Phanerozoic variation of a number of geochemical parameters such as pCO_2, Mg/Ca, and SO_4/Ca. These three models each assume that mid-ocean ridge cation exchange reactions has dominated the Mg cycle over the Phanerozoic, as it does today.

The results of these modeling studies are remarkably coherent (Figure 2-8), and they uniformly indicate early Mississippian Mg/Ca of 1–3 mol/mol. This similarity likely arises because all of these models rely on the same oceanic crust production curve to calculate Mg fluxes (Gaffin, 1987). Gaffin (1987) constructed this curve of pre-Jurassic ocean crust production by calibrating the production record of extant ocean crust to estimates of synchronous sea-level change (Vail et al., 1977).

Others, while agreeing that seawater exchange reactions at mid-ocean ridges dominate the Mg cycle today, have suggested that the formation of sedimentary dolomite may have has been the primary sink for oceanic Mg (e.g., Wilkinson and Algeo, 1989)

throughout the Phanerozoic on the basis of mass–age data of Phanerozoic carbonate accumulation and dolomite abundance. Nevertheless, this yields a generally similar Phanerozoic Mg/Ca curve.

Estimates of seawater Mg/Ca from modeling (1–3 mol/mol) and from Muleshoe Mound cements (~ 0.2–0.3 mol/mol) differ by a factor of 5 to 10. Mg-calcite cement precipitated from seawater with Mg/Ca in the range of 1 to 3 mol/mol would have had Mg/Ca ratios of 30 to 130 mmol/mol. None of the least altered samples at Muleshoe Mound had Mg/Ca ratios in this range, so it is suggested that this discrepancy has arisen from slight errors in model parameters. The oceanic crust production curves of Gaffin (1987) and Larson (1991) differ by an order of magnitude, yet these models mentioned above use only Gaffin (1987). Also, most of these models incorporate sea level, yet these estimates are prone to periodic and substantial revision (Miller et al., 2005). A synthesis of more recent estimates of sea-level change and crust production could lead to further refinements in these numerical estimates of Phanerozoic geochemical cycles.

For example, values similar to those obtained in this study can be accommodated by flux models provided by Hardie (1996), who used a mixing model of river water (RW) and mid-ocean ridge brine (MOR) to explain Phanerozoic oceanic Mg/Ca. Based on this modeling, which assumes a ratio of MOR/RW of 1.25, he suggests a lower limit of 1.0 mol/mol on Phanerozoic ocean Mg/Ca and a value of ~ 1.25 mol/mol for early Mississippian Mg/Ca. With only minor modification of this ratio to 1.75, his model yields an early Mississippian Mg/Ca of 0.5 mol/mol, which is similar to the seawater Mg/Ca ratio estimated by this study.

Low values of 1 to 2 mol/mol for Mississippian seawater Mg/Ca have also been suggested by Dickson (2004) based on the Mg content of crinoidal carbonate. However, in that study, the degree of diagenetic alteration was characterized solely on the qualitative evaluation of stereom preservation, and thus geochemically altered samples may have been included in the dataset. For example, in this study it was observed that crinoid calcite showing very negative $\delta^{18}O$ (indicative of burial diagenesis) had higher Mg/Ca ratios than crinoid calcite with the most positive $\delta^{18}O$. The absence of paired isotopic data in the study of Dickson (2004) makes it difficult to determine whether some of his data included analyses of crinoid stereom that may have experienced alteration of the primary elemental chemistries.

The analysis of brines in primary fluid inclusions, which has yielded a complementary record of Mg/Ca for many intervals during the Phanerozoic, does not contribute to our understanding of conditions during the Mississippian because of the paucity of evaporite deposition during this time. However, estimates of seawater Mg/Ca from fluid inclusions range from 0.4 to 1.9 mol/mol during the Devonian (Horita et al., 2002; Kovalevich et al., 1998; Petrychenko and Peryt, 2004), and numerous studies suggest that by the latest Pennsylvanian seawater Mg/Ca had risen to ~ 3.5 mol/mol (Lowenstein et al., 2005). The estimated range in Mg/Ca from Muleshoe Mound cements, 0.19–0.29, suggests a lowering of oceanic Mg/Ca from Devonian values and delays the transition to aragonite sea Mg/Ca ratios (i.e., Mg/Ca >2, Hardie, 1996) until after the Tournaisian–Visean.

Mississippian oceanic Sr/Ca was an order of magnitude less at Muleshoe Mound than modern values and that estimated for the Devonian (Carpenter et al., 1991). This suggests

large changes in the Sr budget of the ocean. Today, mid-ocean ridge hydrothermal systems are characterized by a negligible flux of Sr at ridge axes, yet with flank fluxes on the order of 2.5 x 10^9 mol/yr with a Sr/Ca of 2 mmol/mol (Alt and Honnorez, 2003). An order-of-magnitude larger flux of Sr reaches the ocean by the erosion of continental crust (2–8 x 10^{10} mol/yr) with an average Sr/Ca of 20 mmol/mol. The incorporation of Sr into aragonite phases is of minor importance because most is lost to interstitial fluids upon early diagenetic stabilization (Schlanger, 1988); this mechanism would result in very little Sr leaving the oceanic reservoir. It has been suggested, on the other hand that this flux is non-trivial and that in fact approximately 50% of Sr precipitated in aragonite does not return to the ocean (Steuber and Veizer, 2002). Indeed, there must be some mechanism for removal of Sr in the modern oceanic system if it is to maintain an average Sr/Ca of 8.8 mmol/mol, given that the riverine flux is twice this and a higher concentration than the mid-ocean ridge flux.

An aragonite Sr sink is logical from a number of different perspectives. Aragonitic fossils are found in the rock record, and these fossils (e.g., mollusks) have high Sr contents. High Sr contents in calcite cements and fossils are used as geochemical indicators of former aragonite (Sandberg, 1983). And even calcites precipitate with some Sr content, especially Mg-calcite (Mucci and Morse, 1983), so their burial could potentially remove Sr from the oceanic reservoir.

Sr/Mg ratios from the Phanerozoic generally correlate with calcite/aragonite sea modality (Fig 8, Carpenter et al., 1991; Cicero and Lohmann, 2001). Cements from the Cambrian, Silurian, Devonian, and Mississippian all have Sr/Mg > 0.01, while Middle Triassic, Pliocene, and Holocene cements all have Sr/Mg < 0.01. Calcite-sea conditions

are suggested to have been dominant during the former intervals, while the latter intervals are considered to be from aragonite seas. Because Sr incorporation is proportional to Mg incorporation in calcite (Mucci and Morse, 1983), the slope of the line defined by the variable Mg content in modern calcites is the Sr/Mg ratio. If oceanic Ca concentration were to change, Sr/Mg would not be affected. Fluxes of Mg and Ca to the ocean are known to be dominated by one-to-one cation exchange during hydrothermal alteration of mid-ocean ridge basalt (Stanley and Hardie, 1998). Therefore, any change in Mg concentration would involve a concomitant change in Ca concentration. Variation in the Sr/Mg ratio through time (Figure 2-9) reinforces the notion of secular Sr/Ca variation in the ocean (Lear et al., 2003a; Steuber and Veizer, 2002) because changes to the Sr/Mg ratio cannot occur without changes in oceanic Sr/Ca (Carpenter et al., 1991).

During the Devonian to Carboniferous, carbonate precipitation—mostly as calcite—would have precluded much Sr removal (e.g., through aragonite precipitation). An ocean with a reduced sink for Sr could explain a higher late Devonian Sr/Ca (Carpenter et al., 1991), though it would suggest the existence of a Sr sink by the Early Mississippian to account for the reduction in oceanic Sr/Ca witnessed in Muleshoe Mound cements. If this flux were in the form of aragonite, these cements could be recording the initiation of aragonite-sea conditions during a time when Mg/Ca would indicate a calcite sea. Further inquiry into the mechanisms and time scales by which Sr leaves the oceanic reservoir are required to resolve this problem.

2.7 Conclusions

Syndepositional marine carbonate cements and crinoids were collected from Muleshoe Mound, Alamogordo, New Mexico, USA. Optical and cathodoluminescence

petrography, as well as trends in elemental and isotopic data, indicate preservation of near-original geochemical compositions in select samples ($\delta^{18}O$ = –2.5‰, $\delta^{13}C$ = +4.6‰, Mg/Ca = 11 mmol/mol; Sr/Ca = 0.2 mmol/mol; Mn/Ca = 0.2 mmol/mol, and Fe/Ca = 0.4 mmol/mol). Similar geochemical compositions of well preserved crinoids and marine cements indicate complete replacement of crinoid skeletal carbonate by marine carbonate cement, and suggests that crinoid material, having undergone early diagenetic alteration in the marine environment to essentially an abiotic phase, may be a robust *abiotic* record of marine calcite geochemistry. Estimates of paleoseawater elemental ratios from this material imply that Mg/Ca was 0.19 to 0.32 mol/mol and that Sr/Ca was 0.5 to 0.9 mmol/mol during the early Mississippian. This Mg/Ca is consistent with the Early Mississippian ocean being a calcite sea, but the Sr/Ca value is an order of magnitude higher than estimates for the Devonian and suggests some change in the oceanic Sr budget.

2.8 Acknowledgments

We would like to thank Bruce Wilkinson, John Morse, Justin Ries, and Brenda Kirkland for thought-provoking reviews and comments that helped this manuscript fully mature.

2.9 Figures

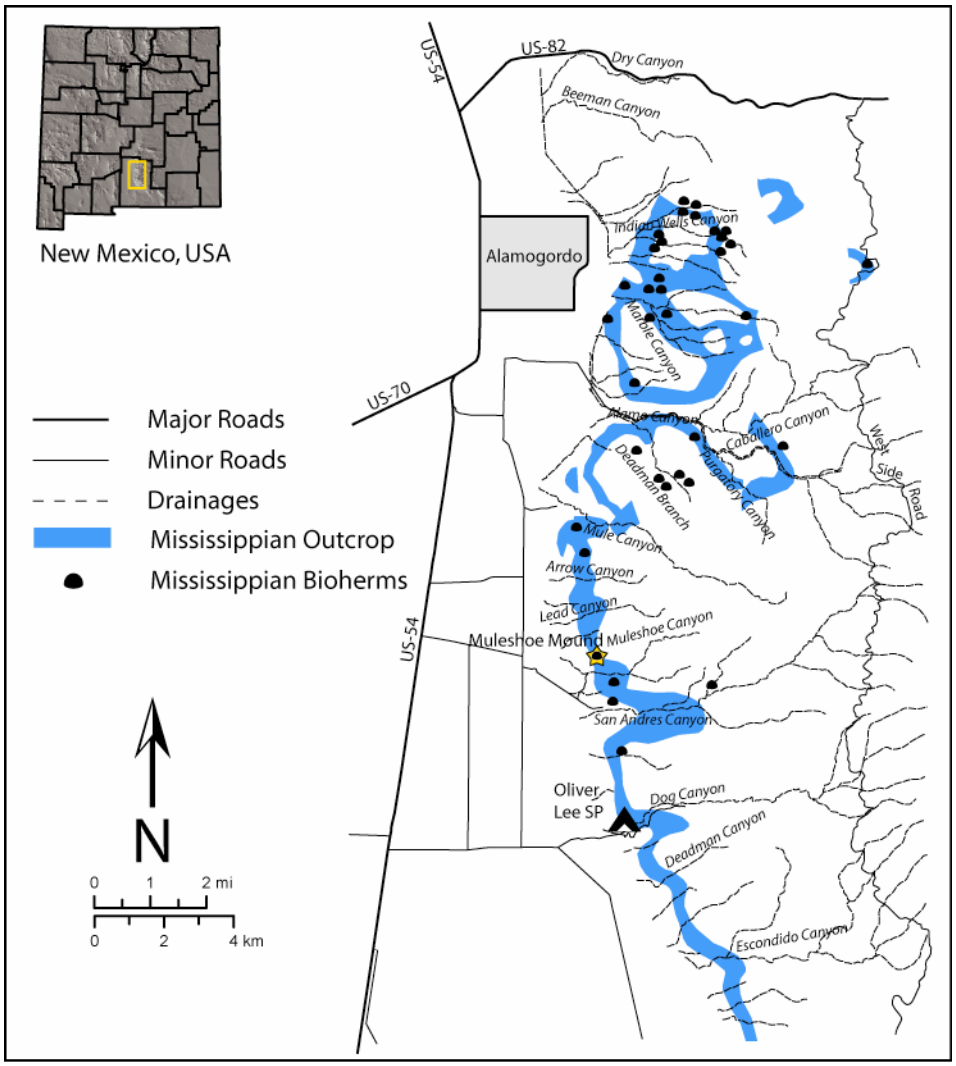

Figure 2-1: Map of study area in the Sacramento Mountains, outside Alamogordo, New Mexico, USA. GIS data from New Mexico Resource GIS System. Bioherm locations are from Ahr (1989).

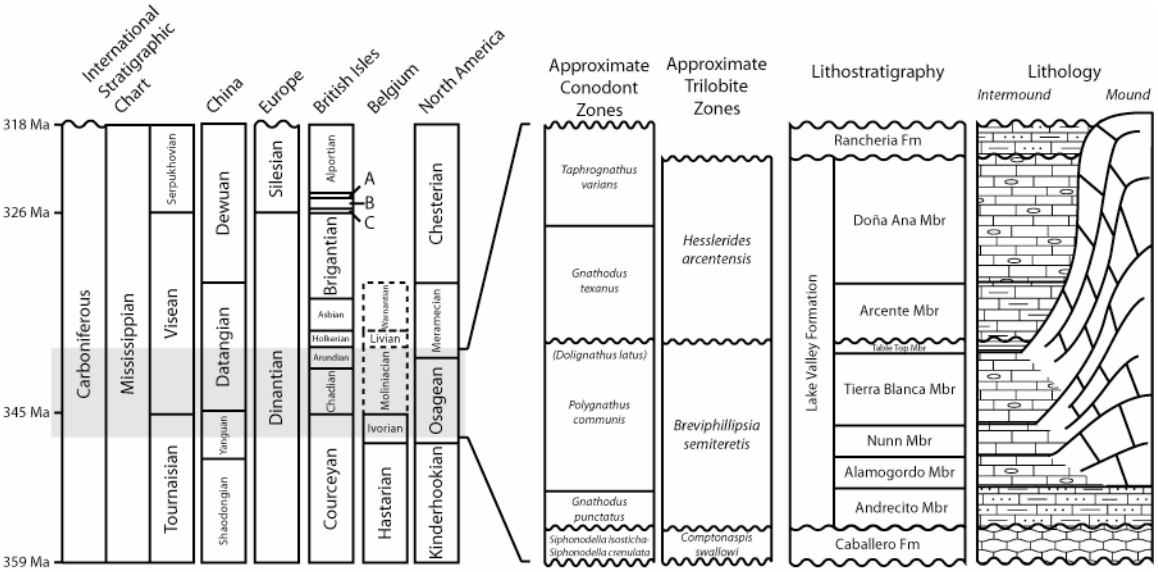

Figure 2-2: Stratigraphic section (Kirkby et al., 1996; Pray and 1961), biostratigraphy (Brezinski, 2000) and correlation diagram (Rohde, 2005) for Muleshoe Mound and associated strata. A, Chokierian; B, Arnsbergian; C, Pendleian.

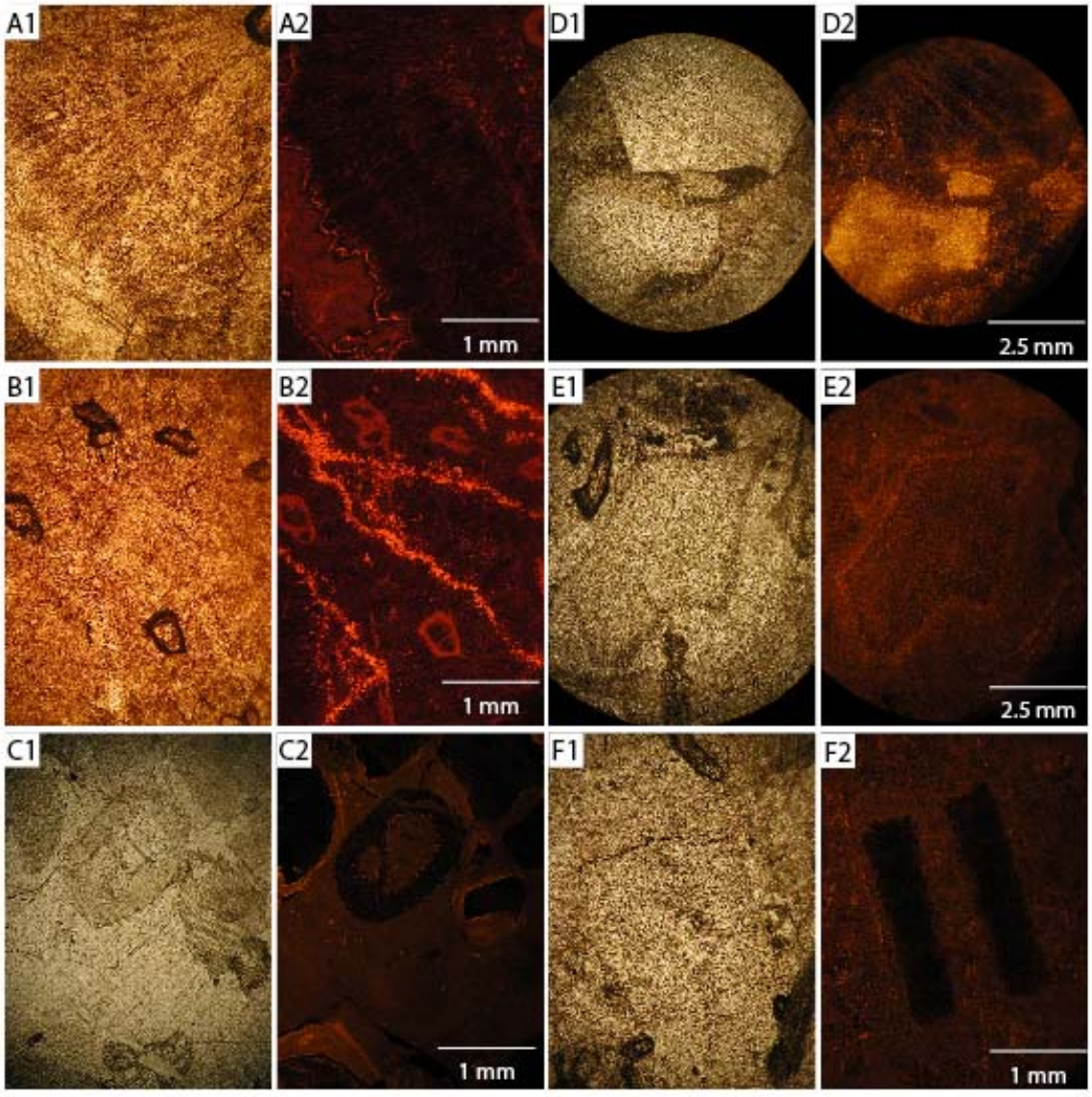

Figure 2-3: PPL and CL photomicrographs of representative phases. A1, 2) Non-luminescent (NL) cloudy, radiaxial cement radiating from a dully-luminescent (DL) bryozoan fragment to a pore filled by a later clear cement. B1, 2) NL cloudy, radiaxial cement (with luminescent fringe) radiating from DL bryozoan fragments. C1, 2) NL bryozoan fragment ensconced in syntaxial cement, but not showing the luminescent (CL) bands zones that appear around the adjacent crinoid fragments (arrows). D1, 2) NL and variably luminescent (VL) crinoid fragments side-by-side. E1, 2) VL crinoid fragment with some stereom structure preserved. F1, 2) Crinoid fragment that is indistinguishable from its syntaxial cement in (1) is visible in the CL photomicrograph.

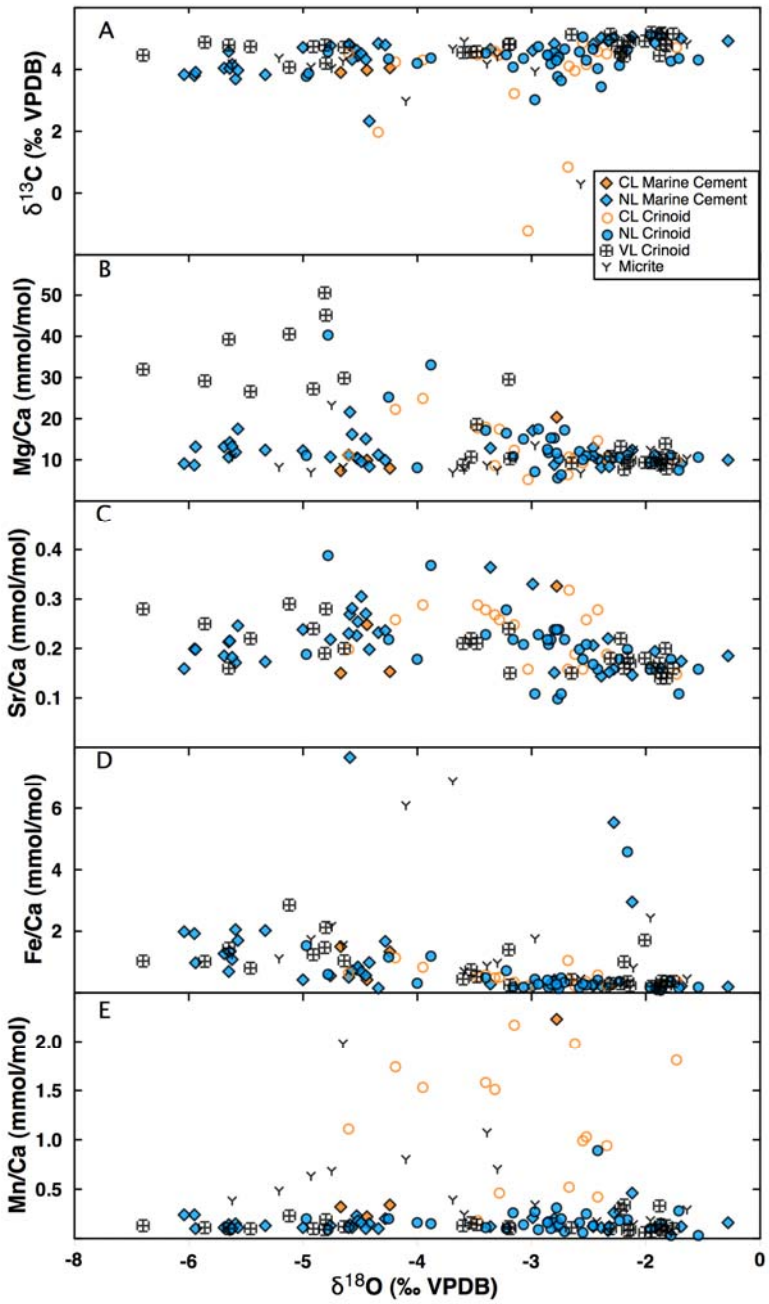

Figure 2-4: Multi-scatter plots against $\delta^{18}O$. A) $\delta^{18}O$ vs. $\delta^{13}C$ shows a burial diagenetic trend follows from (–1.5‰ $\delta^{18}O$, +4.5‰ $\delta^{13}C$) to lighter oxygen values (–6‰ $\delta^{18}O$, +4‰ $\delta^{13}C$). A meteoric diagenetic trend is defined by a meteoric calcite line at ~ –3‰ $\delta^{18}O$. B) $\delta^{18}O$ vs. Mg/Ca shows that Mg contents increase along the burial diagenetic trend. C) Sr/Ca remains relatively unchanged with increasingly more negative $\delta^{18}O$. D) Fe/Ca is very low for most of the samples except for those with the most negative $\delta^{18}O$. E) Mn/Ca is the highest for luminescent phases, but otherwise shows no variation with $\delta^{18}O$.

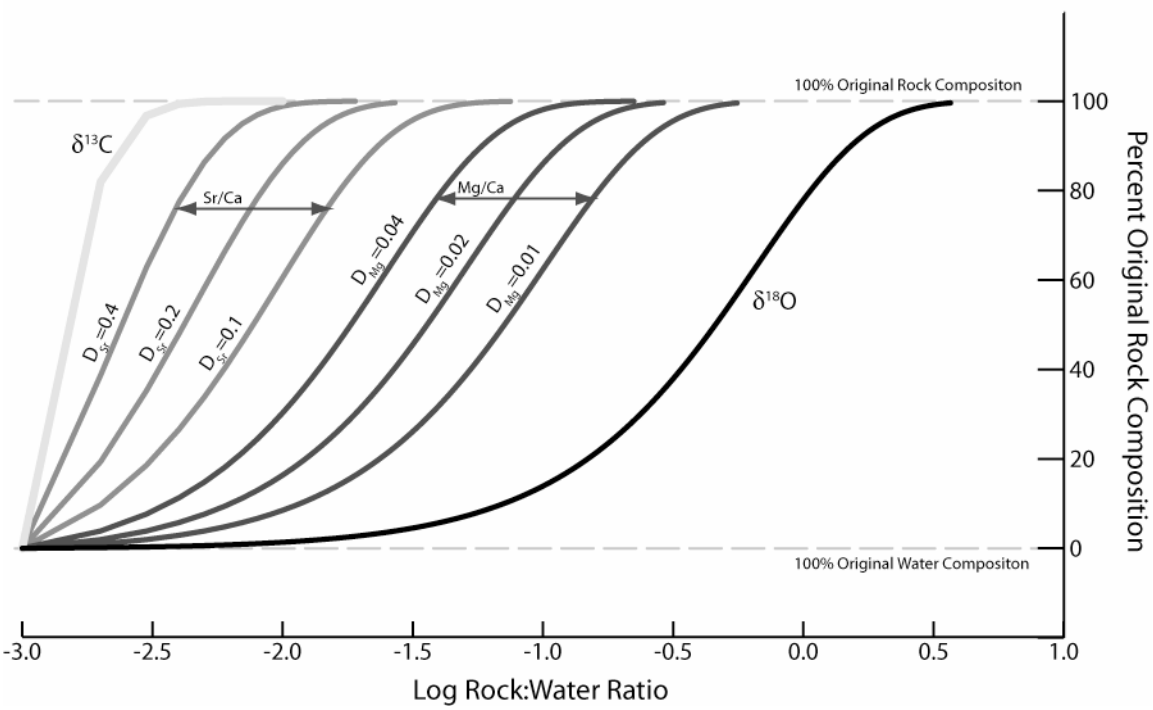

Figure 2-5: With progressive rock–water interaction, the geochemistry of the diagenetic precipitate evolves to reflect the increasing influence of the rock chemistry on the chemistry of the water. Closure of elemental chemistries, here Mg/Ca and Sr/Ca, varies with the partition coefficient. Higher partition coefficients result in faster closure to original rock composition.

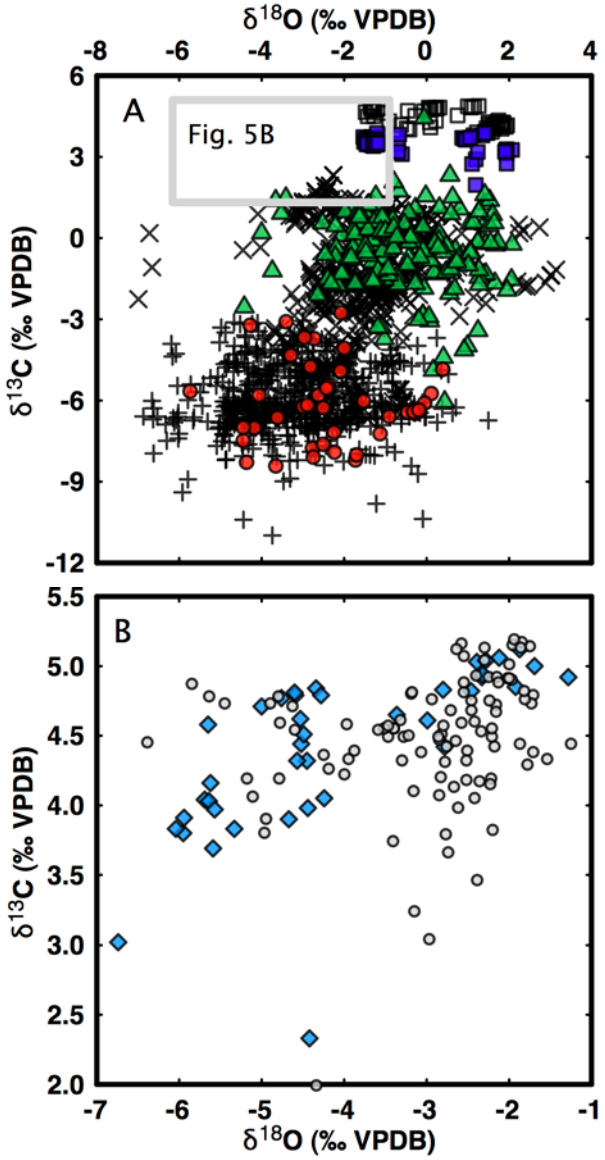

Figure 2-6: A) Isotopic data for modern marine cements (open squares are aragonite, gray squares are Mg-calcite) from Gonzalez and Lohmann (1985), Carpenter and Lohmann (1992), and Aissaoui (1986) as well as isotopic data for modern echinoderms (x's are echinoids, triangles are ophiuroids, circles are crinoids, +'s are asteroids) from Weber and Raup (1966) and Weber (1968). B) Muleshoe mound isotopic data from this study (open circles are crinoids, gray diamonds are cements). Muleshoe marine cement and crinoid isotopic data overlap, whereas modern cements and crinoids do not.

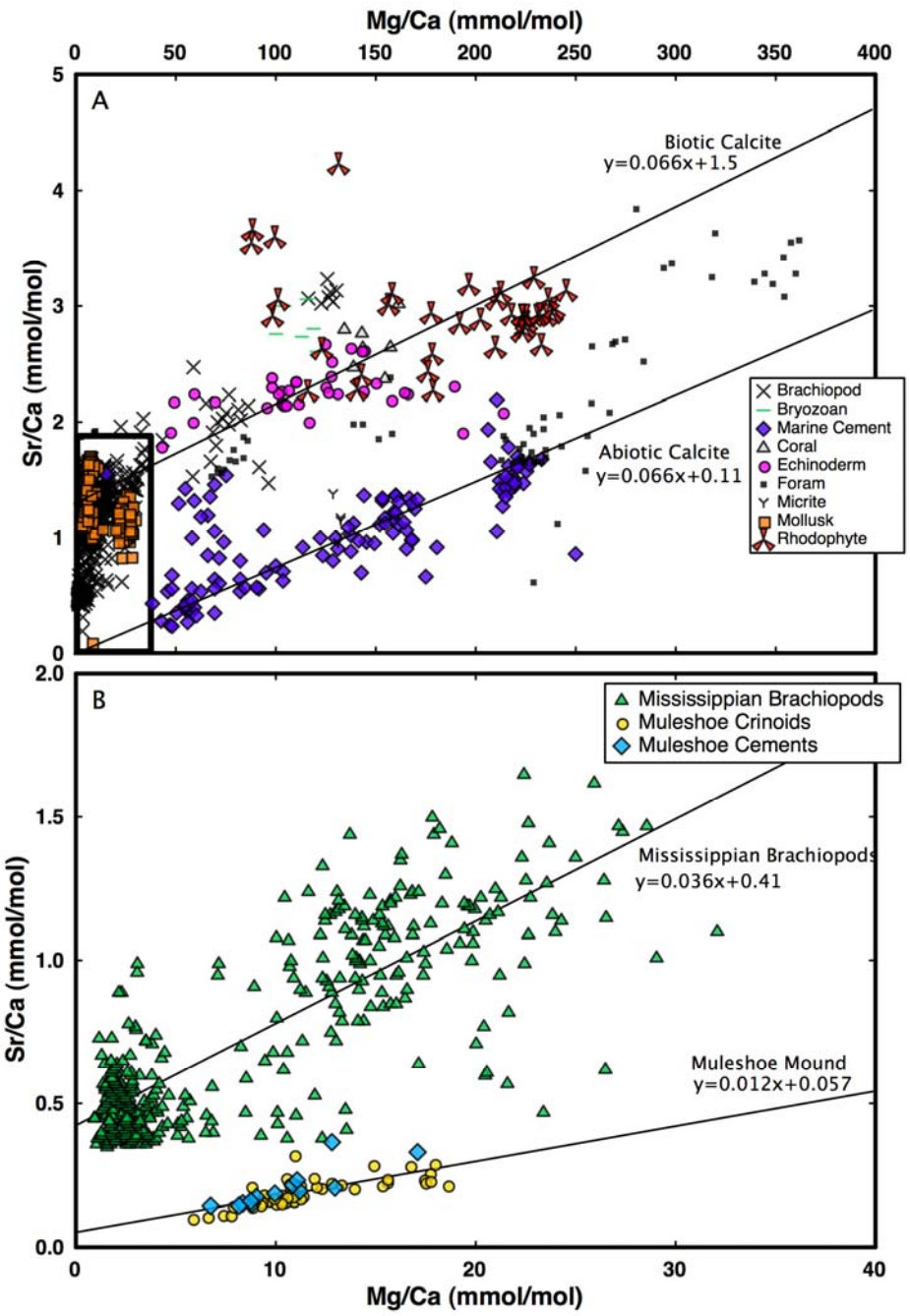

Figure 2-7: A) Sr/Ca–Mg/Ca trends for modern marine Mg-calcite cements and modern biota that which produce magnesian calcite (Brand et al., 2003; Freitas et al., 2005; Klein et al., 1996; Major and Wilber, 1991; Mitsuguchi et al., 2001; Rathburn and De Deckker, 1997; Takesue and van Geen, 2004; Wei et al., 2000; Yu et al., 2005). Gray box represents area of Figure 2-5B. B) Sr/Ca–Mg/Ca trends for least-altered Muleshoe marine cements and crinoids as well as Mississippian brachiopods from the Russian Platform (Mii et al., 1999). Major-axis ellipses represent 95% confidence.

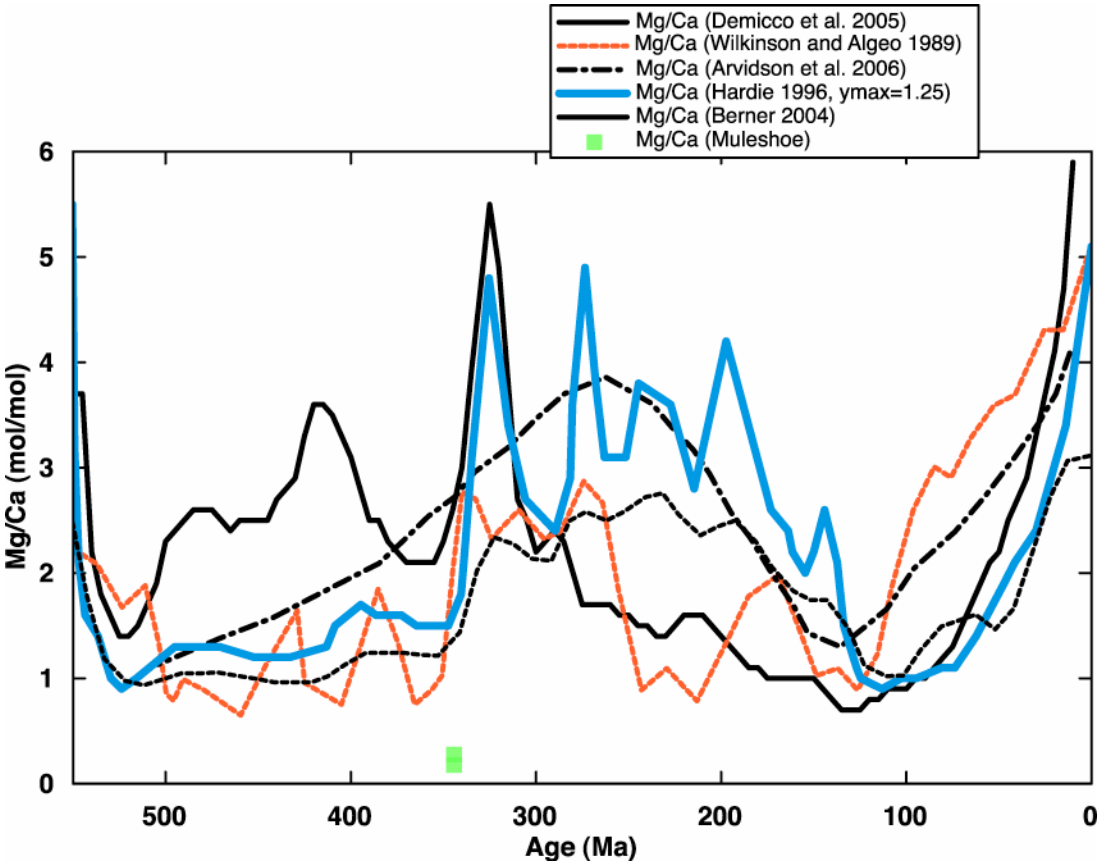

Figure 2-8: Modeled estimates of Phanerozoic Mg/Ca variation (Arvidson et al., 2006; Berner, 2004; Demicco et al., 2005; Hardie, 1996; Wilkinson and Algeo, 1989). The range of oceanic Mg/Ca variation calculated from Muleshoe Mound cements is also included (red squares).

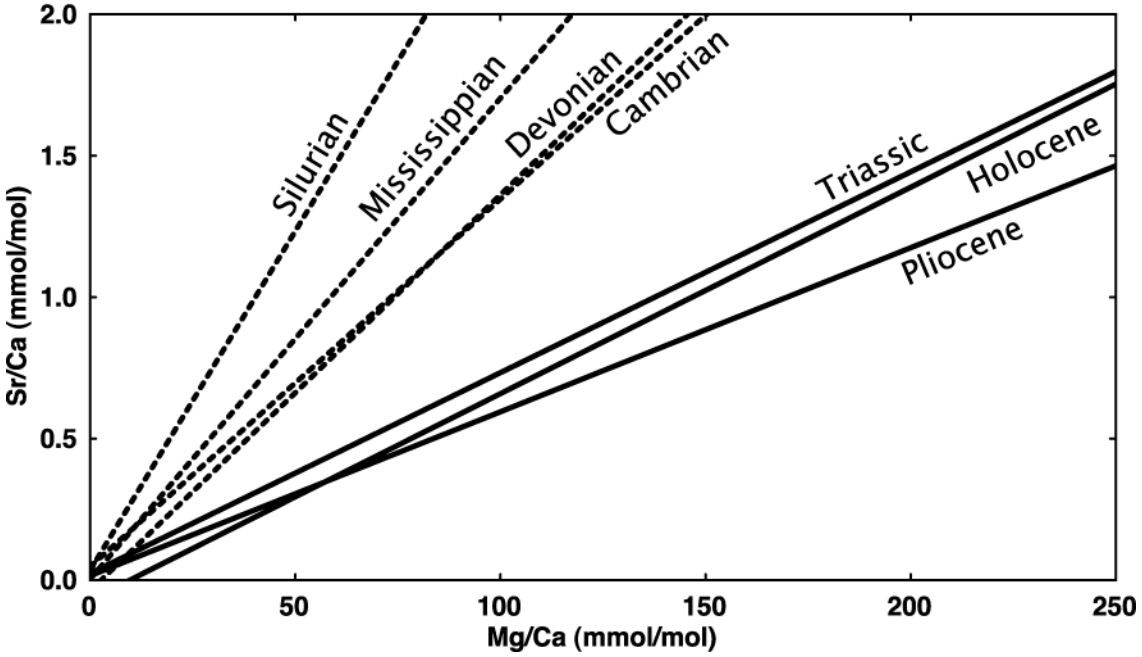

Figure 2-9: Phanerozoic Sr/Mg variation from marine cements. Paleozoic marine cements tend to have a higher Sr/Mg than do Post-Paleozoic marine cements.

Chapter 3: Application of Calcite Trace Element Partitioning Function to the Reconstruction of Paleocean Chemistry

3.1 Abstract

To use the elemental compositions of various marine carbonate phases to understand secular changes in seawater chemistry (e.g., Mg/Ca), one must accurately describe the incorporation of these elements into carbonate minerals. While the Mg/Ca of calcite has been described classically to vary linearly with the Mg/Ca of its parent solution, in reality empirical data are better summarized (i.e., have a higher correlation coefficient) by a power function. Based on these empirically determined "partition power functions," skeletal echinoderm calcite and abiotic marine cements are best suited to investigate variation in paleocean Mg/Ca. Phanerozoic seawater Mg/Ca estimated from echinoderm skeletal material is reduced on average 15% when calculated using a partition power function instead of a partition coefficient. A secular change in the Mg/Ca of marine calcite phases should be apparent if seawater Mg/Ca has changed through geologic time. In addition to an observed secular variation, when partition power functions are considered, the range in concentration measured between calcite phases with the highest and lowest Mg/Ca values would be greatest when seawater Mg/Ca was also high and lowest when seawater Mg/Ca was low. Importantly, it follows that during times of

"calcite seas" when the seawater Mg/Ca was presumed to be lower, the formation of calcite with uniformly low Mg contents would lead to a depressed drive for diagenetic stabilization of these phases and in turn lead to greater preservation of crystal and skeletal microfabrics and primary chemistries in calcitic biotic and abiotic components.

3.2 Introduction

Within the last century, scientific inquiry into the chemistry of limestones has brought us to understand the vital importance of this geomaterial in the global carbon cycle that in turn regulates the Earth's climate. Numerous chemical tracers have been developed to investigate ancient environmental parameters such as temperature, pH, salinity, and seasonality, as well as the fluxes of chemical components into and out of the oceanic reservoir (de Villiers et al., 2005; Hay et al., 2006; Ivany et al., 2004; Pagani et al., 2005; Shackleton, 1974). Carbonates are well suited for this endeavor as they precipitate in a wide variety of aqueous environments and have left a voluminous geological record (>20% of sedimentary rock is limestone). This volume of rock, however, is not uniform in mineralogy, spatial distribution, or chemical composition, and it is through these variations that one hopes to see a signal of paleoenvironment.

The mineralogical signal of most limestones is obscured by the effects of post-depositional alteration (i.e., diagenesis), but methods have been developed to infer primary mineralogy from the petrographic fabric of all but the most intensely altered geological carbonate (Bathurst, 1971). When considering the primary mineralogy of Phanerozoic marine limestones, it has struck many workers that there exists a modality. At some times (e.g., today and the late Paleozoic) aragonite and high-Mg calcite (> 12 mol% $MgCO_3$) are the dominant mineralogies of shallow water shelfal carbonates. Yet,

during other times low-Mg calcite (< 4 mol% $MgCO_3$) is most abundant in this setting. Sandberg (1983) called these times, respectively, "aragonite seas" and "calcite seas." While initially secular variation in atmospheric CO_2 content was causally implicated in this phenomenon (Sandberg, 1983), it has since become commonly accepted that the Mg/Ca ratio of seawater arbitrates this variation by interfering with the growing calcite crystal surface (Stanley and Hardie, 1998) as well as increasing the solubility of the resultant carbonate. At a certain point aragonite, despite being the high pressure/temperature polymorph of $CaCO_3$, becomes kinetically the most favorable structure for marine carbonate. Variations in the mineralogies of dominant reef building organisms (Stanley and Hardie, 1998) have been shown to mirror this carbonate mineralogic trend, as have the mineralogies of evaporite minerals (Hardie, 1996; Holland et al., 1996; Horita et al., 2002). Chemical evidence for variation in seawater Mg/Ca has also come from the analysis of evaporite fluid inclusions (Kovalevich et al., 1998; Lowenstein et al., 2001; Zimmermann, 2000). Change in oceanic Mg/Ca, in turn, is thought to have been dominated by the one-for-one Ca efflux/Mg influx during the hydrothermal alteration of fresh basalt at mid-ocean ridges. Since this flux is directly related to seafloor spreading rates, a record of oceanic Mg/Ca could also illuminate the current debate over whether such rates are constant through the Phanerozoic (Demicco, 2004; Rowley, 2002).

Dickson (2002, 2004) produced a Phanerozoic trend of seawater Mg/Ca (Mg/Ca_{sw}) from the Mg/Ca of crinoid skeletal calcite. Crinoids are well suited for this task as they are generally restricted to living in seawater of open marine composition. If crinoids grew under either brackish or hypersaline conditions, their partitioning might reflect these

highly geochemically variable fluids. In addition, skeletal Mg/Ca_C is suggested to record predictably changes in Mg/Ca_{sw}. Though typically this relationship is quantified by a linear function, it has become clear that a power function describes this behavior better (Ries, 2004, 2005, 2006a, b; Stanley et al., 2005).

In this paper the rationale for a power relationship between the Mg/Ca of an aqueous solution and precipitated calcite is discussed, beginning with its relationship to partition coefficients. We will use these partition power functions for Mg into calcite to model the Mg/Ca of different carbonate phases throughout the Phanerozoic and suggest what might be the most ideal carbonate proxy of paleocean Mg/Ca_{sw}.

3.3 Partition coefficients

During the precipitation of calcite from seawater, trace elements (e.g., Mg, Sr) are incorporated as impurities into the crystal lattice. To quantify the degree to which such an elemental impurity is incorporated within a crystallizing solid, it has been customary to use a partition coefficient (D), which is the ratio of the concentrations of a trace element (Te) in the precipitate and the solution:

$$D = \frac{[Te]_{Precipitate}}{[Te]_{Solution}} \tag{3-1}$$

Trace element to major element ratios (Me) are used because while elemental concentrations may change, the ratios of those elemental concentrations can remain relatively constant. Equation (3-1) is phenomenological and is merely the result of dividing one empirically measured quantity into another. The use of the term "partition coefficient," where others might use "distribution coefficient," follows the suggestion of Morse and Bender (1990) that the latter be used solely to describe coefficients related to

the thermodynamic equilibrium constant while the former be used to describe coefficients that are purely empirical and thus include kinetic effects.

Partition coefficients are used widely to describe trace element incorporation into modern marine biotic and abiotic carbonates because the $[Te/Me]_{Seawater}$ is largely invariant over a broad range of salinities when dilution occurs by fresh waters. This makes *D* essentially a function of $[Te/Me]_{Precipitate}$. However with the realization that through geologic time, elemental ratios in seawater have *not* been constant (Dickson, 2002; Horita et al., 2002; Lowenstein et al., 2001; Zimmermann et al., 2000), it seems more appropriate to rewrite Equation (3-1) in the form of y = *m*x:

$$[Te/Me]_{Precipitate} = D[Te/Me]_{Solution} \quad (3\text{-}2)$$

In this form, Equation (3-2) is identical to the most basic equation that describes sorption, the linear "sorption isotherm." Sorption isotherms are empirically derived and relate the concentration of a chemical species on a mineral surface to the concentration of that chemical species in the adjacent solution. This linear relationship holds for a number of geologically relevant mineral precipitation systems (Arth, 1976; Doerner and Hoskins, 1925; Henderson and Kracek, 1927; McIntire, 1963). Describing the incorporation of trace elements into minerals as a sorption phenomenon is not new (Devore, 1955; Farley et al., 1985), nor even newly applied to calcite (Comans and Middelburg, 1987; Davis et al., 1987; Mucci and Morse, 1983; Rimstidt et al., 1998; Watson, 2004; Zachara et al., 1991).

3.4 Effect of Solution Composition

Numerous studies have investigated the effect of changing solution Mg/Ca on the Mg/Ca of biotic and abiotic calcite. These include investigations of abiotic calcite

(Fuchtbauer and Hardie, 1976; Füchtbauer and Hardie, 1980; Mucci and Morse, 1983), as well as calcite precipitated by echinoids, crustaceans, shrimps, serpulid worms (Ries, 2004), coralline algae (Ries, 2006a; Stanley et al., 2002), coccolithophorids (Stanley et al., 2005), and planktonic and benthic foraminifera (Delaney et al., 1985; Segev and Erez, 2006). To generate a partition coefficient (i.e., Equation (3-2)), a linear function with intercept of zero can be fit to all of these datasets. The intercept must be zero because if there is no Mg in the solution, there can be none in the calcite. As displayed in Table 3-1, these data show strong correlation (high R^2) and high significance ($p < 0.05$).

An inherent feature of the linear partition function is that the slope of the function is constant at all solution compositions. However, when the slope (the partition coefficient, *D*) is plotted against solution Mg/Ca, only the two coralline algae datasets have this feature. The partition coefficient for abiotic cements and calcite produced by crab, echinoid spine, echinoid plate, planktonic and benthic foraminifera, abiotic cement, and the coccolithophorids *P. carterae* and *C. neohelis* decrease exponentially with increasing solution Mg/Ca (Figure 3-1B). While the D_{Mg} of calcite produced by serpulid worms, shrimp, and the coccolithophore *O. neopolitana* increases logarithmically with solution Mg/Ca.

This behavior is analogous to a slightly different sorption equation, known as a Freundlich isotherm. It suggests that a power relationship exists between solution and surface composition. For the incorporation of Mg into calcite precipitating from seawater, it would have the form:

$$Mg/Ca_{Calcite} = F\left(Mg/Ca_{Seawater}\right)^{H} \tag{3-3}$$

Equation (3-3) is referred to as a partition power function. This term is meant to invoke the empirical nature of a partition coefficient, while suggesting a power relationship. In Equation (3-3), *F* is a *partition factor* (not to be confused with a partition coefficient) and *H* is a *partition exponent*. The power function (Equation (3-3) fits data with similar strength and significance as the linear function with zero-intercept, with the exception of the coccolithophorid *C. neohelis*.

To relate Equation (3-3) to Equation (3-1), the equation for the partition coefficient, we find that:

$$D_{Mg} = \frac{Mg/Ca_C}{Mg/Ca_{SW}} = \frac{F(Mg/Ca_{SW})^H}{Mg/Ca_{SW}} = F(Mg/Ca_{SW})^{H-1} \quad (3\text{-}4)$$

With Equation (3-4), we can fit any dataset of calcite D_{Mg} as a function of solution Mg/Ca. This is not the case for Equation (3-2). This holds for most of the functions produced for Mg in calcite. An *H* value near 1 indicates a nearly constant D_{Mg} at differing fluid trace element content, and thus the partitioning behavior could be easily characterized by the traditional partition coefficient. An *H* value greater or less than unity indicates strong changes in D_{Mg} with fluid trace element content. The equation for the partition coefficient (Equation (3-2)) can be viewed as a special case of the partition power function where $H = 1$.

3.4.1 Variation in H

By knowing the range in possible values of the partition factor, *F*, and exponent, *H*, it would be possible to outline the area of possible values of primary calcite Mg/Ca. If a geological sample analyzed outside this area, it could be supposed to have undergone diagenesis. Partition power functions with similar values of *F* and *H* might have similar biochemical pathways for calcite mineralization.

By varying the partition exponent (H), six different types of partition power functions can be identified (

Figure 3-2) based on the following ranges in H: $H = 0$ (Type 1), $0 < H < 1$ (Type 2), $H = 1$ (Type 3), $1 < H < 2$ (Type 4), $H = 2$ (Type 5), $2 < H$ (Type 6). Each range results in a unique expression for Equation (3-3) (for Mg/Ca_C), Equation (3-4) (for D_{Mg}), or both. These expressions are summarized in Table 3-3.

The odd-numbered types have integer values of H. This results in a partition power function with zero slope (Type 1), a partition power function that has a first derivative (i.e., D_{Mg}) of zero (Type 3), or a partition power function that has a constant, positive first derivative (Type 5). The even numbered types are identified by a partition power function that is logarithmically increasing (Type 2), by a partition power function whose first derivative (i.e., D_{Mg}) is logarithmically increasing (Type 4), or by a partition power function whose first derivative (i.e., D_{Mg}) is exponentially increasing (Type 6). Further types could be defined by taking higher and higher derivatives of the partition power function, though the usefulness of such an endeavor is unclear in the present frame of inquiry as the partition power function and its first derivative both have empirical significance.

Partition power functions can exist only in two quadrangles in Mg/Ca_C-Mg/Ca_{sw} space (Figure 3-2A). These quadrangles are delimited by the points (0,0), (1,F), and ($+\infty$,$+\infty$). Outside of these areas, partition power functions cannot exist.

The point (1,F), herein referred to as the "partition nexus," is mathematically necessary because at any H Equation (3-3) reduces to F when $Mg/Ca_{sw} = 1$:

$$Mg/Ca_C = F\left(Mg/Ca_{SW}\right)^H = F(1)^H = F \tag{3-5}$$

At $Mg/Ca_{sw} < 1$, power partition functions with the lowest H have the highest Mg/Ca_C. For example at $Mg/Ca_{sw} = 0.5$, $F(0.5)^0$ will be greater than $F(0.5)^{0.5}$, but when $Mg/Ca_{sw} > 1$, the opposite becomes true and the lowest H value will result in the lowest Mg/Ca_C because at $Mg/Ca_{sw} = 4$, $F(4)^0$ will be less than $F(4)^{0.5}$. Using partition power functions generated by the regression of empirical data, this behavior can be seen in functions with similar F, but varying H (Figure 3-2B).

The first derivative of the partition power function has a similar nexus at (1, F) (Figure 3-2C,D). However, the first derivative of the partition power function is free to occupy all space between (0,0) and ($+\infty$,$+\infty$).

3.4.2 Variation in F

Varying the partition factor (F), in contrast, only translates the partition nexus vertically, either positively or negatively depending on whether F is increased or decreased (Figure 3-3). The characteristics that define each of the six types of partition function remain valid in spite of any change in F.

3.4.3 Other Observations

In addition to the observation that D_{Mg} changes with fluid Mg/Ca, a number of other conclusions can be drawn from the data presented in Figure 3-1. (1) Fluid Mg/Ca and calcite Mg/Ca are positively correlated in all functions, a relation that reinforces the premise that the first order control on the Mg/Ca of these calcite phases is the Mg/Ca ratio of the parent solution. (2) The various biotic and abiotic calcites display different partition power function. This implies that there is an additional physicochemical factor or factors besides the vital effect that are responsible for differences in Mg incorporation behavior among various calcite phases. Vital effect can be ruled out because most of the

biotic partition power functions that have been reported fall within or near the range of the two abiotic calcite partition power functions. (3) There is no limit towards which calcite Mg/Ca converge as fluid Mg/Ca increases. This would imply a calcite of any Mg/Ca could be precipitated provided the requisite high Mg/Ca could be invoked. For example, to produce a calcite with Mg/Ca = 1 (i.e., dolomite), the most favorable partition power function, that of the coccolithophorid *O. neopolitana*, would require Mg/Ca_{sw} of 10, while the rest are in the range of 10 to 1300, except the planktonic foraminifer *G. sacculifer* which would require a Mg/Ca_{sw} of 10^6 (Table 3-4). Since the fossil record is lacking in such primary dolomitic tests and cements, we might assume that Mg/Ca_{sw} has never been above 10.

Maximum and minimum values can be estimated for the partition factor, *F,* through the Phanerozoic from modern considerations. Calcifying organisms today can produce a shell with at most 30 mol% $MgCO_3$ (Milliman, 1974). If we assume that the highest seawater Mg/Ca is that of today (~5.2) and that *H* can only vary between the range we see in modern partition power functions (0.4 to 1.2), then *F* must be between 0.06 and 0.22.

3.5 Other Effects on Trace Element Content

In addition to Mg/Ca ratio of the fluid, partition power functions have been derived to describe the effect of other parent solution parameters on the Mg/Ca of a calcite. These include temperature (e.g. Katz, 1973; Lear et al., 2002; Mucci, 1987; Nürnberg et al., 1996), precipitation rate/supersaturation (e.g., Mucci and Morse, 1983), $pH/CO_3^{2-}/pCO_2$ (e.g. Burton and Walter, 1987; Rathmann and Kuhnert, 2008; Russell et al., 2004),

depth/pressure, and salinity/ionic strength (Zhong and Mucci, 1989; Zuddas and Mucci, 1998).

3.5.1 Temperature

While the effects of Mg/Ca_{sw} on Mg/Ca_C have been generally neglected in the literature, investigations have been made into the effect of temperature on the incorporation of magnesium (Chave, 1954; Elderfield et al., 2006; Katz, 1973; Lear et al., 2002; Nürnberg et al., 1996; Rosenthal and Lohmann, 2002), or strontium (Katz et al., 1972; Malone and Baker, 1999) or both (Elderfield et al., 2002; Rathmann and Kuhnert, 2008; Rosenthal et al., 1997; Rosenthal et al., 2006). However, this work has mostly occurred on abiotic calcite or cultured foraminifera at modern ocean Te/Me ratios.

3.5.2 Combining the Effects of Solution Composition and Temperature

The two dominant factors affecting the Mg/Ca of calcite are the temperature and Mg/Ca of its parent solution. Since empirical partition functions have been described for both, it seems reasonable to combine them to produce a single equation. Two methods have been proposed to accomplish this: Lear et al. (2000; 2002) and Ries (2004, 2006a).

Lear et al. (2000; 2002) first suggested that to account for the Mg/Ca_{SW} variation, the temperature partition function could be amended by multiplying it by the ratio of past-to-present Mg/Ca_{SW}. This has the form:

$$Mg/Ca_C = \left(\frac{Mg/Ca_{SW-past}}{Mg/Ca_{SW-present}} \right) \times Be^{AT} \qquad (3\text{-}6)$$

where B and A are empirical constants and T is temperature (in °C). This methodology has been used in all published studies that have calculated

paleotemperatures over long spans of geologic time from calcite Mg/Ca (Dutton et al., 2005; Lear et al., 2004; Tripati et al., 2003; Zachos et al., 2003).

More accurately, Ries (2004) combined the partition power functions he derived from empirical data with temperature partition functions from Chave (1954) and Fuchtbauer and Hardie (1976). In the case of coralline algae (rhodophyta), Ries (2004) combined the partition power function:

$$Mg/Ca_c = F\left(Mg/Ca_{SW}\right)^H = 0.0421\left(Mg/Ca_{SW}\right)^{1.01} \quad (3\text{-}7)$$

and an temperature partition function:

$$Mg/Ca_C = Be^{AT} = 0.0709e^{0.0457T} \quad (3\text{-}8)$$

simultaneously at Mg/Ca_{sw}=5.2 to generate a unified Mg–T partition function for:

$$Mg/Ca_C = E\left(Mg/Ca_{SW}\right)^H e^{AT} = 0.0134\left(Mg/Ca\right)^{1.01} e^{0.0457T} \quad (3\text{-}9)$$

Where *E* is a constant that is explained as follows:

$$E = \frac{B}{\left(Mg/Ca_{SW}\right)^H} = 0.01341 \quad (3\text{-}10)$$

3.6 Ideal Carbonate Proxies of Paleocean Mg/Ca

3.6.1 Biotic Phases

Partition power functions, and the data from which they are estimated, can be used to investigate what might constitute the best carbonate proxy of paleoseawater Mg/Ca. To do this, we investigate the two parameters of the partition power function, *F* and *H*, and the R^2 of the fit. The distribution exponent, *H*, describes to what extent the partition function deviates from linearity.

The Mg/Ca of an ideal carbonate proxy should vary predictably with seawater Mg/Ca. All of the partition power functions in Table 3-1 meet this except the

coccolithophorid *C. neohelis* (Stanley et al., 2002), whose calcite Mg/Ca does not change with changes in Mg/Ca_{sw}. In addition, the ideal proxy would have a strong correlation (high R^2) between calcite and seawater Mg/Ca. All of the power fits for calcites in Table 3-1 have an $R^2 > 0.79$ except the planktonic foraminifer, which has an R^2 of 0.55 (Delaney et al., 1985). However, all of the regressions, with the exception of *C. neohelis*, are highly significant at the $p < 0.01$ level.

If secular variation in seawater Mg/Ca is to be discerned from measurements of carbonate, the measured amplitude in carbonate Mg/Ca must be greater than the analytical errors. For example, it would be difficult to identify changes in Mg/Ca_{sw} from an organism whose shell Mg/Ca varied from 59 to 61 mmol/mol between $Mg/Ca_{sw} = 1$ and 5, respectively. Conversely, the calcite should have a low enough Mg/Ca to minimize diagenetic stabilization to a secondary carbonate that does not preserve original values. Here, we adopt an upper limit of 10 mol% (110 mmol/mol Mg/Ca), which is suggested because below this point the solubility of Mg-calcite is less than that of co-occurring aragonite (Milliman, 1974). Therefore, during the diagenesis of a poly-mineralic assemblage of abiotic and biotic carbonate particles, the diagenetic fluid will reach saturation with respect to calcite even though aragonite phases will continue to undergo dissolution and alteration.

The requirement that the partition function will result in a large amplitude signal of Mg/Ca variation largely precludes the use of carbonate phases whose Mg-content varies little between times of high and low seawater Mg/Ca. This discounts benthic foraminifera (Segev and Erez, 2006) and echinoid spine material (Ries, 2004) because they range less than 0.03 mol/mol Mg/Ca in their precipitate as fluid Mg/Ca varies between 1 and 10. On

the other hand, calcite phases whose Mg content varies considerably between high and low seawater Mg/Ca might have poor preservation of high-Mg material precipitated during times of high seawater Mg/Ca. This would preclude the remaining coccolithophores (Stanley et al., 2005) and the coralline algae (Ries, 2006a; Stanley et al., 2002). It can be noted that the original bulk geochemistry of a carbonate could be preserved in a diagenetic carbonate phase if alteration occurs in a closed system (Given and Lohmann, 1985; Lohmann and Meyers, 1977).

The remaining carbonate phases, comprised of the crab carapace, serpulid worm tube, shrimp carapace and echinoid plates (Ries, 2004) should be acceptable proxies. Of these, echinoid plates (i.e. echinoderm material) are the most abundant in the geologic record and thus should serve as the ideal records of Phanerozoic Mg/Ca based on currently available partition power functions.

There are numerous taxa for which partition power functions do not exist, but might be quite useful. For example, brachiopods have been used to document secular change in $\delta^{18}O$, $\delta^{13}C$, Sr/Ca and $^{87}Sr/^{86}Sr$ (McArthur et al., 2001; Steuber and Veizer, 2002; Veizer et al., 1999). Generally considered to have been obligate low-Mg calcifiers for the entire Phanerozoic, they could be disqualified under the notion that the Mg/Ca signal might be too small to identify in the geologic record. Some modern brachiopods, though, precipitate calcitic shells with up to 130 mmol/mol Mg/Ca (Brand et al., 2003) and if their ancient relatives can be identified with a high degree of accuracy, they could be a useful paleoproxy of Mg/Ca_{sw}.

3.6.2 Abiotic Phases

Two datasets exist for abiotic marine carbonate cements from which Mg partition power functions can be calculated ("MM83"Füchtbauer and Hardie, 1980; Mucci and Morse, 1983). The resulting functions are not identical with the *F* of one (Füchtbauer and Hardie, 1980) about twice that of the other (Mucci and Morse, 1983). Which is more appropriate? At modern Mg/Ca_{sw}, these two functions both produce values within the range of modern marine cements: the former produces a high-Mg calcite (150 mmol/mol), while the latter produces a low-Mg calcite (85 mmol/mol). Peculiarities to the experimental procedures of each study are the likely cause of this discrepancy. At Mg/Ca < 1.5 the difference between the two is negligible. It is probably necessary to use both functions when estimating the paleoseawater Mg/Ca and acknowledge that a range of compositions might exist.

3.7 Modeling Phanerozoic Mg/Ca

Partition power functions can be applied to improve understanding of Phanerozoic change in seawater Mg/Ca. Using the Phanerozoic seawater Mg/Ca model of Hardie (1996), hypothetical secular Mg/Ca trends of various biotic and abiotic calcites can be generated based on their empirically determined Mg-partition power functions. These model results (Figure 3-4) clearly show that a given seawater Mg/Ca will produce a range of Mg/Ca values for biotic and abiotic calcites and that this range increases with an increase in seawater Mg/Ca. For example, during the calcite sea of the Ordovician, the highest Mg/Ca in a calcite phase would have been ~ 60 mmol/mol, the lowest ~ 15 mmol/mol, for a range of ~ 45 mmol/mol. Today, where the Mg/Ca_{sw} is at a high of 5.2, the range observed range is ~ 200 mmol/mol.

One of the primary drivers of diagenetic alteration in carbonate rocks is the stabilization of aragonite and high-Mg calcite, both metastable, to low-Mg calcite (Bathurst, 1971; James and Choquette, 1990). An important, but rarely mentioned, corollary to the calcite sea/aragonite sea theory is that during calcite seas the tendency for diagenesis based on the stabilization of metastable mineralogies should be reduced. This results from the small range and low average Mg content of both biotic and abiotic calcite phases as well as the general paucity of metastable aragonite during these times.

Many carbonate diagenetic paradigms assume that the primary Mg/Ca of a fossil carbonate phase is equal to its modern composition. If a phase is found in the geologic record with a lower Mg/Ca than expected for a modern analog, a "loss" of Mg is estimated. This is untenable even when thinking in terms of partition coefficients because modern organisms that produce skeletons of high-Mg calcite would have produced skeletons of low-Mg calcite during calcite seas. Even modern aragonitic taxa have been shown to produce calcitic skeletons in artificial seawater with Mg/Ca < 2 (Ries, 2006a).

When attempting to use calcites from the geologic record to reconstruct paleoseawater Mg/Ca, the variation in Mg/Ca among calcites of a given age can only be corrected by using biota-specific partition power functions and suggests caution when attempting to construct a single Mg/Ca time-series from a variety of calcite phases. Further empirical study is needed to assess whether this extends to other elemental ratios in calcite (e.g. Sr/Ca, Steuber and Veizer, 2002).

Dickson (2004) published a curve for Phanerozoic seawater Mg/Ca derived from crinoidal skeletal material in which only those specimens with well-preserved stereom microstructure were analyzed. To calculate Mg/Ca_{SW} from Mg/Ca_C, a fixed D_{Mg} of

0.03182 (derived from a single modern echinoid) was employed for all fossil echinoderm material. In his paper, Dickson states that this method was used because it was the most accurate method at the time to describe the relationship between Mg/Ca_{SW} and Mg/Ca_{C}. It was noted that a future calibration might change the interpretation of paleoseawater Mg/Ca from the echinoderm Mg/Ca data. Applying the partition power function for echinoid plate calcite from Ries (2004) to this fossil echinoderm dataset yields a secular trend in seawater Mg/Ca (Figure 3-5) that is on average 0.5 mol/mol lower than that reported by Dickson (2004). This represents ~15% of the total range of Phanerozoic Mg/Ca variation proposed by most authors (e.g., Hardie, 1996; Lowenstein et al., 2001).

The effectiveness of using partition power functions over partition coefficients can also be illustrated by reconstructing past seawater Mg/Ca from published data on the Mg-contents of marine cements (Figure 3-6). As stated above, the two partition power functions for marine cement likely represent end-member scenarios. From these, a range of Mg/Ca_{sw} can be calculated from measured marine cement Mg/Ca. Interestingly, the cement data suggest that pre-Cenozoic marine cements had Mg/Ca ratios no higher than ~1, and only began to rise to modern values (~5) during the Mid-Mesozoic. This is at odds with previously published data from both modeling studies and the geochemistry of fluid inclusions, which all suggest a Late Paleozoic to Early Mesozoic high (>3 mol/mol) in seawater Mg/Ca (Demicco et al., 2005; Hardie, 1996; Kovalevich et al., 1998; Lowenstein et al., 2001).

3.8 Conclusions

Partition power functions for Mg incorporation into calcite extend the predictive power of partition coefficient theory by recognizing and characterizing the variation in Mg partition coefficients with changes in seawater Mg/Ca.

By applying these power functions to suggested models of secular variation in Mg/Ca_{sw}, we can estimate the secular variation in the Mg/Ca of various calcite phases. This leads to the understanding that there is a much wider range in the Mg/Ca of calcite phases during aragonite seas than during calcite seas. In other words, during a calcite sea, biotic and abiotic calcite have about the same Mg/Ca. During aragonite seas, some taxa steadfastly produce low-Mg calcite (e.g., brachiopods), while the Mg content of other changes in tune with seawater Mg/Ca (e.g., the echinoderms). Thus, the key to identifying alternation between calcite and aragonite seas is not identifying calcite seas (in reality this is the null hypothesis as diagenetic alteration tends to result in low-Mg calcite), but rather in identifying phases with higher-Mg contents. From the functions presented here, crab carapace, serpulid worm tube, shrimp carapace and echinoid plates seem suited for this purpose. As echinoid plates (and likely all echinoderm plates) are the most abundant of these in the fossil record they could be considered ideal (Dickson, 2002).

The general low-Mg character of all carbonates precipitated from a calcite sea also implies a reduced mineralogical drive for diagenesis. This would result in a fundamentally different diagenetic style for shelfal carbonates based on the reduction in the volume of metastable carbonate minerals.

The starting material for meteoric diagenesis today is a mixture of low-Mg calcite, high-Mg calcite and aragonite, which has formed both as primary precipitates and during early diagenesis. These materials have characteristic and different elemental and isotopic compositions. For example, there is a 1‰ difference in the $\delta^{13}C$ of aragonite and high-Mg calcite marine cements (Gonzalez and Lohmann, 1985) and a much higher Sr/Ca aragonite than calcite (Milliman, 1974). During a calcite sea, the ingredients for diagenesis change to predominantly low-Mg calcites. During meteoric diagenesis of an aragonite sea carbonate parasequence, layers at the bottom are bathed in the diagenetic fluids that are sequentially dissolving the most soluble to the least soluble minerals above them. On the other hand, during alteration of a calcite sea parasequence, the geochemistry of the diagenetic fluid would be much more homogeneous. There will still likely be differences based upon such factors as the enhanced solubility of small particles and biotic particles, as well as slight differences in Mg content.

3.9 Acknowledgements

This paper has benefited greatly from the thoughtful insight and kind encouragement of Tom Baumiller, Joel Blum, George Kling, Matt Wasson, and Bruce Wilkinson.

3.10 Figures

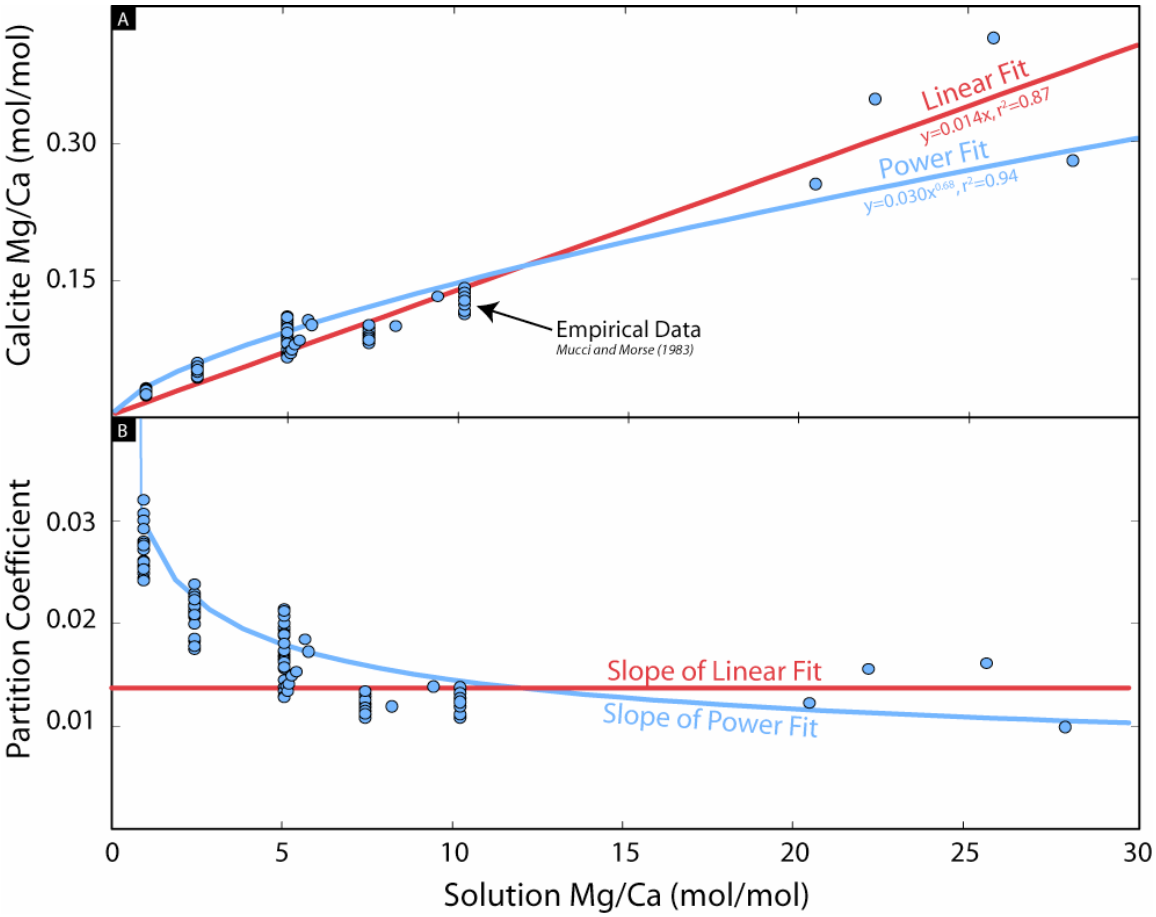

Figure 3-1: There is a power relationship between Solution Te/Me and Precipitate Te/Me. Here we use the data describing the partitioning of Mg into abiotic calcite (Mucci and Morse, 1983) to demonstrate this concept. A) A standard Mg-fractionation plot (i.e., Mg/Ca of the solution on the *x*-axis, calcite Mg/Ca on the *y*-axis). A linear fit to the data seems more appropriate visually, despite the higher R^2 value for the power function. B) When the partition coefficient is calculated (Calcite Mg/Ca divided by the Solution Mg/Ca) it becomes obvious how poorly the data are described by a linear function.

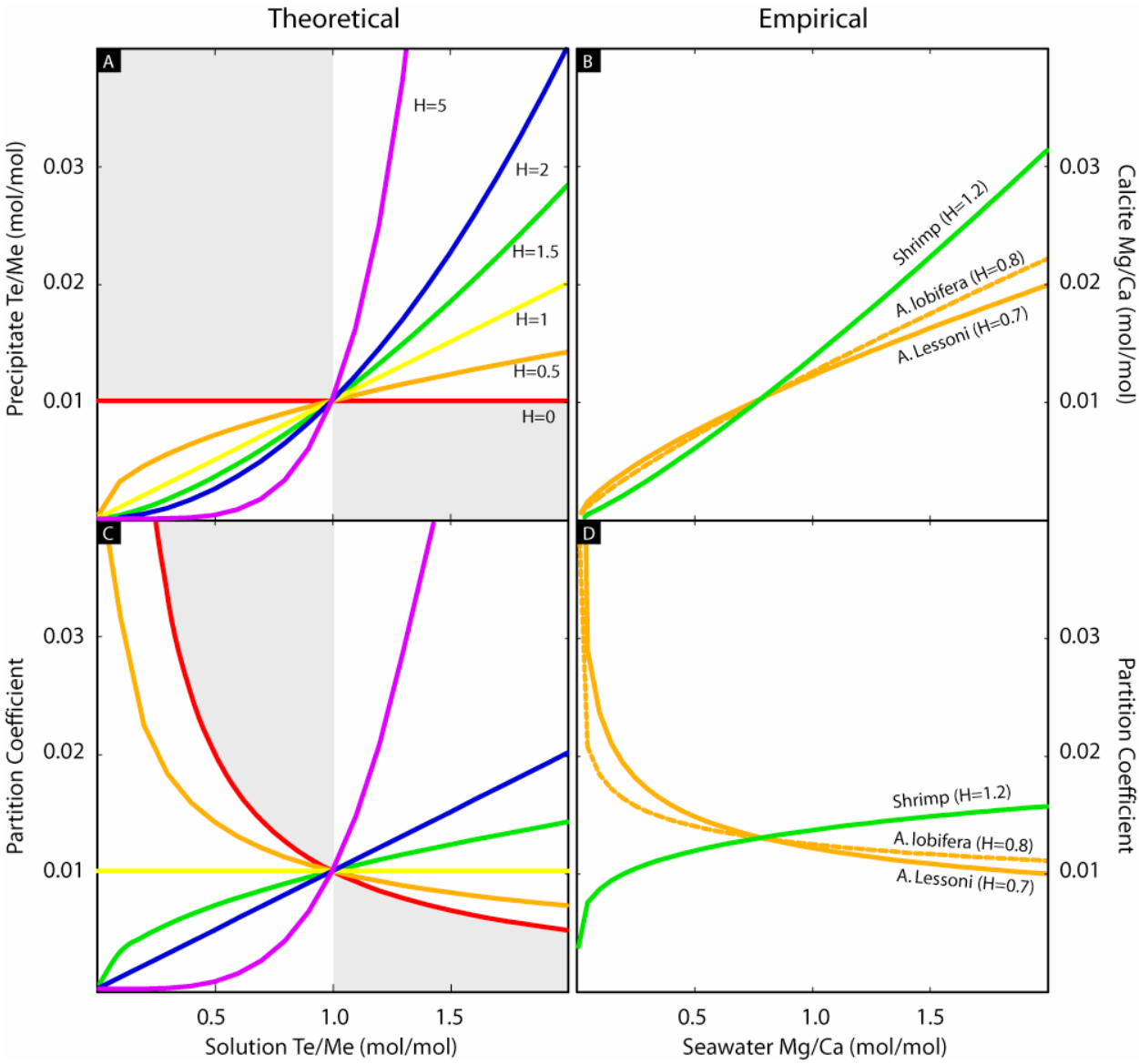

Figure 3-2: Modeled variation in the partition exponent (H), holding the partition factor (F) constant, where Precipitate Te/Me = F(Solution Te/Me)^H. A) Variation in H produces the six types of partition power function: $H=0$, $0<H<1$, $H=1$, $H>1$, $1<H<2$, $H=2$, $H>2$. At any H, Precipitate Te/Me can only exist in the quadrangles between (0,0) and (1,F) and between (1,F) and (∞,∞). All functions of a given F must pass through the point (1,F), the "partition nexus." B) Three partition power functions (for shrimp and two benthic foraminifera) with similar F cross near Solution Mg/Ca = 1. C) While there is little difference in (A) between the last three types, when partition coefficients are calculated it is clear that six domains exist (see Table 3-1 and Table 3-2 and see text for discussion). All six functions and their coefficients cross at the point (1, F). D) The partition coefficients associated with the functions in (B) display similar behavior.

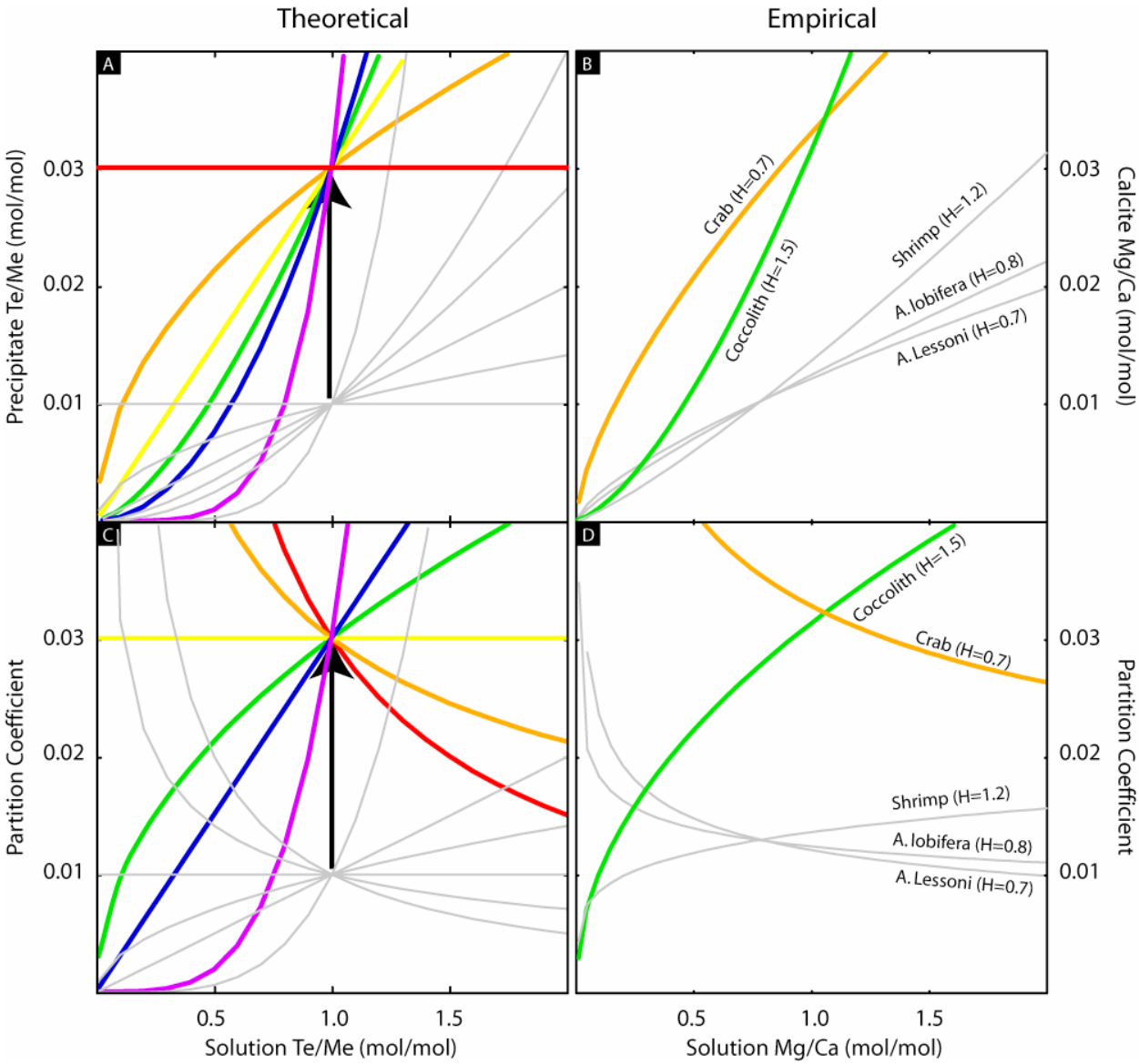

Figure 3-3: A) Increasing the partition factor (F) results in translation of the partition power functions in the positive direction along the y-axis, though they still stay "rooted" at the origin. B) Partition coefficients are translated similarly. Empirical partition power functions (C) and coefficients (D) display identical behavior. Functions with an $F \approx 0.32$ are offset in the positive direction from those with $F \approx 0.12$.

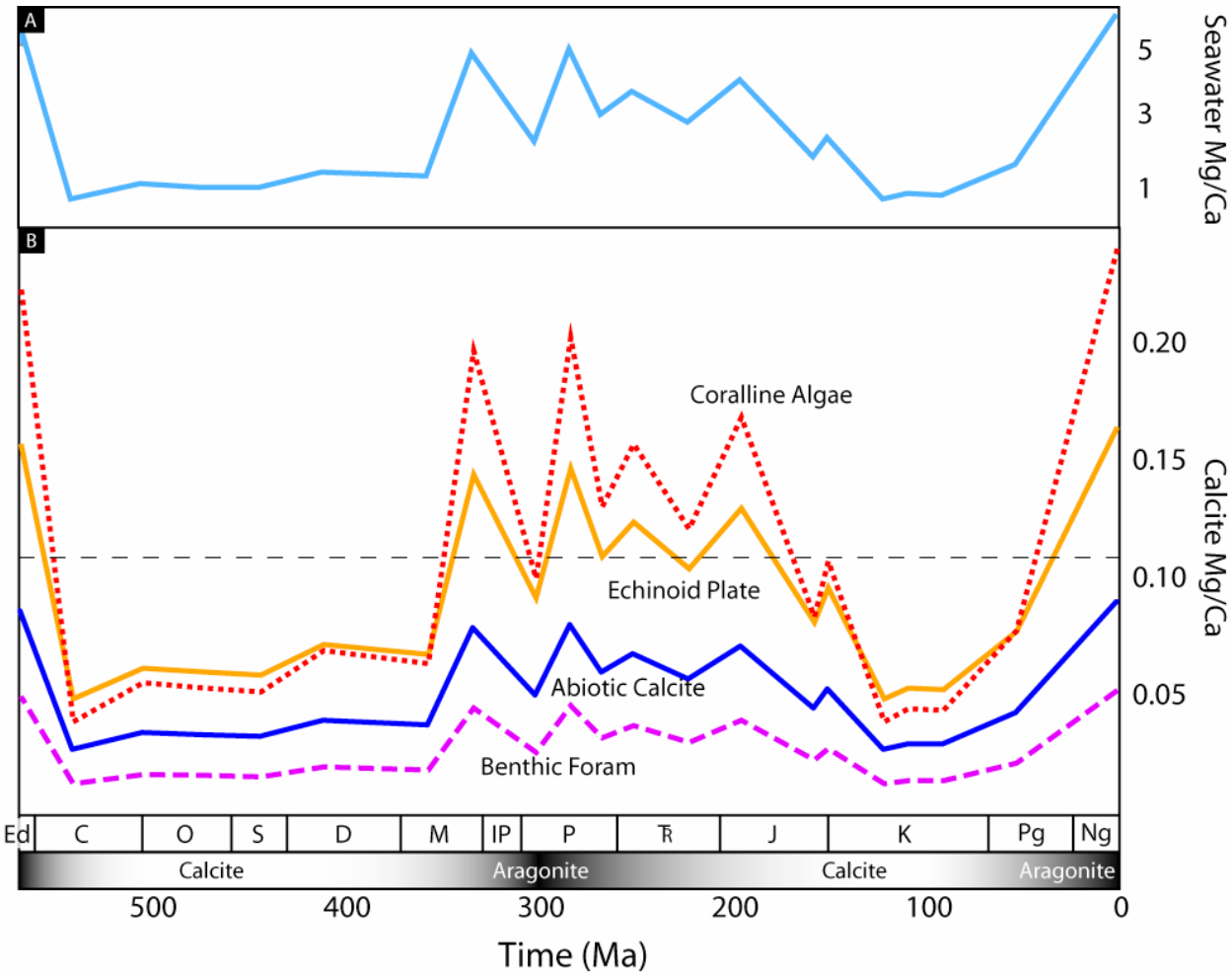

Figure 3-4: Primary calcite Mg/Ca of calcitic taxa throughout the Phanerozoic. A) Phanerozoic seawater Mg/Ca model from Hardie (1996). B) Variation in carbonate Mg/Ca calculated from data in (A) and the partition power functions from Table 3-1 for coralline red algae (Ries, 2006b), echinoid plate calcite (Ries, 2004), abiotic calcite cement (Füchtbauer and Hardie, 1980), and benthic foraminifer *A. lobifera* (Segev and Erez, 2006). Note that the range in calcite Mg/Ca among different carbonate phases is least during times of low seawater Mg/Ca (calcite seas) and greatest during high seawater Mg/Ca (aragonite seas).

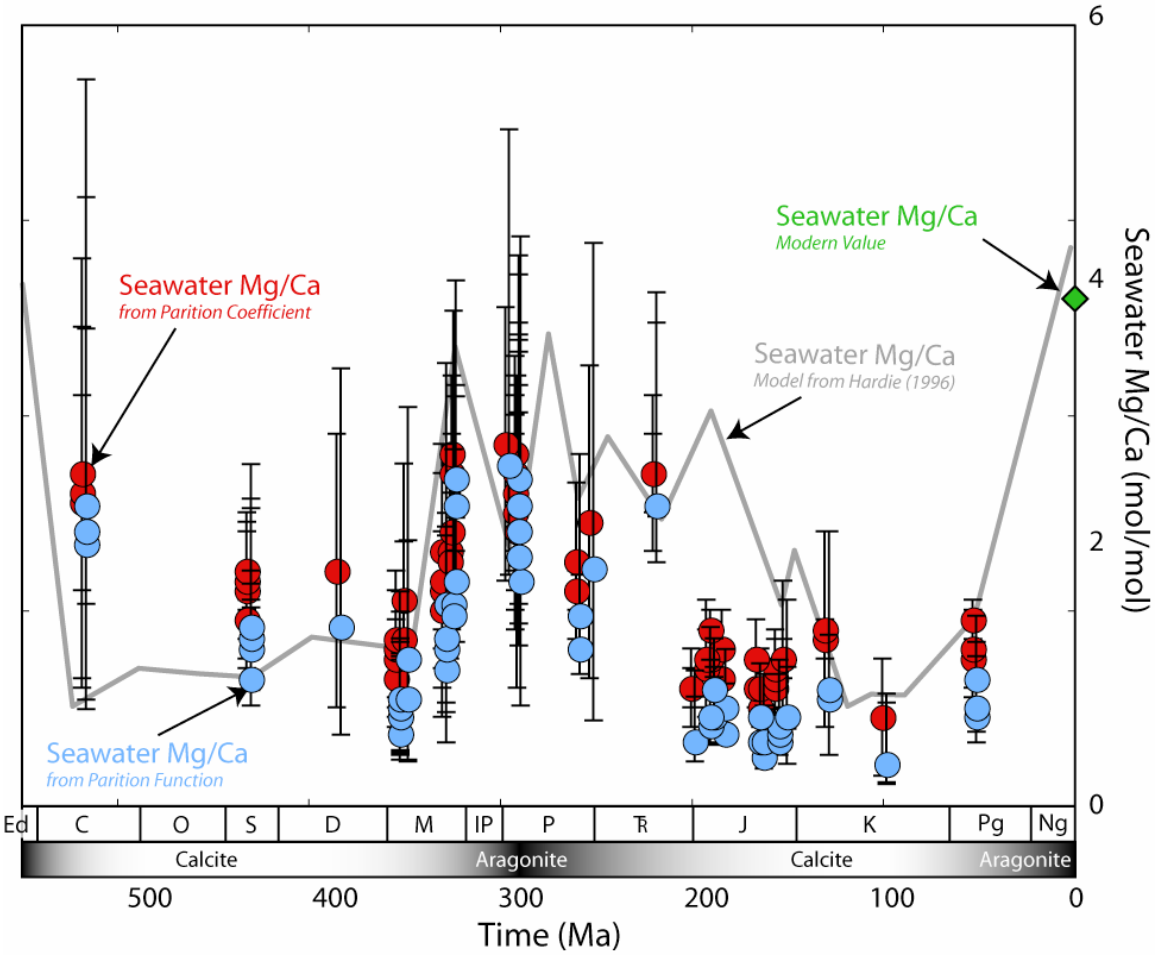

Figure 3-5: Difference between the calculated values of seawater Mg/Ca determined from data on echinoderm Mg/Ca (Dickson, 2004) employing a partition coefficient ($Mg/Ca_C = 0.3182(Mg/Ca_{SW})$) shown as red circles, and a partition power function ($Mg/Ca_C = 0.051(Mg/Ca_{SW})^{0.67}$) from Ries (2004) shown as blue circles. Differences vary between 1 and 50% (average 24%). Error bars represent 2 standard deviations. Blue data points have been shifted 2 My younger to prevent their error bars from overlapping with red data point error bars.

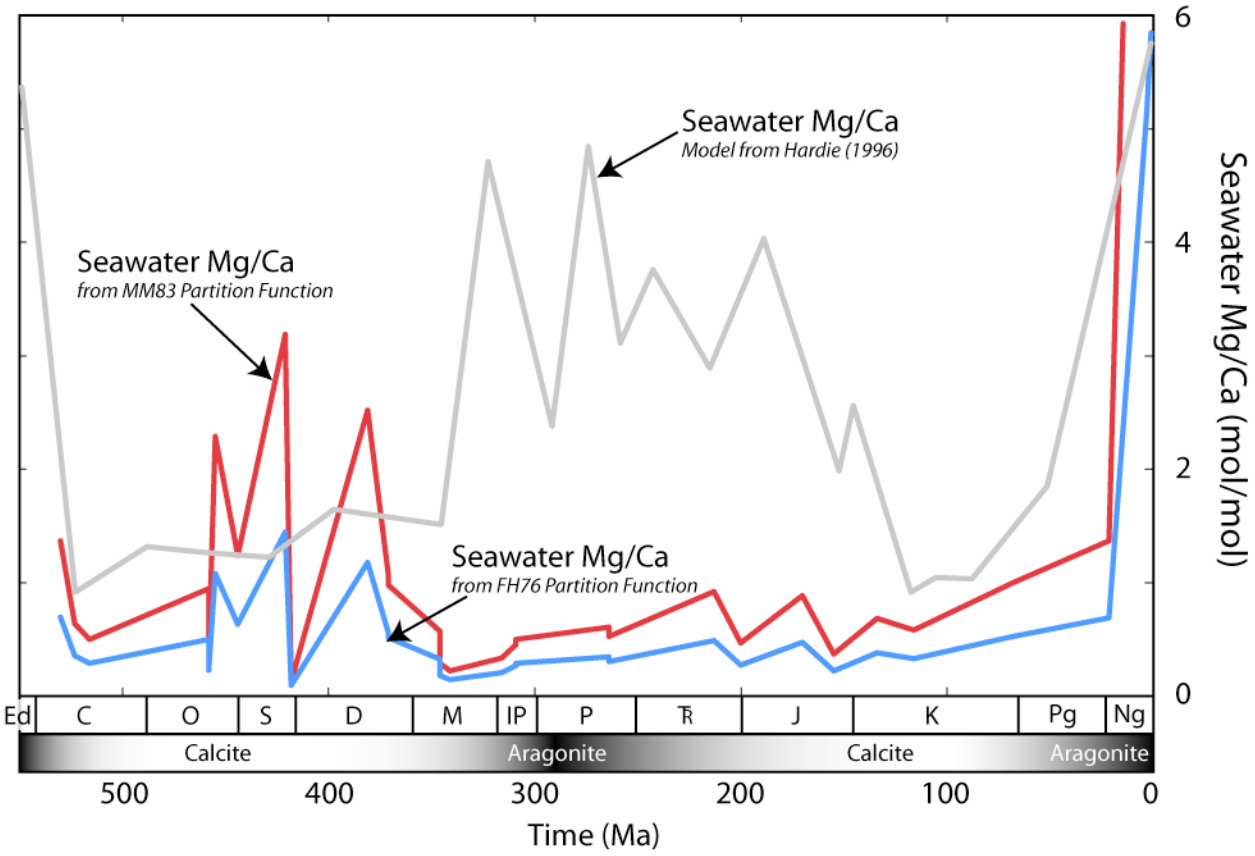

Figure 3-6: Phanerozoic seawater Mg/Ca calculated partition power functions from Fuchtbauer and Hardie (1976; red) and Mucci and Morse (1983; green) using published unaltered marine cement data (Benito et al., 2005; Carpenter et al., 1991; Cicero and Lohmann, 2001; Davies, 1977; Douthit, 1990; Frank and Lohmann, 1996; Hendry et al., 1996; Lohmann and Meyers, 1977; Marshall and Ashton, 1980; Mazzullo et al., 1990; Rahnis, 1995; Saller, 1986; Tobin and Bergstrom, 2002; Tobin and Walker, 1996; Tobin et al., 1997; Whittaker et al., 1994). The Phanerozoic seawater Mg/Ca curve of Hardie (1996) is included for reference (gray line).

Table 3-1: Regression parameters for calcite Mg/Ca vs. solution Mg/Ca. Linear (intercept = 0) and power regressions fit the data with approximately equal significance (p-values). Strength of correlation (R^2) is somewhat higher for linear regressions.

			Linear Function (y = *m*x)				Power Function (y = Fx^H)						
	N	**Temp (°C)**	**R^2**	**m**	**m_SE**	**m_p**	**R^2**	**F**	**F_SE**	**F_p**	**H**	**H_SE**	**H_p**
Abiotic Cement[1]	100	25	0.96	0.014	0.0003	1.1E-70	0.94	0.027	0.0127	3.3E-109	0.68	0.0172	6.6E-62
Abiotic Cement[2]	34	28	0.67	0.026	0.0008	2.3E-27	0.92	0.045	0.0297	1.4E-30	0.77	0.0411	1.0E-18
Echinoid Plate (*E. tribuloides*)[3]	19	25	0.98	0.030	0.0009	1.8E-17	0.95	0.051	0.0245	2.8E-20	0.67	0.0391	3.6E-12
Echinoid Spine (*E. tribuloides*)[3]	16	25	0.96	0.010	0.0005	9.8E-12	0.84	0.021	0.0361	1.0E-16	0.54	0.0627	5.9E-07
Crab Carapace (*P. gibbesi*)[3]	13	25	0.99	0.030	0.0010	8.4E-13	0.96	0.033	0.0318	5.4E-14	0.94	0.0575	4.6E-09
Shrimp (*P. pugio*)[3]	12	25	0.98	0.019	0.0009	3.0E-10	0.95	0.014	0.0433	1.1E-12	1.22	0.0859	6.0E-08
Serpulid Worm Tube (*H. crucigera*)[3]	13	25	0.97	0.029	0.0016	4.1E-10	0.79	0.020	0.1136	1.2E-08	1.24	0.1913	4.6E-05
Red Alga (*Neogoniolithon* sp.)[4]	18	25	1.00	0.043	0.0007	1.1E-21	0.96	0.042	0.0267	3.3E-19	1.02	0.0500	6.9E-13
Red Alga (*Amphiroa* sp.)[5]	9	25	0.99	0.037	0.0012	1.2E-09	0.98	0.038	0.0264	2.0E-10	1.00	0.0532	2.9E-07
Planktonic Foram (*G. sacculifer*)[6]	10	30	0.93	0.001	0.0001	1.6E-06	0.54	0.003	0.1032	6.8E-09	0.42	0.1357	***1.5E-02***
Benthic Foram (*A. lessonii*)[7]	38	24	0.93	0.007	0.0003	1.2E-22	0.89	0.012	0.0257	4.5E-41	0.70	0.0402	3.4E-19
Benthic Foram (*A. lobifera*)[7]	42	24	0.95	0.009	0.0003	3.9E-28	0.89	0.012	0.0281	6.7E-43	0.82	0.0467	1.7E-20
Coccolith (*P. carterae*)[8]	6	25	0.99	0.048	0.0018	1.4E-06	0.98	0.051	0.0281	1.3E-06	0.93	0.0656	1.4E-04
Coccolith (*O. neopolitana*)[8]	6	25	0.91	0.073	0.0101	7.9E-04	0.94	0.031	0.0824	5.3E-05	1.53	0.1860	1.2E-03
Coccolith (*C. neohelis*)[8]	6	25	0.73	0.010	0.0026	***1.4E-02***	0.00	0.032	0.1277	3.0E-04	-0.03	0.2884	**9.1E-01**

Bold values have p > 0.05, ***Bold Italicized*** values have 0.05 > p > 0.01
Source: 1, Mucci and Morse (1983); 2, Fuchtbauer and Hardie (1976; 3, Ries (2004); 4, Ries (2006); 5, Stanley et al. (2002); 6, Delaney et al. (1985); 7, Segev and Erez (2006); 8, Stanley et al. (2005)

Table 3-2: If a linear function best describes the relationship between calcite Mg/Ca and solution Mg/Ca, then the regression of D_{Mg} vs. solution Mg/Ca should be the line y = b, with m = 0 and $R^2 = 0$. On the other hand, if a power function best describes this relationship, then the regression of D_{Mg} vs. solution Mg/Ca should also be a power function that can be evaluated simply in terms of R^2 and p.

	Linear Function (y = *m*x + *b*)							**Power Function (y = Fx^H)**						
	R^2	**m**	**m_SE**	**m_p**	**b**	**b_SE**	**b_p**	**R^2**	**F**	**F_SE**	**F_p**	**H**	**H_SE**	**H_p**
Abiotic Cement[1]	0.43	0.022	0.001	1.8E-54	-0.001	0.000	8.6E-14	0.78	0.027	0.013	3.3E-109	-0.321	0.017	5.1E-34
Abiotic Cement[2]	0.14	0.045	0.005	4.9E-10	-0.001	0.001	***2.7E-02***	0.89	0.019	0.018	9.6E-41	6.719	0.426	1.2E-16
Echinoid Plate (*E. tribuloides*)[3]	0.69	0.048	0.003	7.7E-13	-0.003	0.001	1.1E-05	0.81	0.051	0.025	2.8E-20	-0.330	0.039	1.7E-07
Echinoid Spine (*E. tribuloides*)[3]	0.69	0.022	0.002	3.2E-09	-0.002	0.000	6.6E-05	0.79	0.021	0.036	1.0E-16	-0.461	0.063	3.7E-06
Crab Carapace (*P. gibbesi*)[3]	0.08	0.033	0.002	3.2E-08	-0.001	0.001	**3.3E-01**	0.09	0.033	0.032	5.4E-14	-0.061	0.057	**3.1E-01**
Shrimp (*P. pugio*)[3]	0.45	0.013	0.002	3.9E-05	0.001	0.001	***1.6E-02***	0.39	0.014	0.043	1.1E-12	0.218	0.086	***3.0E-02***
Serpulid Worm Tube (*H. crucigera*)[3]	0.00	0.029	0.007	1.0E-03	0.000	0.001	**9.6E-01**	0.12	0.020	0.114	1.2E-08	0.238	0.191	**2.4E-01**
Red Alga (*Neogoniolithon* sp.)[4]	0.00	0.044	0.003	2.1E-11	0.000	0.001	**8.4E-01**	0.01	0.042	0.027	3.3E-19	0.021	0.050	**6.8E-01**
Red Alga (*Amphiroa* sp.)[5]	0.03	0.039	0.003	1.7E-06	0.000	0.001	**6.5E-01**	0.00	0.038	0.026	2.0E-10	0.005	0.053	**9.3E-01**
Planktonic Foram (*G. sacculifer*)[6]	0.53	0.002	0.000	1.0E-04	0.000	0.000	***1.6E-02***	0.70	0.003	0.103	6.8E-09	-0.581	0.136	2.7E-03
Benthic Foram (*A. lessonii*)[7]	0.43	0.013	0.001	4.5E-17	-0.001	0.000	7.3E-06	0.60	0.012	0.026	4.5E-41	-0.295	0.040	1.2E-08
Benthic Foram (*A. lobifera*)[7]	0.22	0.013	0.001	4.7E-19	-0.001	0.000	2.0E-03	0.26	0.012	0.028	6.7E-43	-0.175	0.047	5.4E-04
Coccolith (*P. carterae*)[8]	0.09	0.052	0.005	5.4E-04	-0.001	0.002	**5.6E-01**	0.21	0.051	0.028	1.3E-06	-0.067	0.066	**3.6E-01**
Coccolith (*O. neopolitana*)[8]	0.83	0.015	0.010	**2.1E-01**	0.014	0.003	***1.2E-02***	0.67	0.031	0.082	5.3E-05	0.528	0.186	***4.7E-02***
Coccolith (*C. neohelis*)[8]	0.67	0.035	0.007	7.7E-03	-0.007	0.002	***4.7E-02***	0.76	0.032	0.128	3.0E-04	-1.033	0.288	***2.3E-02***

Bold values have p > 0.05, ***Bold Italicized*** values have 0.05 > p > 0.01
Source: 1, Mucci and Morse (1983); 2, Fuchtbauer and Hardie (1980); 3, Ries (2004); 4, Ries (2006); 5, Stanley et al. (2002); 6, Delaney et al. (1985); 7, Segev and Erez (2006); 8, Stanley et al. (2005)

Table 3-3: Distinguishing characteristics of the six types of the partition power function.

	Type 1	**Type 2**	**Type 3**	**Type 4**	**Type 5**	**Type 6**
H	0	0 < H < 1	1	1 < H < 2	2	2 < H
Mg/Ca_C	$F(Mg/Ca_{SW})^0$	$F(Mg/Ca_{SW})^{0<H<1}$	$F(Mg/Ca_{SW})^1$	$F(Mg/Ca_{SW})^{1<H<2}$	$F(Mg/Ca_{SW})^2$	$F(Mg/Ca_{SW})^{2<}$
Slope	Zero Slope	Logarithmic +	Constant +	Exponential +	Exponential +	Exponential +
D_{Mg}	$F(Mg/Ca_{SW})^{-1}$	$F(Mg/Ca_{SW})^{-1<H<0}$	$F(Mg/Ca_{SW})^0$	$F(Mg/Ca_{SW})^{0<H<1}$	$F(Mg/Ca_{SW})^1$	$F(Mg/Ca_{SW})^{1<}$
Slope	Exponential –	Exponential –	Zero Slope	Logarithmic +	Constant +	Exponential +

Table 3-4: Fit parameters and type for partition power functions for all empirical datasets evaluated in this study. While partition power functions of types 1, 5 and 6 are theoretically possible, none of the calcite phases examined here had these types.

	R^2	F	H	Type	Mg/Ca_{sw} for Dolomite
Abiotic Cement[1]	0.94	0.027	0.68	2	200
Abiotic Cement[2]	0.92	0.045	0.77	2	56
Echinoid Plate (*E. tribuloides*)[3]	0.95	0.051	0.67	2	85
Echinoid Spine (*E. tribuloides*)[3]	0.84	0.021	0.54	2	1300
Crab Carapace (*P. gibbesi*)[3]	0.96	0.033	0.94	3	38
Shrimp (*P. pugio*)[3]	0.95	0.014	1.22	4	33
Serpulid Worm Tube (*H. crucigera*)[3]	0.79	0.020	1.24	4	23
Red Alga (*Neogoniolithon* sp.)[4]	0.96	0.042	1.02	3	22
Red Alga (*Amphiroa* sp.)[5]	0.98	0.038	1.00	3	26
Planktonic Foram (*G. sacculifer*)[6]	0.54	0.003	0.42	2	10^6
Benthic Foram (*A. lessonii*)[7]	0.89	0.012	0.70	2	560
Benthic Foram (*A. lobifera*)[7]	0.89	0.012	0.82	2	220
Coccolith (*P. carterae*)[8]	0.98	0.051	0.93	3	25
Coccolith (*O. neopolitana*)[8]	0.94	0.031	1.53	4	10
Coccolith (*C. neohelis*)[8]	0.00	0.032	-0.03	N/A	N/A

Source: 1, Mucci and Morse (1983); 2, Fuchtbauer and Hardie (1976; 3, Ries (2004); 4, Ries (2006); 5, Stanley et al. (2002); 6, Delaney et al. (1985); 7, Segev and Erez (2006); 8, Stanley et al. (2005)

Chapter 4: Revised Mg/Ca Paleothermometry in Foraminifera

4.1 Abstract

It has become widely accepted that a power relation exists between the Mg/Ca ratio of a calcite and the Mg/Ca ratio of the fluid from which it precipitates. This can be coupled with the exponential relation describing the effect of temperature on the Mg/Ca ratio of calcite to produce a "Mg-T distribution function" which accurately estimates paleoenvironmental temperatures of calcite formation from calcite (usually foraminiferal) and fluid (usually seawater) Mg/Ca ratios. More precise paleotemperature calculations in turn allow for estimation of the $\delta^{18}O$ of ancient seawater, a proxy for the extent of continental glaciation. Applying this concept to published marine foraminiferal carbonate geochemical data suggests that either there has been less cooling since 50 Ma or more change in seawater Mg/Ca than have been recently estimated. The latter interpretation is favored as it reinforces results from studies on the geochemistry of fluid inclusions and echinoderms that argue for an increase in seawater Mg/Ca from ~2 at 50 Ma to 5.2 today.

4.2 Introduction

Within the last century, scientific inquiry into the chemistry of limestones has brought us to understand the importance of $CaCO_3$ in the global carbon cycle, which regulates the

Earth's climate. From these studies, various elemental and isotopic tracers have been developed as proxies of ancient environmental parameters. The most important of these is the $\delta^{18}O$ paleothermometer (Epstein et al., 1951; Kim and O'Neil, 1997; Urey, 1947), which describes the relation between the oxygen isotopic composition of calcite ("δ_C") and that of the water ("δ_W") from which the calcite formed as a function of temperature. Unfortunately, while the geologic record offers abundant marine carbonate for measuring δ_C, without an independent knowledge of δ_W, these data provide ambiguous temperature estimates. Because continental glaciation is a dominant control on Cenozoic δ_W, the oxygen isotopic composition of seawater can be expected to change greatly during global climate transitions between icehouse and greenhouse modes.

If, however, another paleothermometer can be developed that is independent of the ice volume effect, it could be coupled with the $\delta^{18}O$ paleothermometer to uniquely estimate δ_W and in turn the temporal record of continental glaciation, the dominant feature of the Cenozoic climate. The Mg/Ca ratio of marine calcite has been suggested as just such a paleothermometer. Mg/Ca paleothermometry in calcite is based on the exponential relation between the Mg/Ca of calcite and its temperature of formation (Nürnberg et al., 1996; Rosenthal et al., 1997). However just as the $\delta^{18}O$-paleothermometer requires knowledge of δ_W, the Mg-paleothermometer requires knowledge of the seawater Mg/Ca. Although initially the Mg/Ca paleothermometer was developed to investigate the Pleistocene when changes from the modern oceanic Mg/Ca would likely have been negligible, the utility of the Mg-paleothermometer over longer time intervals requires knowledge of possible secular variations in seawater Mg/Ca (cf. Billups and Schrag, 2002, 2003; Lear et al., 2000; Tripati et al., 2003).

The effects of change in seawater $\delta^{18}O$ and Mg/Ca on calculated paleotemperature can be investigated simultaneously by describing Mg incorporation into calcite both as a function of the Mg/Ca of seawater and as a function of temperature (Ries, 2004, 2006b). Here we expand on previous studies by clarifying key concepts necessary to calculate paleocean temperature, Mg/Ca, and δ_W from the trace element and isotopic compositions of marine calcite.

4.3 Mg Partitioning in Calcite

It is common to use a partition coefficient to describe the relationship between the elemental ratios of a mineral and the fluid from which it was precipitated (McIntire, 1963; Morse and Bender, 1990). As was discussed in Chapter 3, the partition coefficient for Mg into calcite has been shown to decrease with increasing fluid Mg/Ca for a number of biotic and abiotic calcite phases (Delaney et al., 1985; Fuchtbauer and Hardie, 1976; Mucci and Morse, 1983; Ries, 2004, 2006a; Segev and Erez, 2006; Stanley et al., 2002, 2005). As this relationship is probably a sorption phenomenon, it is more appropriate to use a power function to describe the equilibrium relation between fluid and calcite Mg/Ca.

$$Mg/Ca_C = F(Mg/Ca_{SW})^H \quad (4\text{-}1)$$

The incorporation of Mg into calcite as a function of temperature has been formalized as an exponential function (e.g. Lear et al., 2002; Nürnberg et al., 1996; Rosenthal et al., 1997):

$$Mg/Ca_C = Be^{AT} \quad (4\text{-}2)$$

Where T is temperature in °C and A and B are empirically derived constants.

Two attempts to combine equations for the effects of Mg/Ca_{sw} and temperature on Mg/Ca_C have been reported in the literature. Lear et al. (2000; 2002) combined Mg/Ca and temperature functions by using an equation of the form:

$$Mg/Ca_C = \left(\frac{Mg/Ca_{SW-Ancient}}{Mg/Ca_{SW-Modern}}\right) \times Be^{AT} = 0.00019\left(Mg/Ca_{SW-Ancient}\right)e^{0.114T} \qquad (4\text{-}3)$$

Where *B* and *A* are empirical constants, and T is bottom water temperature (in °C). This suggests that for foraminifera the Mg partition power function is:

$$Mg/Ca_C = \frac{Mg/Ca_{SW-Ancient}}{Mg/Ca_{SW-Modern}} \qquad (4\text{-}4)$$

In the light of the previous discussion of partition power functions, it is unclear on what basis they assume that *F* is the reciprocal of the present Mg/Ca_{sw}. *F* is an empirical constant and has no mathematical or phenomenological relation to the Mg/Ca_{sw}. Or why $H = 1$ which, while appropriate in some cases (e.g., the red algae), does not hold for any reported foraminifera. Correctly, Ries (2006a) solved an empirically derived partition power function and an empirically derived temperature partition power function to generate a unified Mg–T partition power function for the red alga *Neogoniolithon*:

$$Mg/Ca_C = 0.0134\left(Mg/Ca_{SW}\right)^{1.01} e^{0.0457T} \qquad (4\text{-}5)$$

This equation accommodates the condition that at $Mg/Ca_{sw} = 0$, $Mg/Ca_C = 0$, which would not be met if the Mg and T partition power functions were simply added.

4.4 Revised Mg/Ca Paleothermometer

Several recent papers (e.g. Billups and Schrag, 2002; Lear et al., 2000; Lear et al., 2004; Tripati et al., 2003) have attempted to use Mg/Ca of foraminiferal calcite as a paleothermometer of Cenozoic oceans independent of the ice-volume effect that is

incumbent upon the $\delta^{18}O$ paleothermometer. These attempts however all incorporate some variant of Equation (4-3), which imperfectly describes the dependence of D_{Mg} on Mg/Ca_{sw}. Given the relations described above, it is appropriate to characterize the effect of Mg/Ca_{sw} on foraminiferal Mg/Ca_C using the approach of Ries (2006b), based on the dataset of Lear (2000), and then evaluate any differences.

Estimates by Hardie (1996) and Wilkinson and Algeo (1989) provide two end-member models describing the change in oceanic Mg/Ca over this time span. The former varies from ~1.4 at 50 Ma to 5.2 today, while the latter from ~3.5 at 50 Ma (Figure 4-1A) to 5.2 today. Mg partition power functions exist for both benthic (*Amphistegina* sp.) and planktonic (*Globigerinoides sacculifer*) foraminifera. By combining these with the estimates of oceanic Mg/Ca, secular variation in foraminiferal calcite Mg/Ca for the past 50 My can be estimated (Figure 4-1B).

Both trends in foraminiferal calcite Mg/Ca are suggested to increase from 50 Ma to present, while the data of Lear et al. (2000) show a decrease over the same interval. If foraminiferal calcite Mg/Ca were only affected by seawater Mg/Ca, then the data of Lear et al. (2000) should also have a positive slope. To resolve this discrepancy, Lear et al. (2000) argued that this decrease documents cooling of ocean bottom waters of ~12°C between 50 Ma to present. However, as shown above, their method rather imperfectly describes the effect of changing Mg/Ca_{SW} on Mg/Ca_C. An alternative is to employ a Mg-T partition power function in the manner of Ries (2004).

The benthic foraminifera used in the analysis of Lear et al. (2000) are, however, much lower in Mg contents (1-5 mmol/mol) than the benthic foraminifera *Amphisteginae* sp. for which Mg/Ca partition power functions have been developed (50-60 mmol/mol).

Benthic foraminiferal calcite Mg/Ca (normalized to *O. umbonatus*) is similar to that of the planktonic foraminifer reported in Delaney et al. (1985). If it can be assumed that *O. umbonatus* and *G. sacculifer* have similar partition power functions, we can then use *G. sacculifer*'s partition power function with a more recent temperature partition power function for *O. umbonatus* (Lear et al., 2002) to produce a Mg/Ca_{sw}–T partition power function for low-Mg calcite benthic foraminifera:

$$Mg/Ca_C = 0.0005(Mg/Ca_{SW})^{0.42} e^{0.114T} \quad (4\text{-}6)$$

Using Equations (4-3) and (4-6), Mg-paleotemperatures are calculated (Figure 4-2A) for the past 50 My using end-member models of Mg/Ca_{sw} (Hardie, 1996; Wilkinson and Algeo, 1989). The four models suggest that bottom water temperatures have cooled by at least 10°C since 50 Ma. This cooling seems to be divided into four phases: steep cooling from 50 Ma to 33 Ma (interrupted by a 2 My warming pulse at 39 Ma), gradual cooling from 33 to 11 Ma, slight warming from 11 to 7 Ma, and steep cooling from 7 Ma to the present.

In their original treatment, Lear et al. (2000) preferred the Mg/Ca_{sw} model of Wilkinson and Algeo (1989) over that of Hardie (1996) because the Hardie model gave Mg-paleotemperatures that were too high to be considered reasonable (e.g., Figure 4-2A). The difference between the two Mg/Ca_{sw} models is significant at all times from 50 Ma (~8.2°C) to ~2 Ma (~1°C) using the method of Lear et al. (2000). When using the Mg-T partition power function suggested here, Mg-temperatures do not begin to diverge greatly until 6 Ma, and only differ by about ~3.5°C at 50 Ma. From this it seems that the Mg-T partition power function used here reduces the differences between the two models of

secular Mg/Ca_{sw} on Mg-temperatures, and makes it more difficult to discount the Hardie model of Mg/Ca_{sw} (Billups and Schrag, 2002; Lear et al., 2000; Tripati et al., 2003).

By calculating Mg-paleotemperatures using the refined method described above, the impact of secular variation in Mg/Ca_{sw} on the final temperature is reduced. In other words, the final Mg-paleotemperature is less sensitive to which model of Mg/Ca_{sw} is employed. This can be clearly seen by comparing the range separating Mg-paleotemperatures trends calculated using the method of Lear et al. (2000) and that using a partition power function in Figure 4-2. This reduced range likely brackets the real trend in the variation of Cenozoic bottom water temperatures. The trend resulting from Wilkinson and Algeo's estimates produces lower temperatures and thus would suggest less overall cooling over the last 50 My. (This is also the Mg/Ca_{sw} model employed by Lear et al. (2000) and all Mg-paleothermometry studies since.) On the other hand, the Mg-paleotemperature trend calculated from the Hardie model is would imply greater bottom water cooling over the last 50 My. And indeed the Hardie model might be considered more realistic as it treats Mg cycling in the oceans as dominated by the ratio of riverine flux to brine flux from mid-ocean ridge hydrothermal alteration.

4.5 Paleoseawater $\delta^{18}O$

The paleotemperature trends (Figure 4-2A) can be transformed into δ_W trends (Figure 4-2B) employing Cenozoic benthic foram δ_C data (Zachos et al., 2001) and the $\delta^{18}O$-paleotemperature equation (Shackleton, 1974):

$$\delta_W = \delta_C + \delta_W^* - \left(\frac{16.9 - T}{4}\right) \qquad (4\text{-}7)$$

Where δ_W* is the difference (–0.27‰, Hut, 1987) between δ_W in SMOW and δ_C in PDB reference scales. According to this equation if δ_C is constant, an increase in temperature will lead to an increase in δ_W. The differences apparent in the Mg-temperature trends carry over into δ_W. Again, the trends provided by the two models of Mg/Ca_{sw} are widely separated (up to 2.1‰) using method of Lear et al. (2000), yet considerably closer using the method suggested here (0.9‰). In nature, there exist certain constraints on δ_W (Dwyer et al., 1995) that suggest that if all glacial ice on continents were to melt, $\delta_W \approx -1$ and if there were a volume of continental ice equivalent to that at the height of the Pleistocene, $\delta_W \approx +1$. When measured against this scale, δ_W from the Lear method (incorporating the Hardie model) would require substantial glaciation in the late Eocene, Oligocene glaciers of similar magnitude to the Pleistocene, and gradually decreasing, but continuously abundant, glacial ice through the present. This is not in accord with literature estimates of at most ephemeral glaciers during the late Eocene, an early Oligocene with at most a fully glaciated Antarctica, and a Miocene-Pleistocene of increasing glacial ice. The other three trends, however, match this record.

The four phases of Cenozoic temperature evolution described above apply to the δ_W record, with cooling in general associated with more positive δ_W. As temperature decreased from 50 to 33 Ma, δ_W increased by about +1‰, interrupted by a 0.5‰ positive excursion at 39 Ma when temperatures increased by several degrees. This Eocene cooling trend is generally consistent with recent estimates based on the $\delta^{18}O$ of bivalve carbonate (Ivany et al. 2008). The δ_W record shows a return to approximately late Eocene δ_W values by 25 Ma while temperatures remained almost constant over this interval. From 25 to 7

Ma, δ_W increased gradually by about 0.4‰. Then δ_W sharply increased by about 0.8‰ from 7 Ma to the present.

In Figure 4-2, three excursions in the δ_W record occur at 39 Ma, 30 Ma, 12 Ma, and from 7 to 4 Ma are associated with excursions in the Mg-temperature record that are not mimicked in the δ_C record. The spike in temperatures at 39 Ma, which lead to a positive excursion in δ_W by our calculations could represent the MECO (Bohaty et al., 2003). However, this event is generally assumed to have lasted from 43 to 41 Ma, where no temperature spike is present in the Mg/Ca data of Lear et al. (2000). The low-resolution nature of the Mg/Ca dataset might have precluded the recognition of the MECO. Conversely, the ages for the Mg/Ca data may be slightly incorrect, thus placing the MECO between 40 and 38 Ma. The negative excursions (at 30 Ma, 12 Ma, and from 7 to 4 Ma) are associated with a drop in δ_W and thus would require a reduction in continental ice perhaps through reduced continental precipitation.

The effects of partition power functions on shorter time-scales are just as profound. One of the main points argued by Lear et al. (2000) was that ocean cooling was not responsible for the onset of Antarctic glaciation at the Eocene-Oligocene (E-O) boundary. Their high-resolution benthic foraminiferal Mg-paleotemperature record showed, if anything, slight warming from 34.5 to 32 Ma. In Figure 4-2A, the Mg-temperature trends calculated by our method and the two end-member models of Mg/Ca_{sw} differ consistently by 3°C. This difference translates into a δ_W difference of 0.75‰, well within the total range of Cenozoic δ_W of 3.3‰ between full Pleistocene glaciation and complete absence of glacial ice. If these differences had been calculated with the Lear formula, the

temperature difference would have been 7.1°C, corresponding to a δ_W difference of 1.8‰.

In contrast to Lear et al. (2000), we do not fit a linear trend to these temperature data. A more nuanced trend is thus presented that shows cooling across the E-O boundary of about 1°C followed by warming of a little more than 1°C when the benthic δ_C record is at the steepest part of its positive excursion. How could deep sea warming be correlated with initiation of Antarctic glaciation? It is possible that the slightly warmer Oligocene allowed for a stronger hydrologic cycle that was able to move more water from ocean to continent. The more positive δ_W trend (calculated from the Hardie Model) would also be in closer agreement with recent suggestions of the presence of ephemeral glaciations in late Eocene (Eldrett et al., 2007; Moran et al., 2006; Tripati et al., 2005) as the more negative model sits at –1‰ (i.e., ice-free) for this interval..

4.6 Figures

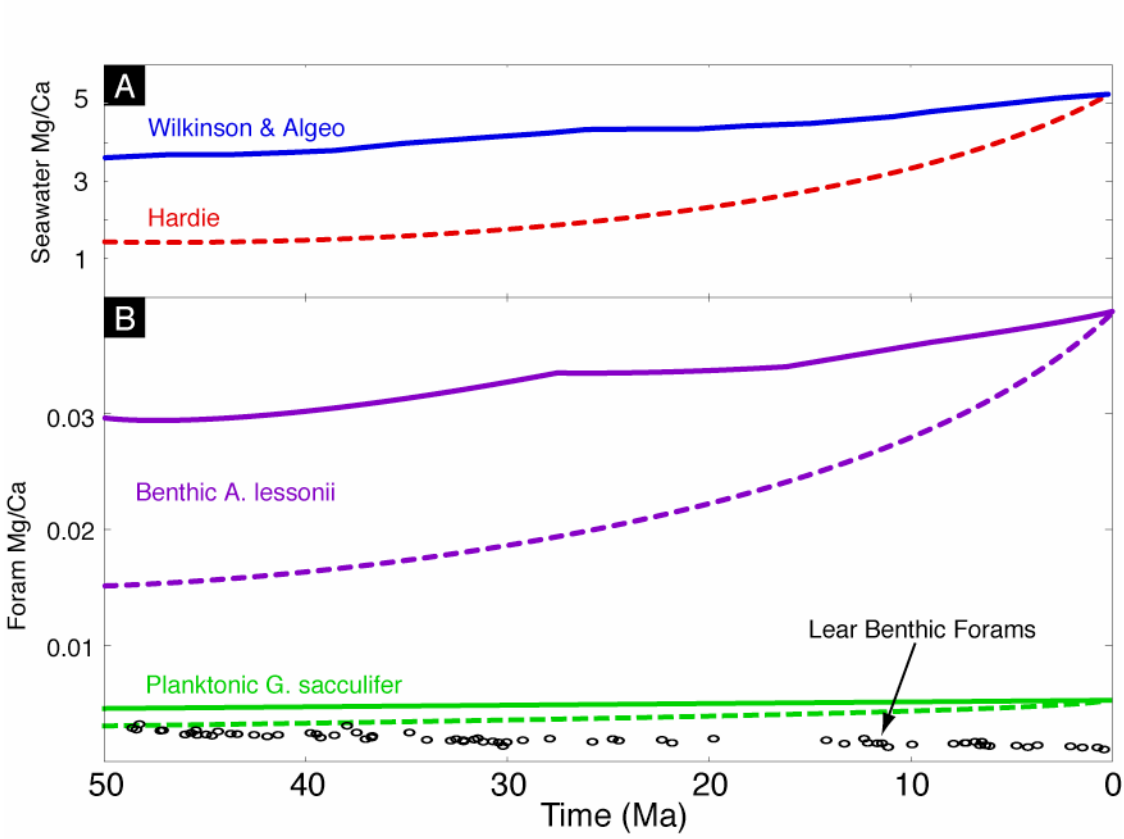

Figure 4-1: A) Models of global oceanic Mg/Ca (50 Ma to present) as suggested by Wilkinson and Algeo (1989; solid blue) and Hardie (1996; dashed red). B) Change in foraminiferal calcite Mg/Ca in response to change in oceanic Mg/Ca over the last 50 My from (A). Values from Hardie's model would produce the dashed lines, Wilkinson and Algeo's model the solid lines. Benthic foram Mg/Ca, normalized to *O. umbonatus*, of Lear et al. (2000) are plotted as open circles.

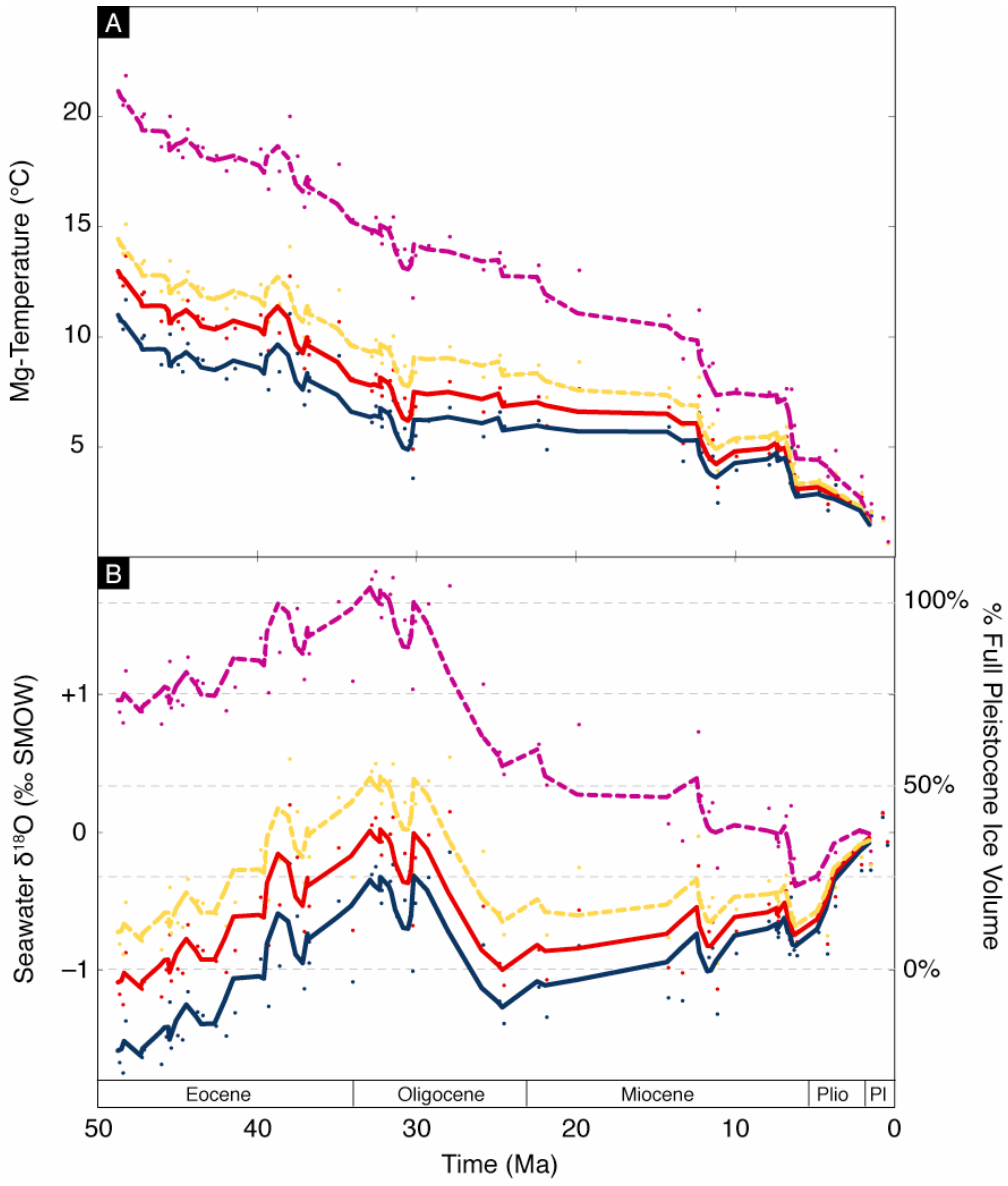

Figure 4-2: A) Cenozoic bottom water temperature trends derived from benthic foram calcite Mg/Ca, normalized to *O. umbonatus* (2000). Dashed trends use the Mg/Ca_{sw} model of Hardie (1996), solid trends use Wilkinson and Algeo (1989). Purple and Red trends are calculated using the Mg-T partition power function of Lear (2002); at 50 Ma they differ by ~7°C. The yellow and blue trends use the Mg-T partition power function advocated in this study and only differ by ~3.5°C at 50 Ma. B) Cenozoic δ_W calculated from Mg-temperature trends from (A), benthic foram $\delta^{18}O$ (Zachos et al., 2001, calibrated to "equilibrium"), and a benthic foram $\delta^{18}O$-paleothermometer (Shackleton, 1974). Again, there exists a wide difference between the δ_W estimates of the purple-red trends (~2‰ at 50 Ma) versus the yellow and blue trends (~1‰ @ 50 Ma). Dwyer et al. (1995) provided a model of how δ_W related to extent of continental glaciation. This is represented as a percentage of full Pleistocene ice volume. (Mg-temperature and δ_W trends represent three-point moving averages.)

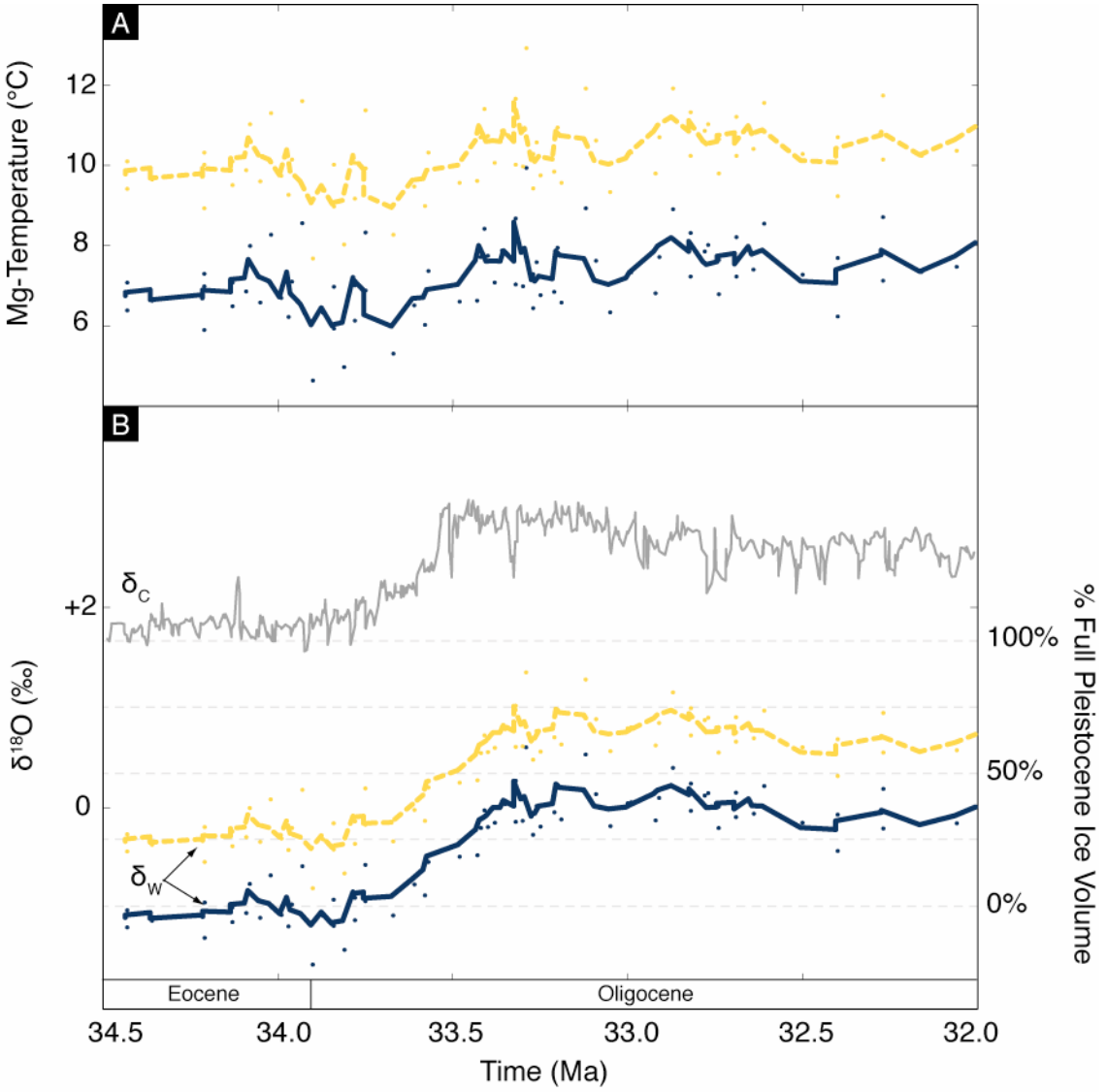

Figure 4-3: A) Paleotemperature trends from Mg/Ca of benthic foraminifera (normalized to *O. umbonatus*) across the Eocene-Oligocene boundary. The *blue curve* was calculated from the same Mg/Ca_{sw} model, but with updated Mg-T partition power function (Delaney et al., 1985; Lear et al., 2002). The *yellow dashed curve* was calculated similarly except with the Mg/Ca_{sw} model of Hardie (1996). B) δ_C and δ_W across the Eocene-Oligocene boundary. The yellow and blue curves were calculated with the gray δ_C curve (Zachos et al., 2001) and the same-color Mg-temperature trends in (A). All trends represent three-point moving averages.

Chapter 5: Accurate Mg/Ca Paleothermometry at Cenozoic Time-Scales

5.1 Abstract

The $\delta^{18}O$ of foraminiferal calcite has long been the standard proxy of ancient ocean temperatures. However, it is confounded by the fact that foraminiferal calcite $\delta^{18}O$, in addition to temperature, is also a function of the $\delta^{18}O$ of the ambient seawater. Therefore, it has become common recently to use the Mg/Ca ratio of foraminiferal calcite as a paleothermometer independent of ice volume. Paleotemperatures calculated thus can be applied to the $\delta^{18}O$-paleothermometer to calculate the $\delta^{18}O$ of ancient seawater. Unfortunately, in a similar way to the $\delta^{18}O$ paleothermometer, foraminiferal calcite Mg/Ca is a function of ambient seawater Mg/Ca. Attempts to date to employ the Mg/Ca paleothermometer to calculate paleotemperatures and paleoseawater $\delta^{18}O$ have been hampered by an inaccurate treatment of the effect of seawater Mg/Ca on calcite Mg/Ca. By using a power function, the Mg/Ca paleothermometer can be more accurately applied to deep geologic time (i.e., ages older than 5 Ma). While previous methods assumed little to no change in seawater Mg/Ca over the last 60 My to produce realistic paleocean temperatures and $\delta^{18}O$, the updated methodology presented here is compatible with the prevailing opinion that seawater Mg/Ca has changed dramatically since 60 Ma.

5.2 Introduction

Over the last 60 million years, conditions at the surface of the earth have undergone dramatic changes as climate has evolved from the greenhouse of the mid-Cretaceous to the Plio-Pleistocene icehouse. This global change has manifested itself in a number of ways including: a cooling of the atmosphere and oceans; a reduction in atmospheric pCO_2; lowering of sealevel; and an increase in continental ice volume. Understanding the history of this global climate transition is necessary if we are to accurately predict long-term effects of anthropogenic perturbations to the carbon cycle.

One of the most fruitful methods for characterizing these phenomena has been to use the oxygen isotopic composition of calcite as a proxy of past ocean temperatures. The $\delta^{18}O$ of calcite precipitated in the marine environment depends on three factors, one physical (temperature), one chemical (solution $\delta^{18}O$) and one biological (presence or absence of biotic vital effects). When calibrated to specific biotic or abiotic calcite phases, marine calcite can be used as a paleothermometer when seawater $\delta^{18}O$ is known or, if temperature can be constrained, it can document changes in seawater $\delta^{18}O$ which is influenced by continental ice volume and the $\delta^{18}O$ of that ice.

Because of the confounding nature of this glacial influence on $\delta^{18}O$ paleothermometry, it has been suggested that calcite Mg/Ca can be used as a geochemical proxy of paleotemperature as it would be independent of the ice effect (Lea et al., 1999; Lear et al., 2002; Nürnberg et al., 1996; Rosenthal et al., 1997). By employing a combined approach that utilizes Mg-paleotemperatures and marine calcite $\delta^{18}O$ accurate estimates of paleoseawater $\delta^{18}O$ can be obtained.

For this holistic approach of using both the elemental and isotopic chemistry of marine calcite to succeed in calculating paleocean $\delta^{18}O$, several factors must be constrained. First, accurate and precise measurement of calcite $\delta^{18}O$ and Mg/Ca is required: a condition easily accomplished with modern analytical instrumentation. Secondly, we must be reasonably sure that these represent primary calcite and not a diagenetic or secondary precipitate. This can be accomplished through a variety of petrographic and geochemical tests for diagenetic alteration. Third, a $\delta^{18}O$ paleothermometer must be known for the specific calcite phase, whether of biotic or abiotic origin. Numerous studies have provided empirical calibrations for numerous biotic and abiotic calcites (e.g. Kim and O'Neil, 1997; Shackleton, 1974). Fourth, the Mg/Ca paleothermometer must accurately account for the effects of temperature and seawater Mg/Ca on calcite Mg/Ca. Understanding the effect of solution Mg/Ca is fundamental to the application of the Mg/Ca paleothermometer as it directly affects how sensitive the resulting paleotemperature and seawater $\delta^{18}O$ estimates are to secular variation in seawater Mg/Ca.

While studies of the paired effect of temperature and solution $\delta^{18}O$ on calcite $\delta^{18}O$ have been published by numerous authors and for numerous biotic and abiotic calcite phases, only one such simultaneous investigation exists for calcite Mg/Ca (Fuchtbauer and Hardie, 1976; 1980). Therefore, even though Mg/Ca paleothermometry has been applied in numerous studies (Billups and Schrag, 2002, 2003; Lear et al., 2000; Tripati et al., 2003), it has been hampered by a poor calibration for the effect of solution Mg/Ca. This poor calibration has contributed to the prevailing opinion within the paleoceanographic community that seawater Mg/Ca has changed less than suggested by

modeling studies and data from other geochemical proxies (Demicco et al., 2005; Dickson, 2002; Hardie, 1996; Kovalevich et al., 1998; Stanley and Hardie, 1998).

This paper directly addresses this controversy surrounding the Mg/Ca paleothermometer by incorporating a more accurate calibration which accommodates changes in seawater Mg/Ca. The implications of this revision on estimates of paleoseawater Mg/Ca, temperature, and $\delta^{18}O$—and by proxy the history of plate tectonics, climate, and continental ice volume—over the last 60 million years are explored.

5.3 Methodology

5.3.1 Introduction

The dominant factors controlling the Mg/Ca of a calcite phase are the Mg/Ca of the solution from which it precipitates and the temperature of that solution. This can be summarized in the following relation:

$$Mg/Ca_{Calcite} = f\left(Mg/Ca, T\right)_{Solution} \tag{5-1}$$

The intricacies of biomineralization also affect the Mg/Ca of a biotic carbonate phase in a way peculiar to each taxonomic group. These "vital effects" are used by the organism to vary the chemistry of their biomaterial to meet their needs of strength, weight, permeability, etc. By characterizing Equation (5-1 for each biotic or abiotic calcite phase, it is only necessary to formulate an equation with coefficients for temperature and seawater chemistry.

Mg/Ca paleothermometry is a paleoceanographic tool for understanding past ocean temperatures. It's main application has been to study changes in ocean temperatures over the last million years because during this span of time it can reasonably be assumed that

seawater Mg/Ca was essentially the same as that of today. These studies have focused primarily on the Mg/Ca of skeletal calcite of foraminifers, as they are easy to identify and are relatively cosmopolitan, and there exists a long history of using this order for paleo-geochemical studies. However, to apply Mg/Ca paleothermometry on deep time scales (i.e. on time intervals greater than the residence times of Ca and Mg in the oceans), secular variation in seawater chemistry must be considered. Thus, a method is needed to quantify the combined effect of changing seawater temperature and Mg/Ca on the Mg/Ca of a foraminiferal test.

5.3.2 The Lear Method

To accommodate the paired effects changing seawater temperature and chemistry, Lear et al. (2000) suggested amending the temperature partition function for *C. floridanus* (Rosenthal et al., 1997):

$$Mg/Ca_{foram} = 0.00136 \times 10^{0.044T} \tag{5-2}$$

This is accomplished by multiplying Equation (5-2) first by a factor "*f*," a "species correction factor," which adjusted the function from the species against which it was originally calibrated (*C. floridanus*) to *O. umbonatus*, the species to which all data were normalized. To account for changing seawater Mg/Ca, they proposed multiplying the species-adjusted temperature partition function by the ratio of past-to-present seawater Mg/Ca:

$$Mg/Ca_{foram} = \left(\frac{Mg/Ca_{sw-Ancient}}{Mg/Ca_{sw-Present}} \right) \times \left(0.00136\, f \times 10^{0.044T} \right) \tag{5-3}$$

Formalizing the relationship between seawater and calcite Mg/Ca in this manner allows the equation to reduce to the simple temperature partition function when past and present seawater Mg/Ca are equal. This method, however, is only based on empirical data

describing the effect of temperature on shell Mg/Ca. Neither theoretical nor empirical reasoning substantiate Equation (5-3). While subsequent incarnations of this equation have updated the temperature partition function used in this method (Lear et al., 2004; Lear et al., 2002; Lear et al., 2003b), the portion of the equation handling Mg/Ca_{sw} has never been changed to reflect the power nature of the relationship between the Mg/Ca of seawater and calcite. In contrast, it has become the accepted method employed when "accounting" for changes in past Mg/Ca_{sw} (Billups and Schrag, 2002, 2003; Dutton et al., 2005; Shevenell et al., 2004; Tripati et al., 2003).

5.3.3 The Ries Method

A more empirically rigorous method of accommodating paired variation in temperature and Mg/Ca seawater was provided by Ries (2004, 2006a). In these studies, various calcifying taxa were cultured in artificial seawaters of different Mg/Ca to investigate concomitant changes in the Mg/Ca of their skeletal calcite. A least-squares linear regression of each taxon's dataset revealed a power function of the form:

$$Mg/Ca_C = F\left(Mg/Ca_{SW}\right)^H \tag{5-4}$$

These "partition power functions" are best-fit equations relating the Mg/Ca of the organism's shell and the Mg/Ca of the water in which it grew. To account for the effects of temperature on shell Mg/Ca, the results of previous studies were used. The work of Chave (1954) and Weber (1969) suggest that Mg content of a calcitic skeleton changes exponentially with temperature:

$$Mg/Ca_C = Be^{AT} \tag{5-5}$$

By solving this equation simultaneously with Equation (5-4), the following function, a "Mg-T partition function," was derived to describe the combined effects of temperature and Mg/Ca_{sw} on Mg/Ca_C:

$$Mg/Ca_C = E\left(Mg/Ca_{SW}\right)^H \left(e^{AT}\right) \tag{5-6}$$

To solve for *E*, we note that:

$$B = E\left(Mg/Ca_{SW}\right)^H \tag{5-7}$$

$$F = Ee^{AT} \tag{5-8}$$

And thus:

$$E = B\left(Mg/Ca_{SW}\right)^{-H} = Fe^{-AT} \tag{5-9}$$

It should not matter whether *E* is calculated from Equation (5-7) or (5-8). For example, it was shown (Ries, 2006b) in the case of *Neogoniolithon* (coralline red algae) that estimates of *E* calculated from Equation (5-7) or (5-8) were identical to three significant figures (0.01341 vs. 0.01343, respectively). This may be a serendipitous outcome resulting from the Ries's calibration of Chave's temperature data "to *Neogoniolithon*." If this calibration is removed, the *E* calculated by Equation (5-8) becomes 0.02573. A dilemma results: the two equations that can be used to calculate E produce different results. Is the value of *E* equal to 0.01341 from Equation (5-7) or 0.02573 from Equation (5-8)? The answer is not readily apparent.

Despite this, the method provided by Ries (2004, 2006a) is much preferable to the method of Lear et al. (2000) because of the incorporation of the partition power function. When one parses Mg-T partition function of Lear et al. (2000) in the manner of Ries (2004), it becomes clear that it is untenable, because it would imply the Mg partition function for benthic foraminifera is:

$$Mg/Ca_C = \frac{Mg/Ca_{SW-Ancient}}{Mg/Ca_{SW-Present}} = \frac{1}{5.2}\left(Mg/Ca_{SW-Ancient}\right)^1 \quad (5\text{-}10)$$

In other words, the incorporation of Mg into the skeletons of all calcifying organisms proceeds in the same manner and it is related to the Mg/Ca of modern seawater. This is not borne out by culture experiments that have been performed on calcifying organisms (Segev and Erez, 2006; Stanley et al., 2005).

The method of Ries (2004) has other drawbacks besides the conundrum concerning calculating *E*. It generates the equation for a surface from two best-fit equations, not the original data, which would seem the more reasonable approach. This method also lacks utility when addressing more complicated systems of equations. For example, if it were necessary to combine a Mg partition power function and two exponential temperature partition functions.

5.3.4 Method of Multiple Linear Regression

It might be possible to bypass the difficulty in selecting *E* by using the method of a multiple linear regression to fit a surface to empirical data in the three dimensional space defined by the variables Mg/Ca_{SW}–*T*–Mg/Ca_C. Fuchtbauer and Hardie (Fuchtbauer and Hardie, 1976; 1980) provide the only study in which calcite Mg/Ca was measured as a function of solution Mg/Ca at different temperatures (13.5°C, 28°C, 50°C). Because Mg/Ca_C varies exponentially with temperature and as a power function of Mg/Ca_{sw}, the appropriate equation for multiple linear regression in this case is:

$$Mg/Ca_C = \beta_0 + \beta_1\left(Mg/Ca_{SW}\right)^X + \beta_2 e^T \quad (5\text{-}11)$$

Where β_0, β_1, and β_2 are fitting parameters. To perform a multiple *linear* regression, the equation must be linearized, in this case, by taking the natural log of both sides of the equation:

$$\ln\left(Mg/Ca_C\right) = \beta_0 + \beta_1 \ln\left(Mg/Ca_{SW}\right) + \beta_2 T \quad (5\text{-}12)$$

For the Fuchtbauer and Hardie (1976) dataset, the following values were returned for β_0, β_1, and β_2 by a standard statistical software package (i.e., Analysis Toolpak in Microsoft Excel 2004):

$$\ln\left(Mg/Ca_C\right) = -3.9 + 0.80 \ln\left(Mg/Ca_{SW}\right) + 0.022T \quad (5\text{-}13)$$

Equation (5-13) yields:

$$Mg/Ca_C = 0.020 + 2.2\left(Mg/Ca_{SW}\right) + e^{0.022T} \quad (5\text{-}14)$$

Not only does this method provide an excellent R^2 (0.84) signifying a strong correlation, but also p-values for all variables are « 0.01 suggesting the relationship is highly significant as well.

It also obviates the confusion about whether to use Equation (5-7) or (5-8) when calculating *E*. However, one major drawback to this method is that at $Mg/Ca_{sw} = 0$, there are still temperatures at which Equation (5-14) can give non-zero Mg/Ca_C. This is not possible as there must be some Mg in the solution for it to be incorporated into the precipitating calcite.

When seeking to create a single equation from two or more partition power functions, this method of multiple linear regression is ideal. However, large enough high quality datasets necessary to perform these regressions are scarce. For this reason, the Ries method remains the most broadly applicable to extant datasets.

5.3.5 Deriving Mg-T partition functions for foraminifera

To assess the impact of this revised methodology on foraminiferal Mg/Ca and δ_W records, Mg-T partition functions must be generated for benthic and planktonic foraminifera. Only three foraminiferal Mg partition functions have been published

(Figure 5-1A): for two benthic species (Segev and Erez, 2006) and one planktonic (Delaney et al., 1985):

Amphistegina lessonii (benthic) $$Mg/Ca_C = 0.012\left(Mg/Ca_{SW}\right)^{0.71} \quad (5\text{-}15)$$

Amphistegina lobifera (benthic) $$Mg/Ca_C = 0.012\left(Mg/Ca_{SW}\right)^{0.83} \quad (5\text{-}16)$$

Globigerinoides sacculifer (planktonic) $$Mg/Ca_C = 0.0026\left(Mg/Ca_{SW}\right)^{0.42} \quad (5\text{-}17)$$

The partition power functions for the benthic functions are well correlated ($R^2 > 0.89$) and significant (p-values < 0.05). For the planktonic function, the correlation is also strong ($R^2 = 0.54$) and significant (p-values < 0.05).

With these functions, it is possible to model the response of planktonic and benthic foraminifera to changes in oceanic Mg/Ca over the past 60 My. Hardie (1996) and Wilkinson and Algeo (1989) provide two end-member models estimating the change in Mg/Ca over this time span. The former varies from Mg/Ca = 2 at 60 Ma to Mg/Ca = 5.2 today, while the latter has Mg/Ca = 4 at 60 Ma (Figure 5-2A). Using Equations (5-15), (5-16), and (5-17), the change in foraminiferal Mg/Ca in response to changes in seawater Mg/Ca can be estimated (Figure 5-2B).

The first attribute of Figure 5-2B is that the two benthic foraminifers display a much higher Mg/Ca than the single model from a planktonic foram and that the secular trend in benthic foraminiferal calcite Mg/Ca data (Lear et al., 2000) is much closer to the planktonic model than to either of the benthic models. These uniformly low Mg contents could be rationalized as the diagenetic loss of Mg; however, this is unlikely as modern examples of the species analyzed by Lear et al. (2000) all produce calcite of similarly low Mg/Ca. As has been shown above, there exists a range in Mg partition functions among calcifying invertebrates and thus we cannot preclude the conclusion that the benthic

foraminifers analyzed by Lear et al. (2000) likely have Mg partition functions more similar to that of the modern planktonic foraminifer, *G. sacculifer*, which produces a test of low-Mg calcite.

The second feature of Figure 5-2B is that all the models produce positive trends in foraminiferal calcite Mg/Ca from 60 Ma to present, while the data of Lear et al. (2000) display a negative slope. If foraminiferal calcite Mg/Ca were only affected by seawater Mg/Ca, then they should also exhibit a positive slope. As the data of Lear et al. (2000) do not mimic this Cenozoic increase, we can conclude that either a diagenetic enrichment in Mg or depletion in Ca has occurred in older samples, or that some other factors are affecting foraminiferal calcite Mg/Ca. Lear et al. (2000) argue that this decrease results from the secular trend of decreasing bottom water temperatures from 60 Ma to present.

To account for this secular change in bottom water temperatures, we must incorporate a temperature partition function into Equations (5-15), (5-16), and (5-17). Numerous temperature partition functions for foraminifera exist (Anand et al., 2003; Lea et al., 1999; Lear et al., 2002; Martin et al., 2002; Nürnberg et al., 1996; Russell et al., 2004), and these describe the effect of temperature on foraminiferal Mg/Ca as exponential, a variant of the Arrhenius equation. The planktonic foraminiferal temperature calibration of Anand et al. (2003) was chosen after an extensive literature review of planktonic foraminiferal Mg/Ca data from multiple taxa:

Planktonic foraminifera $$Mg/Ca_C = 0.00038e^{0.090T} \quad (5\text{-}18)$$

For benthic species we use the calibrations for *O. umbonatus* and *Cibicidoides spp.* of Lear et al. (2002) as these are the most recent and highest quality core-top calibrations (See Table 5-2 for fit parameters to Equations (5-18), (5-19), and (5-20).):

Oridiosalis umbonatus $$Mg/Ca_C = 0.0010e^{0.11T} \quad (5\text{-}19)$$

Cibicidoides spp. $$Mg/Ca_C = 0.00087e^{0.11T} \quad (5\text{-}20)$$

For consistency, when combining Mg partition power functions (Equations (5-15), (5-16), and (5-17)) and exponential temperature calibrations (Equations (5-18), (5-19), and (5-20)), *E* was calculated with Equation (5-7). The resulting Mg-T partition functions for benthic and planktonic foraminifera are:

O. umbonatus $$Mg/Ca_C = 0.00050\left(Mg/Ca_{SW}\right)^{0.42}\left(e^{0.11T}\right) \quad (5\text{-}21)$$

Cibicidoides spp. $$Mg/Ca_C = 0.00045\left(Mg/Ca_{SW}\right)^{0.42}\left(e^{0.11T}\right) \quad (5\text{-}22)$$

Planktonic foraminifera $$Mg/Ca_C = 0.00019\left(Mg/Ca_{SW}\right)^{0.42}\left(e^{0.09T}\right) \quad (5\text{-}23)$$

These functions define surfaces in the three-dimensional space across which foraminiferal Mg/Ca_C can vary. Ideally, they would be generated by the multiple linear regression of a truly three-dimensional dataset, however no such dataset exists.

5.4 Results

5.4.1 Mg/Ca Paleotemperatures

The effect of using a Mg-T partition function can be seen when data are re-evaluated from two recent papers (Lear et al., 2000; Tripati et al., 2003), which have employed the Mg/Ca of foraminiferal calcite as a paleothermometer of Cenozoic oceans. The planktonic foraminiferal Mg/Ca data from 60 Ma to 40 Ma (Tripati et al., 2003) shows an oscillation about a mean value, but no positive or negative trend through this time interval. Mg-temperatures were calculated with Equation (5-23). The differences between temperature estimates of Equation (5-23) and the common method (Equation (5-3)) are evident in Figure 5-3. Calculating Mg-paleotemperature in the manner of Tripati et al.

(2003), i.e. using the Mg-T partition function of Lear et al. (2000) and the Mg/Ca_{sw} model of Wilkinson and Algeo (1989) produces an average sea surface Mg-paleotemperature of 31°C. Substituting the Hardie (1996) model of Mg/Ca_{sw}, temperatures average 41°C. This estimated temperature was so high that it led Tripati et al. (2003) to discount the Mg/Ca_{sw} model of Hardie (1996).

However, in the same case when a partition power function (Equation (5-23)) is employed with the seawater Mg/Ca model of Wilkinson and Algeo (1989), calculated temperatures are lowered by about 3°C to an average of 28°C. More importantly, when using Equation (5-23), realistic temperatures are also estimated when Hardie's Mg/Ca_{sw} model. The resulting trend averages 32°C, only 1°C higher than estimates of Tripati et al. (2003). This suggests that the Hardie (1996) model of Cenozoic Mg/Ca_{sw} may not be unreasonable as they suggested because application of the revised Mg-T partition functions can accommodate secular changes in seawater Mg/Ca and result in more realistic temperature estimates.

Lear et al. (2000) estimated oceanic paleotemperatures for the last 60 My from benthic foraminiferal calcite Mg/Ca. The same phenomenon as seen with the planktonic data occurs with Mg-paleotemperatures calculated from benthic foraminiferal calcite Mg/Ca (Figure 5-4). Using Equation (5-3) and the Wilkinson and Algeo model of Cenozoic Mg/Ca_{sw}, the Cenozoic paleotemperature trend averages 8°C. Using the Hardie (1996) model of Cenozoic Mg/Ca_{sw} paleotemperatures average 14°C, this large discrepancy led Lear et al. (2000) to prefer the Wilkinson and Algeo Mg/Ca_{sw} model. By using the revised Mg-T partition power function, estimates of bottom water temperatures average 7°C and 9°C for the Wilkinson and Algeo (1989) and Hardie (1996) models of

Cenozoic Mg/Ca_{sw}, respectively. As with the planktonic dataset, the differences between using the two Cenozoic Mg/Ca_{sw} models is reduced (to only 2°C from 6°C) when using the a Mg-T partition function.

5.4.2 Paleoseawater $\delta^{18}O$

A central objective of studies of paleoceanographic and paleoclimatic studies is to estimate the temperatures of marine surface and bottom waters to gain insight into global environmental conditions. Application of the Mg-paleothermometer in combination with $\delta^{18}O$ paleothermometer offers a unique opportunity to estimate changes in marine oxygen isotope composition, which serves as a direct proxy of continental glacial ice volume. To accomplish this, it is standard to measure the $\delta^{18}O$ of carbonate phases ("δ_C") that precipitate from seawater as temperature and δ_C are related by a simple equation. For planktonic foraminiferal calcite (Erez and Luz, 1983) the equation is:

$$T = 17.1 - 4.58\left[\left(\delta_C - \delta_C^*\right) - \left(\delta_W - \delta_W^*\right)\right] \qquad (5\text{-}24)$$

Where:

T =	Temperature (in °C)
δ_W =	$\delta^{18}O$ of seawater (‰ SMOW)
δ_C =	$\delta^{18}O$ of foraminiferal calcite (‰ PDB)
δ_C* =	Species "offset," which accounts for non-equilibrium $\delta^{18}O$ compositions
δ_W* =	Difference between δ_W in SMOW and in PDB = –0.27‰ (Hut, 1987)

A confounding factor in this equation is the difficulty in obtaining an independent estimate of "δ_W," the $\delta^{18}O$ of seawater, which can vary over long time scales in response to rock-water exchange (Lohmann and Walker, 1989; Walker and Lohmann, 1989) and during short term fluctuations in the volume of glacial ice on continents. With the present configuration of continental glaciation in Antarctica and Greenland, $\delta_W \approx 0$‰ SMOW.

Based on a mass-balance, if all glacial ice were to melt, $\delta_W \approx -1‰$ SMOW. At the last glacial maximum (LGM, ca. 8 ka), $\delta_W \approx +1.6‰$ SMOW. These three values could be converted into percentages where –1‰ SMOW equals 0% glacial ice, 0‰ SMOW equals 40%, and +1.6‰ SMOW equals 100% of LGM ice volume.

However, it is difficult to estimate δ_W for periods during geologic history (e.g., the Cenozoic) when ice volume was intermediate between these two extremes. On this basis, the implementation of independent proxies for seawater temperature (i.e., Mg/Ca contents of foraminifers and ostracods) has allowed estimation of δ_W, and likewise reconstruction of temporal changes in ice volume (e.g. Lear et al., 2000). In light the changes in temperature estimates that derive from the revision of the Mg-paleothermometer (Figure 5-3 and Figure 5-4), we provide a new estimate of Cenozoic δ_W based on the following methodology and assumptions.

When solved for δ_W, the planktonic foraminifer $\delta^{18}O$-paleotemperature equation becomes:

$$\delta_W = \delta_C + \delta_C^* - \delta_W^* + \frac{T - 17.1}{4.58} \tag{5-25}$$

To estimate Paleocene/Eocene of tropical sea surface δ_W, Mg-paleotemperatures (Figure 5-3) and δ_C (Bralower et al., 1995, from the same core and sample intervals) from planktonic foraminiferal calcite are combined (Figure 5-5). The first two trends provide estimates of seawater δ_W using the unrevised Mg-paleothermometer (Equation (5-3)) with Cenozoic Mg/Ca_{sw} estimates for both Hardie (1996) and Wilkinson and Algeo (1989). The δ_W trend using Wilkinson and Algeo (1989) averages 1.5‰, while that using Hardie (1996) averages 3.6‰, a difference of 2.1‰. However, when the revised Mg-T

partition function thermometer is employed (Equation (5-23)), the estimates of δ_W exhibit a much smaller difference (~0.4‰). This emphasizes the utility of employing the partition function approach as temperature estimates become relatively insensitive to different models of secular change in Mg/Ca_{SW}.

A similar approach can be applied to calculate Cenozoic δ_W from the revised benthic Mg-temperatures calculated above (Figure 5-4), benthic foraminifera δ_C of Zachos et al., (2001), and the $\delta^{18}O_C$-paleotemperature equation of Shackleton et al. (1974):

$$T = 16.9 - 4\left[\left(\delta_C - \delta_C^*\right) - \left(\delta_W - \delta_W^*\right)\right] \tag{5-26}$$

$$\delta_W = \delta_C + \delta_C^* - \delta_W^* + \frac{T - 16.9}{4} \tag{5-27}$$

Figure 5-6 plots four different trends in Cenozoic δ_W derived from the benthic foraminifer data of Lear et al. (2000). In a similar fashion, two trends use the Mg/Ca_{sw} model of Hardie (1996) and two use the Mg/Ca_{sw} model of Wilkinson and Algeo (1989). Of the two trends produced from each model, one was calculated with the original method (Lear et al. (2000), Equation (5-3), but with the updated temperature function of Lear et al., 2002) and one with the method suggested in this paper (Equation (5-21).

The trends calculated with the method of Lear et al. (2000) show the same wide discordance as they did for the planktonic foraminifera. The results from the Hardie model average 0.9‰, the Wilkinson and Algeo model results average –0.3‰, a difference of 1.2‰. When calculated with Equation (5-21), they are much more in accordance averaging –0.1‰ and –0.6‰, respectively, a difference of only 0.5‰.

5.4.3 Paleoseawater $\Delta^{18}O$

Estimates of Cenozoic seawater $\delta^{18}O$ from planktonic and benthic foraminifera give us a rough estimate of the differences between tropical sea surface δ_W and bottom water δ_W ("Δ_W") for the time period during which the two records overlap, a 15 My span from 55 Ma to 40 Ma. For time interval, Δ_W varies between 1.2‰ and 2.4‰ using the Wilkinson and Algeo (1989) model of Mg/Ca_{sw}, and between 1.9‰ and 3.1‰ using the Hardie (1996) model (Figure 5-7). Both of these ranges in Δ_W are larger than the estimate for today, 0.74‰ (Figure 5-8). However, the observed range for modern seawater between the highest sea-surface $\delta^{18}O$ and the lowest bottom water $\delta^{18}O$ is ~ 3.8‰. Thus it seems possible to accommodate the large ranges in Paleocene-Eocene Δ_W calculated here in the context of modern δ_W variation. Spatial variation in evaporative flux is a major contributor to the modern variability of sea surface δ_W. Therefore, some of this Δ_W discrepancy might be explained by a heightened evaporative flux during Paleocene-Eocene times due to "greenhouse" climatic conditions.

5.5 Discussion

5.5.1 Seawater Mg/Ca

While it has been shown above based on theoretical grounds that the Mg-paleotemperature and δ_W trends calculated with Equation (5-3) are untenable, it remains necessary to discuss whether it is better to use the Mg/Ca_{sw} model of Hardie (1996) or of Wilkinson and Algeo (1989). To a first approximation, they can both be considered appropriate because neither model of secular change in Mg/Ca_{sw} generates patently unreasonable Mg-paleotemperature or δ_W trends from either planktonic or benthic

foraminiferal calcite. When Mg-paleotemperatures are carried through to the estimation of δ_W, results are within reasonable limits for the secular variation of δ_W during a time of increasing continental glaciation. It could be argued that these two models establish boundaries within which the actual secular trends lie because when examining the myriad models for secular change in Mg/Ca_{sw} (Arvidson et al., 2006; Berner, 2004; Demicco et al., 2005; Hardie, 1996; Wilkinson and Algeo, 1989), the Hardie model suggests the greatest change in Mg/Ca_{sw} over the last 60 My, and the Wilkinson and Algeo model suggests the least. However, independent lines of reasoning do suggest that one might be more accurate than the other.

First, a substantial number of geochemical and petrographic studies have argued for more rather than less change in Mg/Ca_{sw} since 60 Ma. These include studies of secular change in echinoderm calcite Mg/Ca (Dickson, 2004), in the Mg/Ca of evaporite fluid inclusions (Demicco et al., 2005; Lowenstein et al., 2003; Lowenstein et al., 2001), evaporite mineralogy (Hardie, 1996; Holland et al., 1996; Horita et al., 2002), ooid mineralogy (Sandberg, 1983), and mineralogy of dominant reef building organisms (Stanley and Hardie, 1998). These data provide an independent, quantitative constraint on paleocean Mg/Ca and are more compatible with the Hardie model.

While the difference between the δ_W trends calculated with the two Mg/Ca_{sw} models is small between 0 and 10 Ma, after that they each suggest different histories for the accumulation of continental ice during the Cenozoic (Figure 5-6). If we accept the model, which uses Mg/Ca_{sw} from Wilkinson and Algeo (1989), glacial ice begins to accumulate in the late Eocene, reaches an apex at 25% of the full Pleistocene ice volume (Dwyer et al., 1995) in the early Oligocene, before complete deglaciation by the late Oligocene.

Glacial ice does not begin to accumulate again until the Mid-Miocene. The δ_W trend from the Hardie model of Mg/Ca_{sw} suggests that glacial ice is present in some amount at all times since 60 Ma. It peaks at ~50% of LGM ice volume in the early Oligocene, but remains at least at ~13% during the late Oligocene/Early Miocene deglaciation.

The discriminating factor between these two models of Mg/Ca_{sw} thus appears to be that one (Hardie, 1996) suggests persistent glaciation over the last 60 My, while the other (Wilkinson and Algeo, 1989) only advocates glaciation during the Late Eocene–Early Oligocene and again from the Mid-Miocene to the present.

The most widely accepted version of Cenozoic climate history, based on benthic foraminiferal $\delta^{18}O$, is that of global cooling and the accumulation of ice on continents (Kennett et al., 1990; Miller et al., 1987; Zachos et al., 2001). This begins with a warm, ice-free Paleocene and early Eocene. Global cooling proceeds through the rest of the Eocene followed by an initial buildup of continental ice on East Antarctica at the Eocene-Oligocene boundary. Global warming and deglaciation during the Early to Middle Miocene was followed by renewed cooling in the late Miocene when it is suggested that the West Antarctic Ice sheet formed. Finally, during the Plio-Pleistocene Northern Hemisphere glaciation begins. Neither model produced in this study matches this chronology verbatim. While the model using Hardie Mg/Ca_{sw} produces permanent glaciation from the Oligocene to the present, neither model is ice-free up to that time.

Other studies have offered additional insights into Cenozoic climate that suggest a different pattern of events. For example, the sedimentological record of ice-rafted debris extends back well into the Eocene (Barrett et al., 1987; Birkenmajer, 1998; Eldrett et al., 2007; Mackensen and Ehrmann, 1992; Margolis and Kennett, 1970; Moran et al., 2006;

Tripati et al., 2008; Wise et al., 1992) suggesting at least ephemeral glaciations during this time. Deconto (2003) showed in a modeling study that Antarctic glaciation would proceed stepwise with smaller glaciations first followed by more extensive buildups of continental ice. Based on these suggestions it seems likely that continental glaciations could have been extensive enough during at least the Eocene, if not the Paleocene as well, to affect δ_W. Indeed, numerous authors have even suggested Cretaceous glaciations as a way to explain high frequency sea-level variation (Carpenter et al., 2003; Matthews and Poore, 1980; Miller et al., 2005; Moriya et al., 2007; Stoll and Schrag, 1996).

Despite the numerous lines of evidence for Early to Mid-Miocene warmth (Kennett and Brunner, 1973; Kennett and von der Borch, 1986; Lewis et al., 2007; Zachos et al., 2001), none have argued for completely ice-free continents. The contrary is the case, with these authors and many others (e.g. Browning et al., 1996; Miller et al., 2005) considering Antarctica to have been permanently ice-bound since the Early Oligocene.

The evidence for the continuous presence of glacial ice throughout the last 50 My strongly suggest that the δ_W curve produced using the Hardie (1996) model is more appropriate than that generated with the model of Wilkinson and Algeo (1989).

5.5.2 The Last 60 My

Using the Hardie model of Mg/Ca_{sw}, we can discuss the history of planktonic and benthic paleotemperatures and δ_W. These trends have been plotted as well as benthic foraminiferal δ_C (Zachos et al., 2001) and sea level anomaly (Miller et al., 2005) over the last 60 My (Figure 5-9). During this span of time, several intervals can be distinguished by obvious trends in δ_W: 60-34 Ma, 34-25 Ma, 25-15 Ma, 15-7 Ma, and 7-0 Ma.

The first interval, 60-34 Ma, is characterized by gradual shallow and deep ocean cooling, increasing benthic foraminiferal δ_C, rise in shallow and deep ocean δ_W, and a drop in sea level of ~75 m. This is consistent with a gradually increasing volume of continental ice. A transient warming event (the Early Eocene Climatic Optimum?, Zachos et al., 2001) around 52 Ma causes shallow ocean temperatures to rise, sealevel to rise, and δ_W to fall. Lack of data masks this event in the benthic Mg/Ca data. Ivany et al. (2008) documented a similar Eocene cooling trend from the bivalve calcite $\delta^{18}O$.

During the next interval, 34-25 Ma, benthic Mg-paleotemperatures are relatively invariant. δ_C increases sharply by ~ 1‰ at 34 Ma, remains relatively constant for 9 My, before falling by ~ 1‰ at 25 Ma. δ_W decreases by ~ 1‰ over this interval suggesting a large decrease in continental ice volume. This contradicts the record of further continuous sea level fall of another 50 m. This could be explained by cooling and contraction of the oceanic lithosphere, a first-order control on sea level.

From 25-15 Ma, all three benthic proxies (temperature, δ_W, and δ_C) are generally constant as is sea-level. Slight positive trends in benthic δ_C and δ_W occur as a step-change in benthic temperatures occurs from ~8°C to 6°C from 15 to 7 Ma. During the final interval, 7 Ma to the present, a steep decrease in benthic temperatures coincides with a steep increase in benthic δ_C and δ_W signaling the onset of glaciation in the northern hemisphere.

5.6 Conclusions

It is apparent that Mg-T partition functions refine the Mg-paleotemperature and the subsequent calculations of the isotopic composition of seawater. This is accomplished by

reducing the sensitivity of Mg-paleotemperature calculations to assumptions concerning secular variation in Mg/Ca_{sw}. The extent to which this requires revision of previous paleoenvironmental interpretations is likely small as in all cases examined, the revised Mg-paleotemperature and δ_W trends could be explained by invoking greater changes in Mg/Ca_{sw} than previous authors had accepted. A major implication of this study is to reconcile the Hardie (1996) model of secular variation in seawater Mg/Ca with Cenozoic foraminiferal Mg/Ca records.

The models of Cenozoic δ_W produced by this method argue in favor of persistent continental glaciation from 60 Ma, a major buildup of continental ice beginning in the Middle Eocene, and widespread, but not complete, deglaciation in the Late Oligocene to Early Miocene. These findings do not perfectly correlate with the standard history of δ_W from benthic foraminiferal calcite $\delta^{18}O$, but do match sedimentological records from ice-rafted debris and stratigraphic evidence of glacioeustasy.

5.7 Acknowledgements

This paper has benefited greatly from the thoughtful insight and kind encouragement of Kacey Lohmann, Tom Baumiller, Joel Blum, George Kling, and Bruce Wilkinson.

5.8 Figures

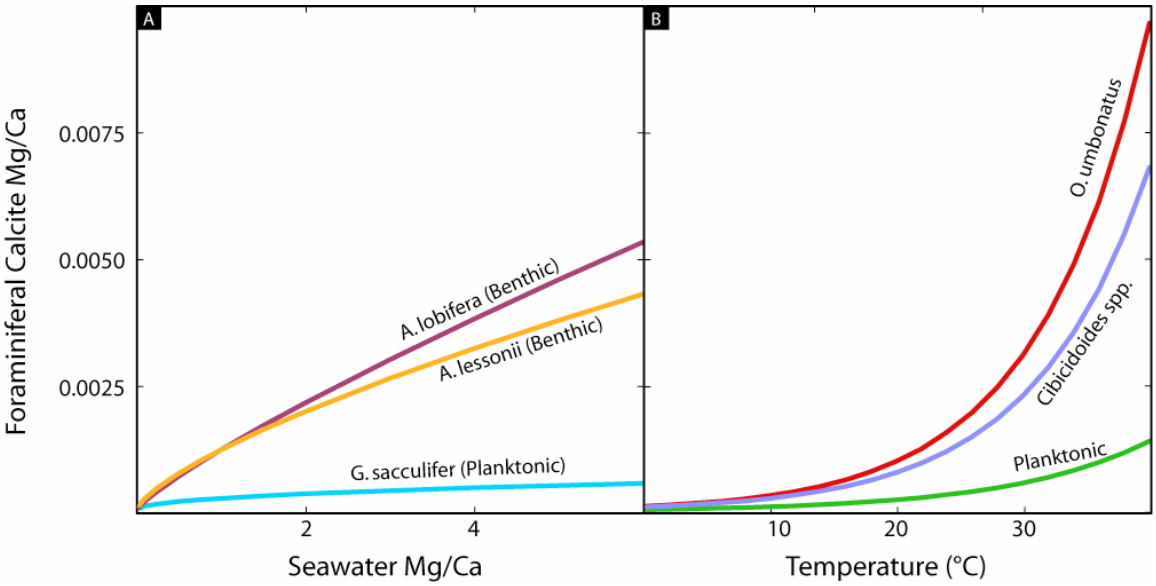

Figure 5-1: A) Mg partition functions for benthic (Segev and Erez, 2006) and planktonic (Delaney et al., 1985) foraminifera. B) Exponential temperature partition functions of Anand et al. (2003) and Lear et al. (2002).

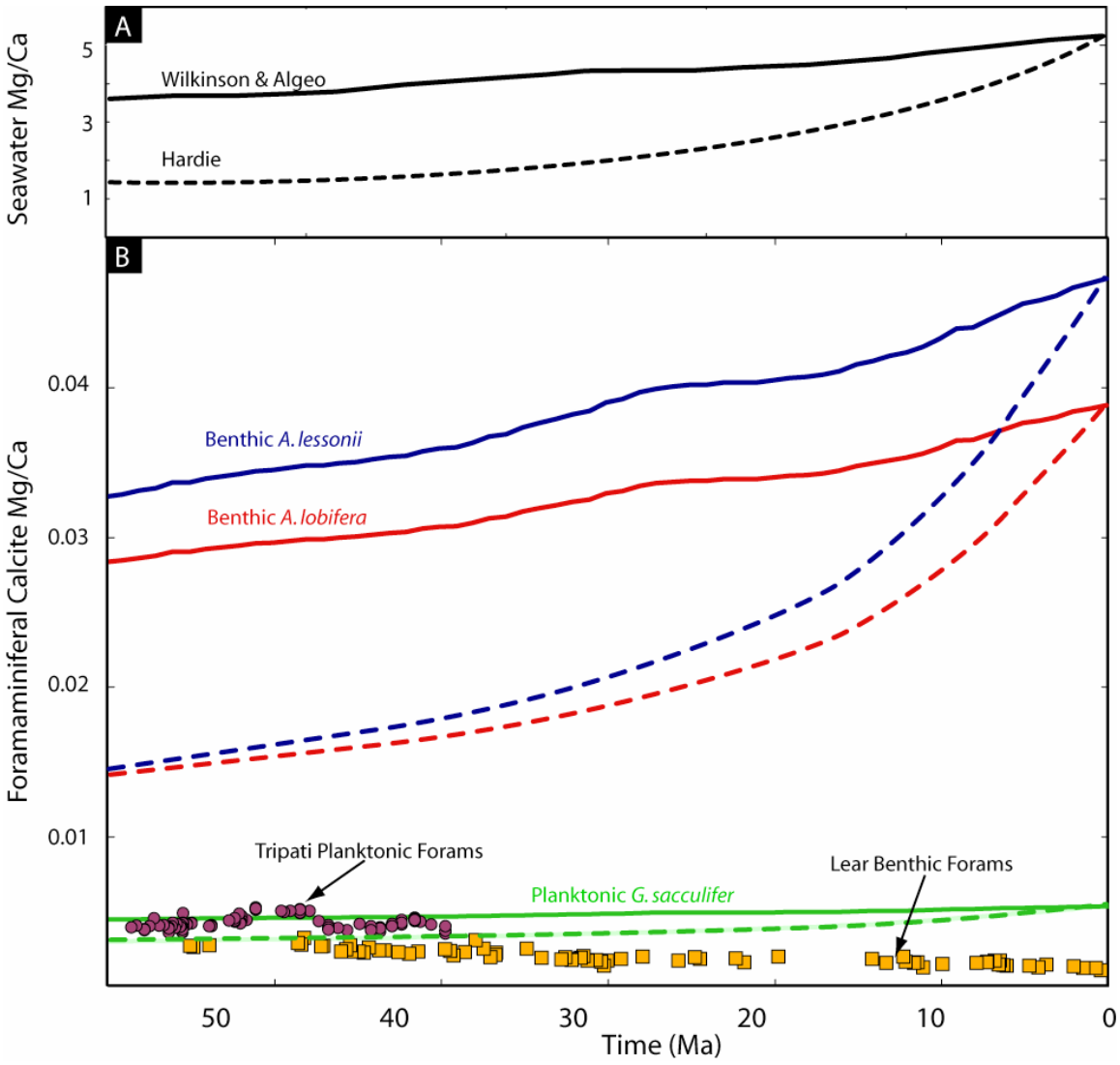

Figure 5-2: A) Models of global oceanic Mg/Ca (60 Ma to present) as suggested by Wilkinson and Algeo (1989; solid) and Hardie (1996; dashed). B) Models of change in foraminiferal calcite Mg/Ca in response to change in oceanic Mg/Ca. Values from Hardie's model would produce the dashed lines, Wilkinson and Algeo's model the solid lines. Data of Lear et al. (2000) are plotted as triangles; data of Tripati et al. (2003) are plotted as purple circles

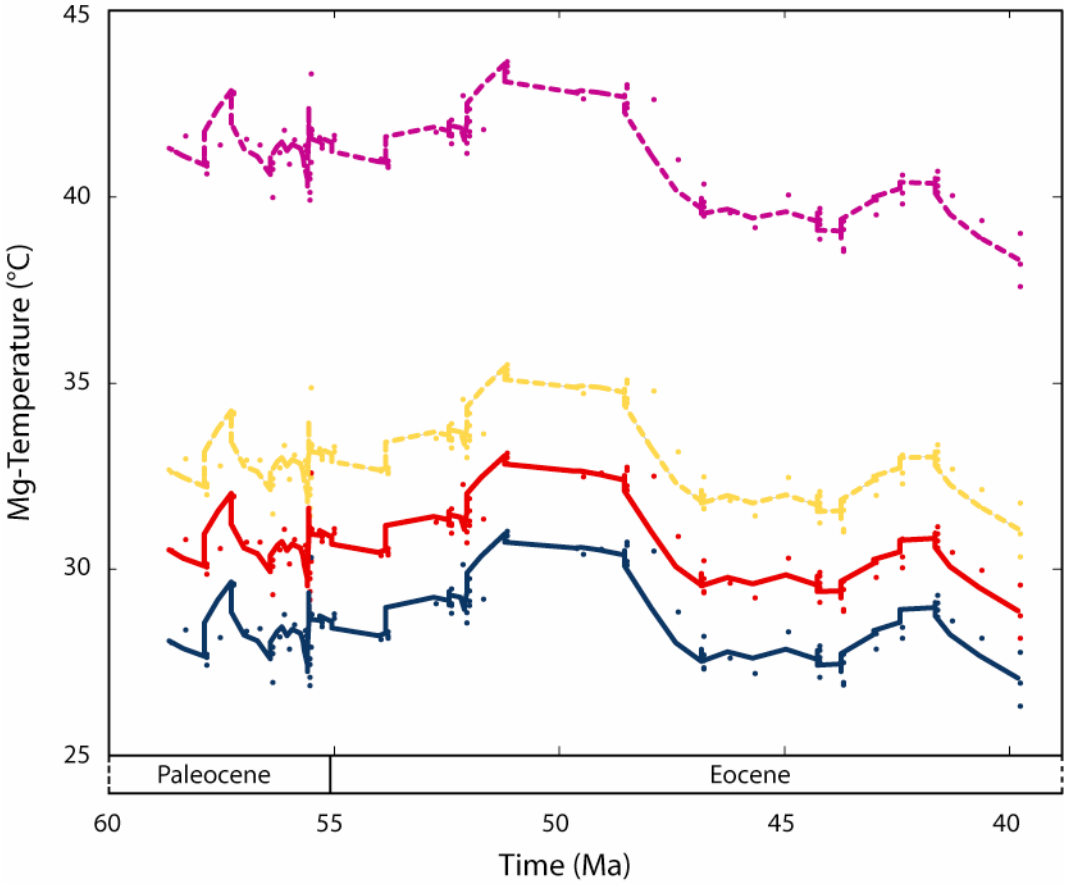

Trend	Symbol	Mg Partition Function	Cenozoic Mg/Ca_{sw} Model	Mean T
Tripati_H	Purple Dash	Lear et al. (2002)	Hardie (1996)	41°C
Hasiuk_H	Yellow Dash	Delaney et al. (1985)	Hardie (1996)	32°C
Tripati_WA	Red Solid	Lear et al. (2002)	Wilkinson and Algeo (1989)	31°C
Hasiuk_WA	Blue Solid	Delaney et al. (1985)	Wilkinson and Algeo (1989)	28°C

Figure 5-3: Paleocene/Eocene tropical temperature trends derived from planktonic foram calcite Mg/Ca (normalized to *M. aragonensis*) of Tripati et al. (2003). All trends use the temperature calibration of Anand et al. (2003). Trends represent three-point moving averages.

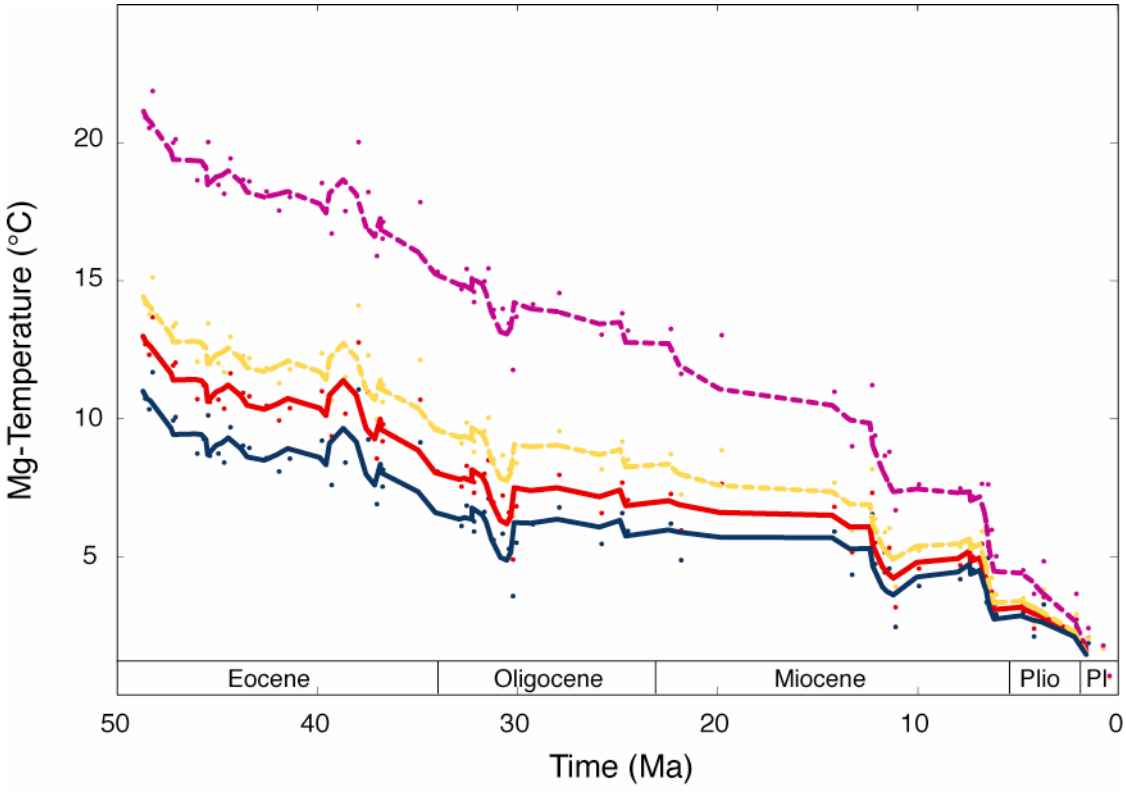

Trend	Symbol	Mg Partition Function	Mg/Ca_{sw} Model	Mean T
Lear_H	Purple Dash	Lear et al. (2000)	Hardie (1996)	14°C
Hasiuk_H	Yellow Dash	Delaney et al. (1985)	Hardie (1996)	9°C
Lear_WA	Red Solid	Lear et al. (2000)	Wilkinson and Algeo (1989)	8°C
Hasiuk_WA	Blue Solid	Delaney et al. (1985)	Wilkinson and Algeo (1989)	7°C

Figure 5-4: Cenozoic bottom water temperature trends derived from benthic foram calcite Mg/Ca (normalized to *O. umbonatus*) of Lear et al. (2000). All trends use the temperature calibration of Lear et al. (2002) for *O. umbonatus*. Trends represent three-point moving averages.

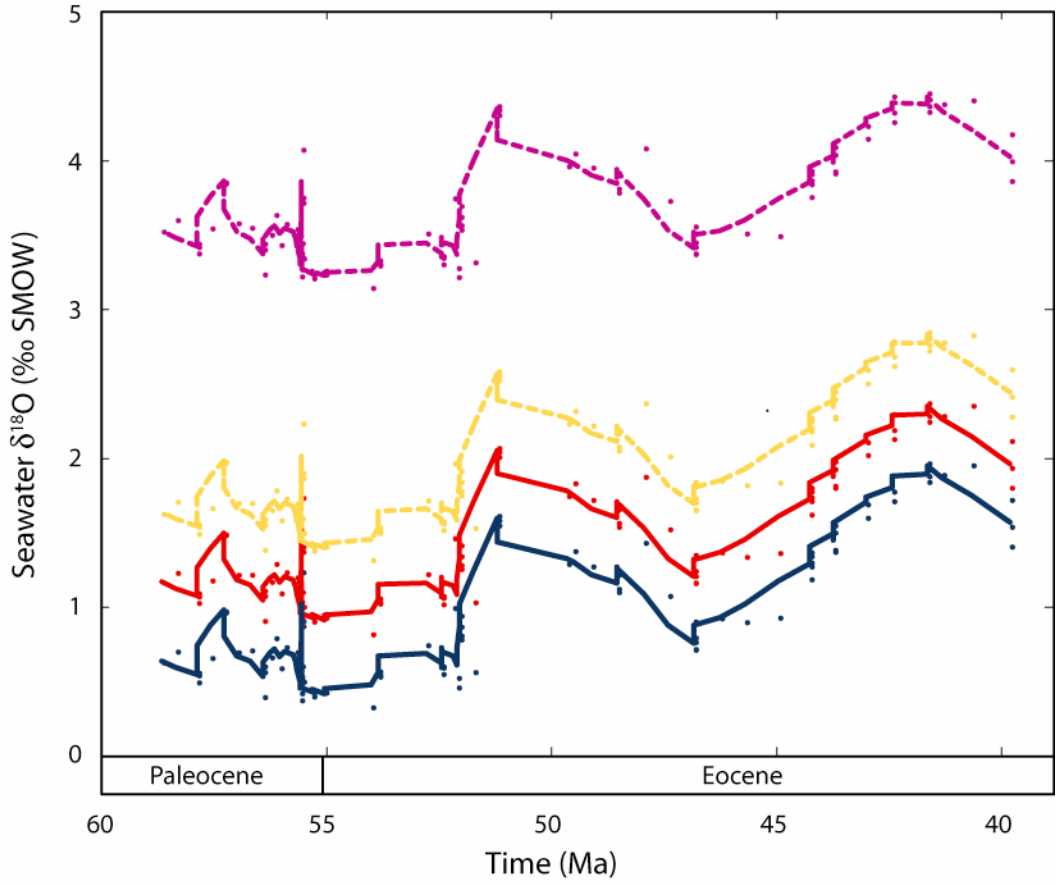

Trend	Symbol	Cenozoic Mg/Ca_{sw} Model	Mean δ_w
Tripati_H	Purple Dash	Hardie (1996)	3.6‰
Hasiuk_H	Yellow Dash	Hardie (1996)	1.8‰
Tripati_WA	Red Solid	Wilkinson and Algeo (1989)	1.5‰
Hasiuk_WA	Blue Solid	Wilkinson and Algeo (1989)	1.4‰

Figure 5-5: Paleocene/Eocene seawater $\delta^{18}O$ calculated by applying the $\delta^{18}O$-paleotemperature equation of Erez and Luz (1983) to planktonic foraminiferal calcite $\delta^{18}O$ data (Bralower et al., 1995) and Mg-paleotemperatures calculated above (Figure 5-3). Trends represent three-point moving averages.

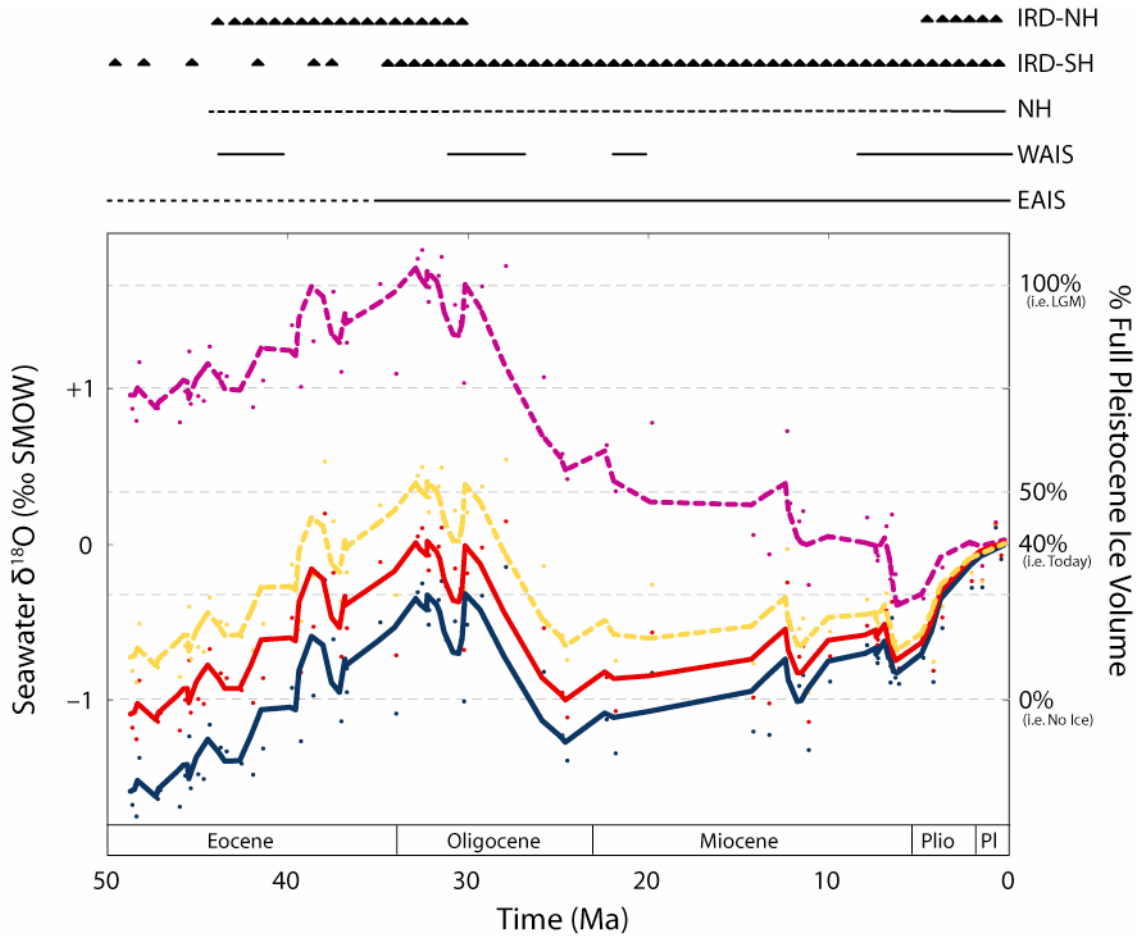

Trend	Symbol	Cenozoic Mg/Ca_{sw} Model	Mean δ_W
Lear_H	Purple Dash	Hardie (1996)	0.9‰
Hasiuk_H	Yellow Dash	Hardie (1996)	–0.1‰
Lear_WA	Red Solid	Wilkinson and Algeo (1989)	–0.3‰
Hasiuk_WA	Blue Solid	Wilkinson and Algeo (1989)	–0.6‰

Figure 5-6: Cenozoic bottom water $\delta^{18}O$ calculated by applying the $\delta^{18}O$-paleotemperature equation of Shackleton (1974) to benthic foraminiferal calcite $\delta^{18}O$ (Zachos et al., 2001, calibrated to "equilibrium") and Mg-paleotemperatures calculated above (Figure 5-4). Dwyer et al. (1995) provided a model of how δ_W and extent of continental glaciation relate. This is represented as a percentage of full Pleistocene ice volume. Trends represent three-point moving averages. Above the plot, small triangle represent the stratigraphic evidence for ice-rafted debris in the northern and southern hemispheres (IRD-NH and -SH, respectively) as well as solid lines representing existence of continental ice in the northern hemisphere (NH), and in the East and West Antarctic Ice Sheets (EAIS and WAIS, respectively). Dashed lines denote possible existence. See text for references.

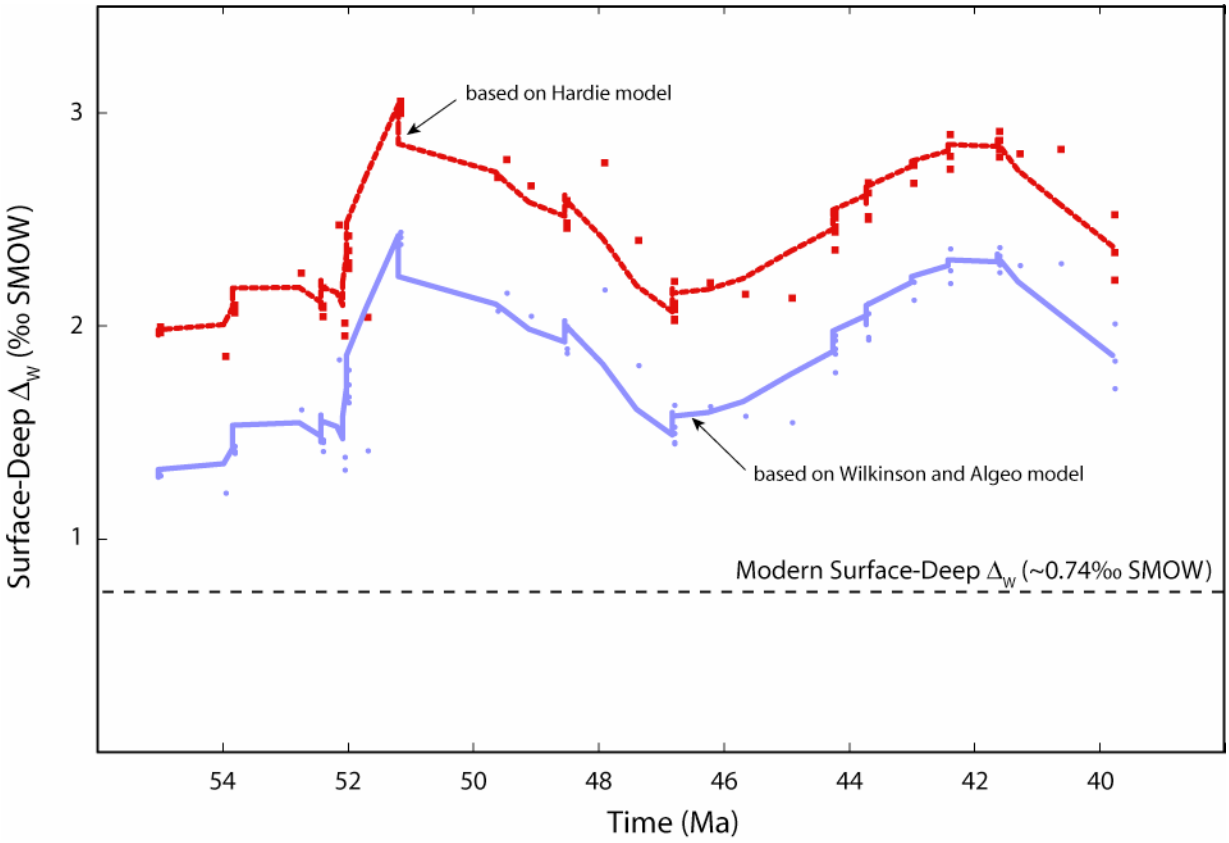

Figure 5-7: Difference in tropical sea surface and bottom water δ_W (i.e., Δ_W). Dashed line is modern Δ_W (0.74‰) derived from NASA Seawater $\delta^{18}O$ Database. (Trends represent three-point moving averages.)

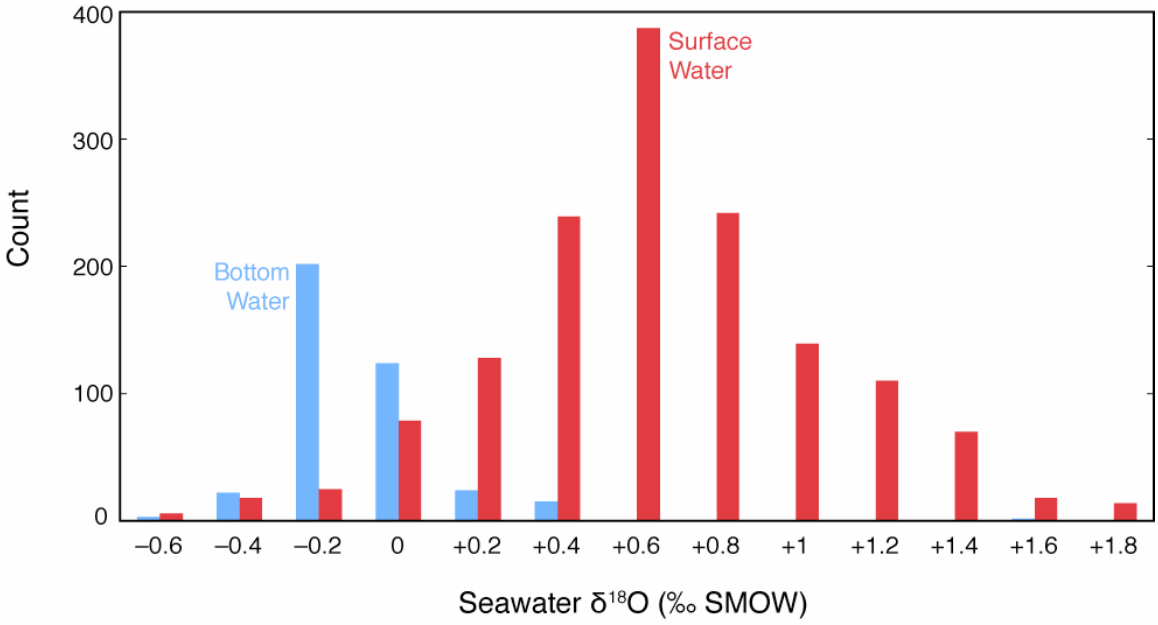

	BW $\delta^{18}O$ (‰ SMOW)	Tropical $\delta^{18}O$ (‰ SMOW)
N =	393	1500
Average	–0.17	0.57
Max	1.67	3.09
Min	–0.70	–1.76
Range	2.37	4.85
SD	0.22	0.47

Figure 5-8: Modern seawater $\delta^{18}O$ statistics. Data are provided for tropical sea surface water (>300m, between 29 and 41‰ salinity, and between 30°N and 30°S latitude) and bottom water (>4000m) from NASA Seawater $\delta^{18}O$ database. The difference between the means ("Δ_W") of the two categories is 0.74‰.

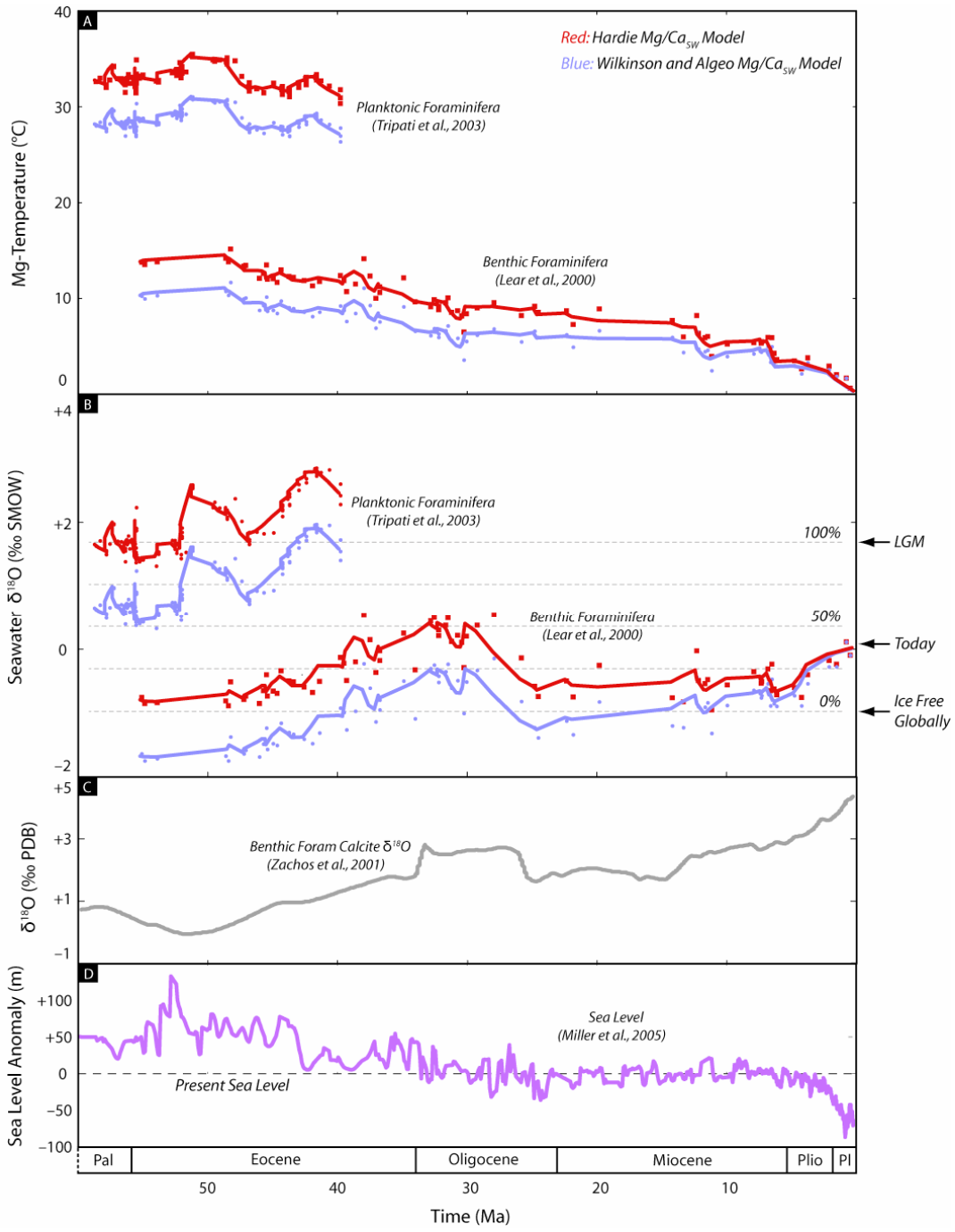

Figure 5-9: Compilation of planktonic and benthic Mg-temperature and δ_W trends from 60 Ma to present, including δ_C trend of Zachos et al. (2001) and sea level anomaly of Miller et al. (2005). A) Mg paleotemperatures. In B, the model of Dwyer et al. (1995) relating δ_W to extent of continental glaciation is provided. This is represented as a percentage of full Pleistocene ice volume. Mg-temperature and δ_W trends represent three-point moving averages. δ_C trend represents a 5-point moving average.

Table 5-1: Mg/Ca partition power function parameters for foraminifera.

			Power Function ($y = Fx^H$)						
	N	**Temp (°C)**	**R^2**	**F**	**F_SE**	**F_p**	**H**	**H_SE**	**H_p**
Planktonic Foram (*G. sacculifer*)[1]	10	30	0.54	0.003	0.1032	6.8E-09	0.42	0.1357	1.5E-02
Benthic Foram (*A. lessonii*)[2]	38	24	0.89	0.012	0.0257	4.5E-41	0.70	0.0402	3.4E-19
Benthic Foram (*A. lobifera*)[2]	42	24	0.89	0.012	0.0281	6.7E-43	0.82	0.0467	1.7E-20

Source: 1, Delaney et al. (1985); 2, Segev and Erez (2006)

Table 5-2: Exponential temperature partition calibration parameters for foraminifera.

			Exponential Regression ($y = Be^{Ax}$)				
	N	**Mg/Ca_{SW}**	**R^2**	**B**	**B_SE**	**A**	**A_SE**
Planktonic Foraminifera (*Multi-taxa*)[1]	341	5.2	0.86	0.00038	0.00002	0.090	0.003
Benthic Foram (*O. umbonatus*)[2]	23	5.2	0.40	0.0010		0.11	
Benthic Foram (*Cibicidoides spp.*)[2]	101	5.2	0.94	0.00087	0.00005	0.11	0.007

Source: 1, Anand et al. (2003); 2, Lear et al. (2002).

Chapter 6: Conclusions

Variation in the character of limestones through geologic time has been noted paleontologically, stratigraphically, petrographically, and geochemically. Thus, it can be supposed that the conditions under which calcium carbonate has precipitated from the seawater have also varied over geologic time.

One major aspect of calcium carbonate production over the Phanerozoic has been that the primary mineralogies of calcium carbonate precipitated from seawater has varied through time between calcite and aragonite plus magnesian calcite . These times have been called “calcite seas” and “aragonite seas,” respectively. While initially it was thought that variation in atmospheric pCO_2 controlled this phenomenon, the Mg/Ca of seawater seems the more likely cause. Seawater Mg/Ca in turn is thought to be dominantly controlled by the hydrothermal alteration of fresh basalt at mid-ocean ridges and to a lesser extent by the riverine input of weathering products. Therefore, analysis of calcite Mg/Ca can elucidate the variability of seafloor spreading rates through time. Because the geologic record contains abundant limestone back into the Neoproterozoic, the opportunity exists to understand the history of oceanic crust production at times for which ocean crust is either scarce or non-existent.

Back-calculating seawater Mg/Ca from calcite Mg/Ca requires care. It has been customary to assume that the relationship between these two quantities is linear and thus that the slope of this function (i.e., the partition coefficient) is constant at all values of

seawater Mg/Ca. However, based on laboratory culturing experiments with both abiotic calcite and marine calcifying organisms, this relationship is more appropriately described by a power function. The power relation, a "partition power function" matches more closely the behavior of calcites because the slope is high at low Mg/Ca because of reduced interference from the Mg ion during growth at the calcite crystal surface.

Partition power functions can be used to model the change in the Mg/Ca of various biotic and abiotic calcite phases in response to secular variation in seawater Mg/Ca. From this it is noted that during times of high ocean Mg/Ca, the range in calcite Mg/Ca among all phases is great (0 to 180 mmol/mol) as is the average calcite Mg/Ca (~85 mmol/mol). During times of low seawater Mg/Ca, the range and average are much less (0 to 40 and ~25 mmol/mol respectively). This implies that there is a secular variation in the potential for diagenesis based on the stabilization of metastable high-Mg calcite.

Calcite Mg/Ca has also been utilized as a thermometer of paleoceans. Applying this methodology to recent geologic history when seawater Mg/Ca was negligibly different from the modern value is straightforward as the thermometer has been calibrated against modern calcites that have precipitated from seawater of differing temperatures. However, when applied to more ancient calcites, those older than 2 My, one must take into account secular variation in seawater Mg/Ca. A revised method to account for this phenomenon is suggested by combining a partition power function with a modern temperature calibration to produce a "Mg-T partition function." Previous attempts at deep-time Mg/Ca paleothermometry have all concluded that little to no change in oceanic Mg/Ca could have occurred over the last 50 My if they are to produce reasonable trends in ocean temperatures and seawater $\delta^{18}O$. This is at odds with geochemical data from evaporite

fluid inclusions and echinoderm calcite, which show variation from about 1 to 5.2 mol/mol Mg/Ca over this interval. Using the Mg-T partition function described here, reasonable paleotemperature and seawater $\delta^{18}O$ trends can be obtained while still accommodating secular variation in seawater Mg/Ca which is independently supported by other geochemical proxy data. When a Mg-T partition function is employed using modeled changes in seawater Mg/Ca, the paleotemperature trend is ~1.5°C higher than that currently proposed, and thus implies a greater degree of deep ocean cooling over the Cenozoic. In a similar fashion, the δ_W trend is ~0.5‰ more positive than currently estimated, which argues for persistent continental ice volume throughout the Cenozoic, for a major buildup of continental ice beginning in the Mid-Eocene, and a major, but not total, deglaciation in the Late Oligocene to Early Miocene.

Appendices

Appendix 1: Geochemical data collected for Chapter 2 at Muleshoe Mound, Sacramento Mountains, Alamogordo, NM, USA.

Column	*Description*
A	Sample ID
B	Site ID
C	UTM Easting (in meters)
D	UTM Northing (in meters)
E	Elevation (in meters)
F	Sample Category
G	Luminescence character (L=luminescent, NL=non-luminescent, VL=variably luminescent)
H	$\delta^{13}C$ (in ‰ VPDB)
I	$\delta^{18}O$ (in ‰ VPDB)
J	Mg/Ca (in mmol/mol)
K	Sr/Ca (in mmol/mol)
L	Fe/Ca (in mmol/mol)
M	Mn/Ca (in mmol/mol)

Cave cement samples (CC-A through -E) were graciously provided by Tracy Frank, University of Nebraska-Lincoln

A	B	C	D	E	F	G	H	I	J	K	L	M
Sample	Site	EAST	NORTH	ELEV	CAT	LUM	$\delta^{13}C$	$\delta^{18}O$	Mg/Ca	Sr/Ca	Fe/Ca	Mn/Ca
01-1	F03	413705	3629109	1573	Bulk Crinoid		4.5	-1.3	9.54		0.39	0.04
01-2	F03	413705	3629109	1573	Bulk Crinoid		4.2	-2.2	7.80		0.33	0.09
02-1	F04	413825	3629282	1619	Bulk Crinoid		4.8	-1.7	11.25		0.77	0.14
02-2	F04	413825	3629282	1619	Bulk Crinoid		4.7	-2.2	8.26		0.28	0.05
03-1	F08	413818	3629090	1648	Bulk Crinoid		4.5	-2.7	6.50		0.72	0.34
03-2	F08	413818	3629090	1648	Bulk Crinoid		4.8	-2.6	7.12		0.39	0.18
05y-1	F10	413855	3629071	1632	Bulk Crinoid		4.9	-2.3	6.17		1.27	0.37
05y-2	F10	413855	3629071	1632	Bulk Crinoid		4.9	-2.4	7.20		0.52	0.84
06-1	F11	413844	3629070	1638	Bulk Crinoid		4.6	-4.0	43.90		2.96	0.30
07-1	F13	413833	3629137	1651	Bulk Crinoid		4.8	-2.5	35.53		1.73	0.20
07-2	F13	413833	3629137	1651	Bulk Crinoid		4.2	-5.2	44.09		2.79	0.51
08a-1	F14	413906	3629190	1649	Bulk Crinoid		4.5	-2.8	6.52		0.66	0.26
08B-1	F14	413906	3629190	1649	Bulk Crinoid		5.0	-2.0	8.64		1.29	0.45
08B-2	F14	413906	3629190	1649	Bulk Crinoid		4.9	-2.0	7.47		0.94	0.10
09-1	F15	413981	3629165	1619	Bulk Crinoid		5.1	-2.3	9.86		1.10	0.13
09-2	F15	413981	3629165	1619	Bulk Crinoid		5.2	-2.6	7.30		0.32	0.12
10-1	F16	414016	3629075	1579	Bulk Crinoid		4.2	-2.4	6.36		0.36	0.50
10-2	F16	414016	3629075	1579	Bulk Crinoid		4.1	-2.9	9.10		0.49	0.50
11-1	F17	414081	3629053	1566	Bulk Crinoid		4.4	-2.5	11.57		2.23	0.26
11-2	F17	414081	3629053	1566	Bulk Crinoid		4.3	-3.3	9.40		0.54	0.16
13-1	F19	414084	3629030	1553	Bulk Crinoid		3.8	-2.2	7.26		2.88	0.10
13-2	F19	414084	3629030	1553	Bulk Crinoid		3.7	-3.4	13.05		0.68	0.23
32-1	H18	413852	3628934	1507	Bulk Crinoid		4.9	-2.0	10.98		1.31	0.12
01-3	F03	413705	3629109	1573	Micrite		3.9	-3.0	13.43		1.75	0.34
02-3	F04	413825	3629282	1619	Micrite		4.8	-1.6	10.25		0.45	0.29
03-3	F08	413818	3629090	1648	Micrite		4.7	-3.7	6.86		6.88	0.39
04-1	F09	413823	3629079	1646	Micrite		4.9	-2.0	12.31		2.43	0.18
04-2	F09	413823	3629079	1646	Micrite		4.9	-2.1	12.36		0.80	0.14
04-3	F09	413823	3629079	1646	Micrite		4.3	-4.6	8.17		1.54	1.98
05x-1	F10	413855	3629071	1632	Micrite		4.1	-4.9	6.95		1.73	0.63
05y-3	F10	413855	3629071	1632	Micrite		4.2	-3.4	8.59		0.87	1.07
05y-4	F10	413855	3629071	1632	Micrite		4.0	-4.7	23.23		2.16	0.68
06-2	F11	413844	3629070	1638	Micrite		4.4	-5.2	8.18		1.10	0.48

A	B	C	D	E	F	G	H	I	J	K	L	M
07-3	F13	413833	3629137	1651	Micrite		4.2	-5.6	10.65		1.24	0.38
08B-3	F14	413906	3629190	1649	Micrite		2.2	-7.0	85.55		49.94	2.20
09-3	F15	413981	3629165	1619	Micrite		4.4	-3.3	7.42		0.96	0.70
10-3	F16	414016	3629075	1579	Micrite		0.3	-2.6	6.71		0.45	7.70
12-1	F18	414095	3629042	1561	Micrite		3.0	-4.1	102.19		6.08	0.80
32-2	H18	413852	3628934	1507	Micrite		4.9	-3.6	7.57		0.69	0.24
32-3	H18	413852	3628934	1507	Micrite		4.7	-2.4	10.09		0.27	0.17
20L-3	H06	413740	3629122	1644	Bryozoan	L	3.5	-5.4	4.87	0.18	2.03	0.48
301-4	H16	413914	3629002	1537	Bryozoan	L	3.9	-4.2	9.02	0.18	0.73	0.41
131-1	F19	414084	3629030	1553	Bryozoan	NL	3.3	-4.2	5.74	0.12	0.57	0.43
131-7	F19	414084	3629030	1553	Bryozoan	NL	3.6	-2.7	6.62	0.13	0.22	0.34
CC-A					Cave Cement		-8.1	-3.0	0.61	0.010	-0.06	0.04
CC-B					Cave Cement		-9.4	-3.1	0.61	0.005	0.23	0.01
CC-C					Cave Cement		-9.0	-3.7	0.62	0.008	0.19	0.05
CC-D					Cave Cement		-8.1	-3.3	1.16	0.017	1.56	0.23
CC-E					Cave Cement		-8.3	-3.0	0.59	0.008	0.27	0.05
21AU-A	H07	413765	3629142	1651	Brachiopod-filling cement		4.1	-7.0	7.72	0.31	3.93	0.66
21AU-B	H07	413765	3629142	1651	Brachiopod-filling cement		3.2	-6.7	413.52	0.14	132.15	3.47
21AU-C	H07	413765	3629142	1651	Brachiopod-filling cement		3.9	-7.7	11.90	0.22	1.69	0.61
21AU-D	H07	413765	3629142	1651	Brachiopod-filling cement		5.0	-6.5	634.96	0.13	75.44	3.61
012-3	F18	414095	3629042	1561	Cement	L	3.0	-6.7				
16L-3A	H02	413546	3629039	1740	Cement	L	4.4	-2.8	20.32	0.326	0.18	2.23
23L-3	H09	413807	3629162	1655	Cement	L	4.0	-4.4	9.93	0.248	0.42	0.22
25U-2B	H11	413832	3629073	1645	Cement	L	3.9	-4.7	7.34	0.150	1.50	0.32
25U-3B	H11	413832	3629073	1645	Cement	L	4.1	-4.2	7.95	0.153	1.33	0.34
071-1	F13	413833	3629137	1651	Cement	NL	4.0	-5.6	17.51	0.246	1.70	0.11
071-2	F13	413833	3629137	1651	Cement	NL	3.9	-5.9	13.16	0.198	0.97	0.10
071-3	F13	413833	3629137	1651	Cement	NL	4.0	-5.6	14.21	0.215	1.33	0.09
072-1	F13	413833	3629137	1651	Cement	NL	4.3	-4.5	15.09	0.270	0.56	0.10
072-2	F13	413833	3629137	1651	Cement	NL	4.3	-4.6	16.19	0.281	0.71	0.11
16L-1	H02	413546	3629039	1740	Cement	NL	4.5	-4.5	9.57	0.305	0.68	0.16
16L-2	H02	413546	3629039	1740	Cement	NL	4.6	-3.4	12.81	0.364	0.28	0.12
16L-3B	H02	413546	3629039	1740	Cement	NL	4.6	-3.0	17.10	0.330	0.21	0.21
16U-1	H02	413546	3629039	1740	Cement	NL	4.4	-4.5	10.34	0.254	0.84	0.18
18L-2	H04	413735	3629133	1646	Cement	NL	4.9	-1.9	11.20	0.194	0.15	0.11

A	B	C	D	E	F	G	H	I	J	K	L	M
18L-3	H04	413735	3629133	1646	Cement	NL	4.8	-2.5	12.97	0.206	0.22	0.12
18U-6	H04	413735	3629133	1646	Cement	NL	4.9	-2.3	10.84	0.22	0.18	0.08
23L-1	H09	413807	3629162	1655	Cement	NL	2.3	-4.4	8.38	0.198	0.98	0.15
25L-1	H11	413832	3629073	1645	Cement	NL	5.0	-1.7	9.04	0.174	0.22	0.12
25L-2	H11	413832	3629073	1645	Cement	NL	4.9	-1.3	9.96	0.185	0.19	0.16
25U-2	H11	413832	3629073	1645	Cement	NL	5.1	-1.9	8.75	0.160	0.10	0.15
25U-2A	H11	413832	3629073	1645	Cement	NL	5.0	-2.3	10.53	0.158	5.53	0.26
25U-3A	H11	413832	3629073	1645	Cement	NL	4.8	-2.8	8.82	0.151	0.41	0.20
27L-1	H13	413835	3629088	1649	Cement	NL	4.6	-4.5	10.43	0.226	0.76	0.23
27L-2	H13	413835	3629088	1649	Cement	NL	4.8	-4.3	9.87	0.236	1.67	0.20
27L-3	H13	413835	3629088	1649	Cement	NL	4.8	-4.6	11.15	0.230	0.50	0.11
27L-5	H13	413835	3629088	1649	Cement	NL	4.8	-4.3	11.21	0.232	0.15	0.10
27U-1	H13	413835	3629088	1649	Cement	NL	4.6	-5.6	10.64	0.213	0.69	0.14
27U-2	H13	413835	3629088	1649	Cement	NL	4.8	-4.6	21.58	0.269	7.67	0.14
27U-3	H13	413835	3629088	1649	Cement	NL	4.7	-5.0	12.25	0.238	0.42	0.11
27U-4	H13	413835	3629088	1649	Cement	NL	4.8	-4.8	10.68	0.218	0.55	0.13
28L-1	H14	413833	3629127	1651	Cement	NL	3.8	-5.3	12.37	0.173	2.02	0.13
28L-2	H14	413833	3629127	1651	Cement	NL	3.7	-5.6	11.86	0.171	2.05	0.15
28L-3	H14	413833	3629127	1651	Cement	NL	3.8	-6.0	8.72	0.199	1.92	0.24
28U-1	H14	413833	3629127	1651	Cement	NL	3.8	-6.0	9.08	0.159	1.98	0.24
28U-2	H14	413833	3629127	1651	Cement	NL	4.0	-5.7	13.19	0.185	1.27	0.11
28U-3	H14	413833	3629127	1651	Cement	NL	4.2	-5.6	13.24	0.182	1.08	0.10
321-1	H18	413852	3628934	1507	Cement	NL	4.9	-2.3	8.35	0.152	0.33	0.12
321-2	H18	413852	3628934	1507	Cement	NL	5.1	-2.1	12.36	0.146	2.95	0.46
321-3	H18	413852	3628934	1507	Cement	NL	5.0	-2.4	8.17	0.144	0.21	0.11
011-2	F03	413705	3629109	1573	Syntaxial Cement	NL	5.0	-0.6	11.07	0.23	0.98	0.08
091-1S	F15	413981	3629165	1619	Syntaxial Cement		5.1	-0.8	6.84	0.12	3.07	0.16
092-3S	F15	413981	3629165	1619	Syntaxial Cement		4.3	-1.9	6.74	0.14	0.50	0.24
18U-2	H04	413735	3629133	1646	Syntaxial Cement	NL	3.8	-8.1	4.78	0.12	2.21	0.48
131-2	F19	414084	3629030	1553	Dull Cement	L			3.61	0.14	2.06	0.91
071-1	F13	413833	3629137	1651	Crinoid	L	4.3	-4.0	25.15	0.29	0.86	1.54
071-2	F13	413833	3629137	1651	Crinoid	L	4.3	-4.2	22.51	0.26	1.17	1.75
091-2	F15	413981	3629165	1619	Crinoid (Core)	L	4.9	-2.6	9.50	0.16	54.43	1.00
092-2	F15	413981	3629165	1619	Crinoid	L	4.7	-1.7	9.98	0.15	0.42	1.82
101-4	F16	414016	3629075	1579	Crinoid (Rim)	L	0.9	-2.7	6.64	0.16	1.08	7.22

A	B	C	D	E	F	G	H	I	J	K	L	M
101-6	F16	414016	3629075	1579	Crinoid	L	-1.2	-3.0	5.45	0.16	0.25	13.12
111-2	F17	414081	3629053	1566	Crinoid	L	4.2	-2.5	11.07	0.26	0.39	1.04
111-4	F17	414081	3629053	1566	Crinoid (Rim)	L	4.1	-2.7	10.94	0.32	0.44	0.53
15-1	H01	413778	3629149	1658	Crinoid	L	4.6	-3.4	18.16	0.28	0.61	1.59
18U-1	H04	413735	3629133	1646	Crinoid	L	4.6	-3.3	8.87	0.27	0.51	1.52
18U-4	H04	413735	3629133	1646	Crinoid	L	4.6	-2.4	14.88	0.28	0.61	0.43
19-3	H05	413734	3629122	1633	Crinoid (Rim)	L	4.5	-3.5	17.95	0.29	0.55	0.19
19-5	H05	413734	3629122	1633	Crinoid (Rim)	L	4.6	-4.6	11.36	0.20	0.67	1.12
20L-2	H06	413740	3629122	1644	Crinoid (Edge)	L	4.5	-3.3	17.70	0.26	0.53	0.47
20L-6	H06	413740	3629122	1644	Crinoid (Small)	L	2.0	-4.4				
31AU-5	H17	413885	3628960	1514	Crinoid (Core, small)	L	4.5	-2.4	10.69	0.19	0.28	0.95
31BU-3	H17	413885	3628960	1514	Crinoid	L	4.0	-2.6	10.77	0.19	0.25	1.99
31BU-8	H17	413885	3628960	1514	Crinoid	L	3.2	-3.2	12.58	0.25	0.37	2.18
011-1	F03	413705	3629109	1573	Crinoid	NL	4.3	-1.6	10.88	0.16	0.21	0.04
012-2	F03	413705	3629109	1573	Crinoid	NL	4.3	-1.8	11.34	0.18	0.39	0.04
092-1R	F15	413981	3629165	1619	Crinoid (Right)	NL	5.2	-2.0	9.63	0.16	0.21	0.11
101-5	F16	414016	3629075	1579	Crinoid (Core)	NL	4.1	-2.4	10.45	0.16	0.44	0.90
101-7	F16	414016	3629075	1579	Crinoid	NL	4.4	-1.7	7.74	0.11	0.19	0.29
111-1	F17	414081	3629053	1566	Crinoid	NL	4.4	-2.8	10.52	0.24	0.17	0.15
111-3	F17	414081	3629053	1566	Crinoid (Core)	NL			13.08	0.23	0.50	0.27
131-3	F19	414084	3629030	1553	Crinoid	NL	3.8	-2.8	5.85	0.10	0.28	0.13
131-4	F19	414084	3629030	1553	Crinoid	NL	3.5	-2.4				
131-5	F19	414084	3629030	1553	Crinoid	NL	3.0	-3.0	7.36	0.11	0.47	0.28
131-6	F19	414084	3629030	1553	Crinoid	NL	3.7	-2.7	6.59	0.11	0.51	0.21
15-2	H01	413778	3629149	1658	Crinoid	NL	4.6	-4.8	40.53	0.39	0.63	0.10
15-3	H01	413778	3629149	1658	Crinoid	NL	4.5	-3.2	16.73	0.28	0.75	0.11
15-4	H01	413778	3629149	1658	Crinoid	NL	4.4	-3.9	33.31	0.37	1.22	0.16
19-2	H05	413734	3629122	1633	Crinoid (Core)	NL	4.7	-2.7	17.47	0.22	0.37	0.08
19-4	H05	413734	3629122	1633	Crinoid	NL	5.1	-2.6	10.29	0.18	0.32	0.07
19-6	H05	413734	3629122	1633	Crinoid (Core)	NL	4.4	-4.3	25.45	0.22	1.19	0.21
20L-1	H06	413740	3629122	1644	Crinoid (Core)	NL	4.6	-3.4	17.41	0.23	0.52	0.12
20L-4	H06	413740	3629122	1644	Cement	NL	3.8	-5.0	11.30	0.19	1.56	0.21
20L-9	H06	413740	3629122	1644	Crinoid	NL	3.9	-5.0				
301-1	H16	413914	3629002	1537	Crinoid	NL	4.2	-2.8	15.56	0.22	0.31	0.11
31AU-1L	H17	413885	3628960	1514	Crinoid (Lower)	NL	4.2	-2.2	10.75	0.18	0.40	0.19

A	B	C	D	E	F	G	H	I	J	K	L	M
31AU-1U	H17	413885	3628960	1514	Crinoid (Upper)	NL	4.7	-2.2	11.40	0.20	4.61	0.20
31AU-2R	H17	413885	3628960	1514	Crinoid (Rectangular)	NL	4.2	-4.0	8.34	0.18	0.34	0.17
31AU-2T	H17	413885	3628960	1514	Crinoid (Triangular)	NL	4.8	-3.0	17.72	0.23	0.31	0.10
31AU-3	H17	413885	3628960	1514	Crinoid (Small)	NL	4.3	-2.5	11.21	0.21	0.28	0.26
31AU-4	H17	413885	3628960	1514	Crinoid	NL	4.1	-3.2	11.03	0.22	0.22	0.27
31AU-6	H17	413885	3628960	1514	Crinoid (Rim, small)	NL	4.3	-2.8	11.89	0.24	0.31	0.32
31BU-1	H17	413885	3628960	1514	Crinoid	NL	4.6	-2.6	12.27	0.20	0.20	0.17
31BU-2	H17	413885	3628960	1514	Crinoid	NL	4.7	-2.5	11.21	0.17	0.30	0.14
31BU-4	H17	413885	3628960	1514	Crinoid	NL	4.4	-3.1	15.31	0.21	0.21	0.15
31BU-5L	H17	413885	3628960	1514	Crinoid (Left)	NL	4.5	-2.9	12.00	0.21	0.21	0.18
31BU-5R	H17	413885	3628960	1514	Crinoid (Right)	NL	4.6	-2.8	15.56	0.24	0.39	0.17
31BU-7	H17	413885	3628960	1514	Crinoid	NL	4.5	-2.9	12.76	0.22	0.44	0.17
031-2	F08	413818	3629090	1648	“Tiger” Crinoid	VL	4.9	-2.2	9.38	0.18	0.36	0.08
031-3	F08	413818	3629090	1648	“Tiger” Crinoid	VL	4.9	-2.0	9.37	0.18	1.71	0.06
071-3L	F13	413833	3629137	1651	“Tiger” Crinoid (Left)	VL	4.2	-4.8	45.11	0.28	2.12	0.19
071-3R	F13	413833	3629137	1651	“Tiger” Crinoid (Right)	VL	4.1	-5.1	40.52	0.29	2.85	0.23
091-1C1	F15	413981	3629165	1619	“Tiger” Crinoid (Right)	VL	5.1	-2.7	9.22	0.15	0.43	0.11
091-1C2	F15	413981	3629165	1619	“Tiger” Crinoid (Left)	VL	5.1	-2.3	10.84	0.18	0.30	0.10
091-3L	F15	413981	3629165	1619	“Tiger” Crinoid (Lower)	VL	5.2	-1.9	10.00	0.15	0.38	0.09
091-3U	F15	413981	3629165	1619	“Tiger” Crinoid (Upper)	VL	5.1	-1.8	10.27	0.16	0.37	0.10
092-3C	F15	413981	3629165	1619	“Tiger” Crinoid	VL	5.2	-2.0	9.29	0.16	0.21	0.07
17AU-1	H03	413751	3629129	1661	“Tiger” Crinoid	VL	4.7	-4.6	29.85	0.20	1.04	0.12
17AU-2	H03	413751	3629129	1661	“Tiger” Crinoid	VL	4.7	-5.5	26.60	0.22	0.80	0.10
17AU-3	H03	413751	3629129	1661	“Tiger” Crinoid	VL	4.5	-6.4	31.99	0.28	1.03	0.13
17AU-4	H03	413751	3629129	1661	“Tiger” Crinoid	VL	4.7	-4.9	27.22	0.24	1.24	0.10
17B-1	H03	413751	3629129	1661	“Tiger” Crinoid	VL	4.9	-5.9	29.18	0.25	1.02	0.11
17B-2	H03	413751	3629129	1661	“Tiger” Crinoid	VL	4.8	-5.6	39.28	0.16	1.45	0.10
17B-3	H03	413751	3629129	1661	“Tiger” Crinoid	VL	4.8	-3.2	29.54	0.24	1.40	0.12
17B-4	H03	413751	3629129	1661	“Tiger” Crinoid	VL	4.8	-4.8	50.57	0.19	1.47	0.09
18U-3	H04	413735	3629133	1646	“Tiger” Crinoid	VL	4.6	-3.5	18.61	0.21	0.52	0.14
18U-5	H04	413735	3629133	1646	“Tiger” Crinoid	VL	4.6	-3.5	10.67	0.22	0.75	0.16
19-1	H05	413734	3629122	1633	“Tiger” Crinoid	VL	4.5	-3.6	8.78	0.21	0.45	0.13
8A1-1	F14	413906	3629190	1649	“Tiger” Crinoid	VL	4.4	-2.2	7.68	0.16	1.01	0.34
8A1-2	F15	413981	3629165	1619	“Tiger” Crinoid	VL	4.8	-2.3				
8A1-3	F16	414016	3629075	1579	“Tiger” Crinoid	VL	4.5	-2.2				

A	B	C	D	E	F	G	H	I	J	K	L	M
8A1-5	F17	414081	3629053	1566	“Tiger” Crinoid	VL	4.8	-1.8	7.85	0.14	0.36	0.13
301-2	H16	413914	3629002	1537	Crinoid	VL	4.6	-2.2	13.25	0.22	0.29	0.30
322-1	H18	413852	3628934	1507	Crinoid	VL	4.8	-1.8	13.90	0.20	0.21	0.06
322-2	H18	413852	3628934	1507	Crinoid	VL	4.9	-2.1	9.90	0.17	0.23	0.09
322-3	H18	413852	3628934	1507	Crinoid	VL	4.8	-3.2	10.26	0.15	0.25	0.10
092-1L	F15	413981	3629165	1619	Crinoid (Left)	VL	5.1	-1.9	8.80	0.14	0.25	0.14
31BU-6	H17	413885	3628960	1514	Crinoid	VL	4.5	-1.9	10.54	0.17	0.13	0.33
031-1	F08	413818	3629090	1648	Brachiopod	NL	3.5	-2.8	4.22	0.83	2.63	0.27

Appendix 2: Echinoderm skeletal chemistry data from Dickson (2004).

Column	*Description*
A	Sample Number
B	
C	Fe (in weight %)
D	Mn (in weight %)
E	Ca (in weight %)
F	Mg (in weight %)
G	$MgCO_3$ (in mole %)
H	Seawater Mg/Ca (in mol/mol)
I	Mg/Ca (in mmol/mol), calculated for this dissertation
J	Fe/Ca (in mmol/mol), calculated for this dissertation
K	Mn/Ca (in mmol/mol), calculated for this dissertation
L	Sample designation
M	Number Analyzed
N	Stage
O	Median Age of Stage (in Ma)
P	Paleolatitude (in degrees), estimated using ‘‘Time Trek-4’’ (Cambridge Paleomap Services Ltd.)

Sample Designations	*Full name*
B. solentois	*Balanocrinus solentois*
E. esculentus	*Echinus esculentus*
L. multi	*Lepidocrinus multi*
Agassiz.	*Agassizocrinus*
Archaeocid.	*Archaeocidaris and crinoid*
E. cassianus	*Encrinurus cassianus*

A	B	C	D	E	F	G	H	I	J	K	L	M	N	O	P
E.e				35.7	1.50	6.1	1.8	57.3			*E. esculentus*			0	
10	a		0.14	38.0	0.84	3.4	0.9	28.6		2.7	Crinoid	2	Albian	100	41°
10	b		0.19	38.5	0.85	3.5	0.9	28.6		3.6	Crinoid	2	Albian	100	41°
61	a			37.5	0.91	3.7	1.0	31.8			Crinoid	2	Callovian	164	39°
32	b			35.8	1.01	4.1	1.2	38.2			Crinoid	2	Bathonian	166	36°
61	b			38.2	1.06	4.3	1.2	38.2			Crinoid	2	Callovian	164	39°
29	a			37.5	1.07	4.4	1.2	38.2			*B. solentois*	3	Oxfordian	156	32°
94	a			37.9	1.07	4.4	1.2	38.2			Crinoid	2	Sinemurian	200	32°
94	b			37.8	1.80	4.4	1.2	38.2			Crinoid	2	Sinemurian	200	32°
29	c			37.6	1.10	4.5	1.3	41.4			*B. solentois*	3	Oxfordian	156	32°
47	a			37.5	1.13	4.6	1.3	41.4			*B. solentois*	2	Domerian	184	40°
76	c			37.8	1.16	4.7	1.3	41.4			Crinoid	3	Osagian	354	-24°
77	b			37.7	1.17	4.8	1.3	41.4			Crinoid	2	Osagian	354	-18°
29	b			37.6	1.19	4.9	1.4	44.5			*B. solentois*	3	Oxfordian	156	32°
101	a			36.9	1.20	4.9	1.4	44.5			Crinoid	2	Pleinsbachian	192	39°
77	a			38.0	1.20	4.9	1.3	41.4			Crinoid	2	Osagian	354	-18°
32	a			35.5	1.22	5.0	1.5	47.7			Crinoid	2	Bathonian	166	36°
38	a			36.6	1.24	5.0	1.5	47.7			Crinoid	3	Pliensbachian	190	36°
17	b			37.0	1.25	5.1	1.5	47.7			Crinoid	2	Kimmeridgian	152	29°
62	a			35.5	1.28	5.2	1.5	47.7			Crinoid	3	Ypresian	53	47°
62	b	0.59		35.4	1.28	5.2	1.6	50.9	12.2		Crinoid	3	Ypresian	53	47°
17	a			37.2	1.30	5.3	1.5	47.7			Crinoid	2	Kimmeridgian	152	29°
38	b			36.7	1.31	5.3	1.5	47.7			Crinoid	3	Pliensbachian	190	36°
47	b			36.7	1.31	5.4	1.6	50.9			*B. solentois*	2	Domerian	184	40°
101	b			36.9	1.33	5.4	1.5	47.7			Crinoid	2	Pleinsbachian	192	39°
66	b			39.1	1.35	5.5	1.5	47.7			Crinoid	2	Osagian	354	-18°
76	b			37.4	1.36	5.5	1.6	50.9			Crinoid	3	Osagian	354	-24°
76	a			37.8	1.38	5.6	1.6	50.9			Crinoid	3	Osagian	354	-24°
66	a			38.1	1.47	6.0	1.7	54.1			Crinoid	2	Osagian	354	-18°
38	c			36.8	1.49	6.1	1.8	57.3			Crinoid	3	Pliensbachian	190	36°
34	a	0.23		37.5	1.49	6.1	1.7	54.1	4.5		Crinoid	2	Hastarian	350	-9°
39	b	0.29		36.3	1.52	6.2	1.7	54.1	5.8		Isocrinus	2	Hauterivian	130	37°

A	B	C	D	E	F	G	H	I	J	K	L	M	N	O	P
39	a			36.7	1.54	6.3	1.8	57.3			Isocrinus	2	Hauterivian	130	37°
104	d			37.7	1.64	6.7	1.9	60.5			Crinoid	7	Telychian	432	-12°
62	c			37.3	1.65	6.7	1.9	60.5			Crinoid	3	Ypresian	53	47°
104	g			37.7	1.69	6.9	1.9	60.5			Crinoid	7	Telychian	432	-12°
104	f			38.0	1.69	6.9	1.9	60.5			Crinoid	7	Telychian	432	-12°
104	a			38.5	1.74	7.0	1.9	60.5			Crinoid	7	Telychian	432	-12°
68	b			37.5	1.77	7.2	2.0	63.6			Crinoid	2	Visean	330	-1°
68	a			37.9	1.79	7.3	2.0	63.6			Crinoid	2	Visean	330	-1°
34	b	0.15		37.2	1.83	7.4	2.1	66.8	2.9		Crinoid	2	Hastarian	350	-9°
83	a			37.0	1.90	7.7	2.2	70.0			Crinoid	2	Artinskian	260	-37°
41	b			37.0	1.93	7.8	2.2	70.0			Crinoid	3	Brigantian	330	7°
104	c			37.5	1.95	7.9	2.2	70.0			Crinoid	7	Telychian	432	-12°
104	e			37.8	2.02	8.2	2.3	73.2			Crinoid	7	Telychian	432	-12°
41	a			37.3	2.03	8.2	2.3	73.2			Crinoid	3	Brigantian	330	7°
26	a			37.2	2.05	8.3	2.4	76.4			*L. multi*	1	M. Devonian	385	-8°
83	b			36.8	2.09	8.5	2.5	79.6			Crinoid	2	Artinskian	260	-37°
104	b			38.6	2.11	8.6	2.4	76.4			Crinoid	7	Telychian	432	-12°
41	c			36.8	2.19	8.9	2.6	82.7			Crinoid	3	Brigantian	330	7°
70	a			37.4	2.22	9.0	2.6	82.7			Agassiz.	2	Chesterian	326	-7°
103	a			36.9	2.37	9.6	2.8	89.1			Crinoid	3	Amsbergian	325	-13°
97	a			37.4	2.38	9.6	2.9	92.3			Crinoid	1	Wordian	253	-4°
98	a			37.5	2.45	9.9	2.8	89.1			Crinoid	1	Virgilian	291	-4°
102	a	0.13		35.9	2.50	10.1	3.0	95.5	2.6		*Archaeocid.*	7	Virgilian	292	-3°
102	c			36.1	2.55	10.3	3.0	95.5			*Archaeocid.*	7	Virgilian	292	-3°
30	b	0.18	0.2	35.3	2.56	10.3	3.1	98.6	3.7	4.1	Crinoid	3	Botomian	518	18°
30	c	0	0.18	35.7	2.61	10.6	3.2	101.8		3.7	Crinoid	3	Botomian	518	18°
70	b			37.6	2.64	10.7	2.5	79.6			*Agassiz.*	2	Chesterian	326	-7°
102	d			36.0	2.69	10.9	3.2	101.8			*Archaeocid.*	7	Virgilian	292	-3°
102	e			36.7	2.73	11.0	3.2	101.8			*Archaeocid.*	7	Virgilian	292	-3°
30	a	0.16	0.18	35.4	2.73	11.0	3.4	108.2	3.3	3.7	Crinoid	3	Botomian	518	18°
102	b			35.3	2.78	11.2	3.4	108.2			*Archaeocid.*	7	Virgilian	292	-3°
102	f			35.2	2.81	11.3	3.4	108.2			*Archaeocid.*	7	Virgilian	292	-3°

A	B	C	D	E	F	G	H	I	J	K	L	M	N	O	P
90	a			36.2	2.82	11.4	3.4	108.2			*E. cassianus*	2	Norian	220	25°
93	a			36.6	2.87	11.6	3.4	108.2			Crinoid	1	Virgilian	292	-3°
103	b			36.2	2.87	11.6	3.4	108.2			Crinoid	3	Amsbergian	325	-13°
102	g			34.9	2.88	11.6	3.6	114.6			*Archaeocid.*	7	Virgilian	292	-3°
90	b			37.0	2.96	11.9	3.4	108.2			*E. cassianus*	2	Norian	220	25°
103	c			36.1	2.98	12.0	3.6	114.6			Crinoid	3	Amsbergian	325	-13°
99	a			36.2	3.11	12.5	3.7	117.7			Crinoid	1	Desmoinesian	297	-3°

Appendix 3: Marine Cement data used to construct Figure 3-6. Bold values indicate original units in which the data were reported. All were subsequently converted to molar ratios.

Period	Formation	Age	$MgCO_3$ (mol%)	Mg (ppm)	Cement Mg/Ca (mmol/mol)	Seawater Mg/Ca[1] (mol/mol)	Seawater Mg/Ca[2] (mol/mol)	Reference
Holocene	Enewetak	0.01			**174.8**	15.59	5.83	(Carpenter and 1991)
Pliocene	Hope Gate Fm	2	**13.7**		158.7	13.53	5.14	(Frank et al., 1996)
Lo Miocene	Enewetak	20.4	**3.2**		33.1	1.35	0.67	(Saller, 1986)
Cretaceous	Scapa Mbr, North Sea	133	**2**		20.4	0.66	0.36	(Hendry et al., 1996)
Jurassic	Torrecillia en Cameros Fm	154	**1.3**		13.2	0.35	0.20	(Benito et al., 2005)
Jurassic	Lincolnshire Ls	169	**2.39**		24.5	0.87	0.45	(Marshall and Ashton, 1980)
Jurassic	Lower Lias, Europe	199	**1.54**		15.6	0.45	0.25	(Mazzullo et al., 1990)
Triassic	Cozzo di Lupo Fm	212			**25.1**	0.90	0.47	(Cicero and Lohmann, 2001)
Permian	Permian Reef (Cements)	263			**16.9**	0.50	0.28	(Smith, 2005)
Permian	Permian Reef (Cements)	263		**4500**	18.8	0.59	0.32	(Rahnis, 1995)
Pennsylvanian	Cements (Can. Arctic)	308	**1.6**		16.3	0.48	0.27	(Davies, 1977)
Pennsylvanian	Crinoids (Can. Arctic)	308	**1.5**		15.2	0.43	0.24	(Davies, 1977)
Pennsylvanian	Cement (Holder Fm)	315		**2951**	12.3	0.32	0.19	(Rasbury et al., 2004)
Mississippian	Irish Waulsortian (Cements)	340			**9.0**	0.20	0.12	(Douthit, 1990)
Mississippian	Lake Valley Fm	345			**11.0**	0.27	0.16	*Chapter 2, This Dissertation*
Mississippian	Lake Valley Fm (Cements)	345			**18.0**	0.55	0.30	(Lohmann and Meyers, 1977)
Devonian	Golden Spike Reef	370	2.6	**6271**	26.2	0.96	0.49	(Carpenter and 1991)
Devonian	Nevis Reef	370	2.8	**6655**	27.8	1.04	0.53	(Carpenter and 1991)
Devonian	Virgin Hills Reef	380	4.9	**12048**	50.3	2.50	1.16	(Carpenter and 1991)
Silurian	Pipe Creek Jr Quarry	417			**6.0**	0.11	0.07	(Cicero and Lohmann, 2001)
Silurian	Gaspé Peninsula, Quebec	420		**14171**	59.2	3.17	1.43	(Bourque and Raymond, 1994)
Ordovician	Boda (Sweden)	443	**3.0**		30.9	1.22	0.61	(Tobin and Walker, 1997)
Ordovician	Kullsberg (Sweden)	454	**4.5**		47.1	2.27	1.06	(Tobin and Walker, 1997)
Ordovician	Alcoa Hwy, Holston Fm (Tennessee, USA)	457	**1.3**		13.2	0.35	0.20	(Tobin et al., 1996)
Ordovician	Effna Ls (Virginia, USA)	457	**2.5**		25.6	0.92	0.48	(Tobin and Bergstrom, 2002)
Ordovician	Dean Quarry, Holston Fm (Tennessee, USA)	457	**2.5**		25.6	0.92	0.48	(Tobin and Walker, 1997)
Cambrian	Forteau	515	**1.6**		16.3	0.48	0.27	(Whittaker et al., 1994)
Cambrian	Wilkawillina	522	**1.9**		19.4	0.62	0.34	(Whittaker et al., 1994)
Cambrian	Pestrotsvet	529	**3.2**		33.1	1.35	0.67	(Whittaker et al., 1994)

Appendix 4: Benthic foraminiferal Mg/Ca and $\delta^{18}O$ data across the Eocene-Oligocene boundary used in Chapter 4.

	Title	*Units*	*Method*	*Reference*
A	Ord			
B	Genus_Species			
C	Age	(Ma)		
D	Mg/Ca, Uncorrected	(mmol/mol)		
E	Normalization Offset	(mmol/mol)		
F	Mg/Ca, Normalized	(mol/mol)		
G	Calcite $\delta^{18}O$	(‰ PDB)		Zachos et al. 1993
H	Calcite $\delta^{18}O$	(‰ PDB)		Zachos et al. 2001
I	Mg/Casw	(mol/mol)		Wilkinson and Algeo (1989)
J	Mg/Casw	(mol/mol)		Hardie (1996)
K	Temperature	(°C)	Lear00	(J)
L	Temperature	(°C)	Lear00	(K)
M	Temperature	(°C)	Lear02	(J)
N	Temperature	(°C)	Lear02	(K)
O	Temperature	(°C)	Diss	(J)
P	Temperature	(°C)	Diss	(K)
Q	Seawater $\delta^{18}O$	(‰ SMOW)	Lear00	(J)
R	Seawater $\delta^{18}O$	(‰ SMOW)	Lear00	(K)
S	Seawater $\delta^{18}O$	(‰ SMOW)	Lear02	(J)
T	Seawater $\delta^{18}O$	(‰ SMOW)	Lear02	(K)
U	Seawater $\delta^{18}O$	(‰ SMOW)	Diss	(J)
V	Seawater $\delta^{18}O$	(‰ SMOW)	Diss	(K)

Method	Mg Calib	Temp Calibration
1	Lear et al. (2000)	Rosenthal et al. (1997)
2	Lear et al. (2000)	Rosenthal et al. (1997)
3	Lear et al. (2000)	Lear et al. (2002)
4	Lear et al. (2000)	Lear et al. (2002)
5	Delaney et al. (1985)	Lear et al. (2002)
6	Delaney et al. (1985)	Lear et al. (2002)

OU	Oridiosalis umbonatus
CP	Cibicidoides praemundulus
NU	Nuttilides umbonifera

A	B	C	D	E	F	G	H	I	J	K	L	M	N	O	P	Q	R	S	T	U	V
1	OU	31.96	2.35	0.00	0.0024	2.26	2.48	4.0	1.8	9.2	17.0	9.9	16.8	8.4	11.3	0.07	2.01	0.45	2.18	0.10	0.82
2	OU	31.96	2.36	0.00	0.0024	2.26	2.48	4.0	1.8	9.2	17.0	9.9	16.8	8.5	11.4	0.08	2.02	0.46	2.18	0.11	0.83
3	OU	32.06	2.10	0.00	0.0021	2.11	2.48	4.0	1.8	8.1	15.9	8.9	15.8	7.5	10.4	-0.36	1.58	0.20	1.93	-0.15	0.58
4	OU	32.16	2.07	0.00	0.0021	2.41	2.50	4.0	1.8	8.0	15.7	8.7	15.6	7.3	10.2	-0.10	1.85	0.19	1.92	-0.16	0.56
5	OU	32.27	2.02	0.00	0.0020	2.45	2.51	4.0	1.8	7.7	15.8	8.5	15.7	7.1	10.1	-0.12	1.91	0.15	1.95	-0.20	0.55
6	OU	32.40	1.82	0.00	0.0018	2.51	2.51	4.0	1.8	6.7	14.8	7.7	14.8	6.2	9.2	-0.30	1.71	-0.07	1.72	-0.43	0.32
7	OU	32.50	2.05	0.00	0.0021	2.37	2.53	4.0	1.8	7.9	16.0	8.7	15.9	7.3	10.3	-0.15	1.86	0.21	2.00	-0.15	0.60
8	OU	32.61	2.37	0.00	0.0024	2.49	2.58	4.0	1.8	9.3	17.4	10.0	17.1	8.5	11.5	0.33	2.34	0.58	2.37	0.22	0.97
9	OU	32.64	2.08	0.00	0.0021	2.67	2.59	4.0	1.8	8.1	16.1	8.8	16.0	7.4	10.4	0.19	2.20	0.30	2.09	-0.06	0.70
10	OU	32.69	2.04	0.00	0.0020	2.69	2.60	4.0	1.8	7.9	15.9	8.7	15.8	7.2	10.2	0.16	2.17	0.27	2.06	-0.09	0.66
11	OU	32.74	2.14	0.00	0.0021	2.33	2.60	4.0	1.8	8.3	16.4	9.1	16.2	7.6	10.7	-0.08	1.93	0.38	2.16	0.02	0.77
12	OU	32.77	2.23	0.00	0.0022	2.47	2.64	4.0	1.8	8.7	16.8	9.4	16.6	8.0	11.0	0.16	2.17	0.51	2.29	0.15	0.90
13	OU	32.82	2.31	0.00	0.0023	2.51	2.66	4.0	1.8	9.1	17.1	9.8	16.9	8.3	11.3	0.29	2.30	0.60	2.39	0.24	1.00
14	OU	32.87	2.47	0.00	0.0025	2.55	2.67	4.0	1.8	9.7	17.8	10.3	17.5	8.9	11.9	0.49	2.50	0.76	2.55	0.40	1.15
15	OU	32.91	2.15	0.00	0.0022	2.55	2.67	4.0	1.8	8.4	16.4	9.2	16.3	7.7	10.7	0.16	2.16	0.47	2.24	0.10	0.85
16	OU	32.99	2.06	0.00	0.0021	2.37	2.72	4.0	1.8	8.0	16.0	8.8	15.9	7.3	10.3	-0.12	1.88	0.42	2.20	0.06	0.80
17	OU	33.05	1.84	0.00	0.0018	2.45	2.73	4.0	1.8	6.9	14.9	7.8	14.9	6.3	9.3	-0.32	1.68	0.19	1.96	-0.18	0.57
18	OU	33.09	2.13	0.00	0.0021	2.77	2.73	4.0	1.8	8.3	16.3	9.1	16.2	7.6	10.6	0.36	2.36	0.51	2.28	0.14	0.89
19	OU	33.12	2.47	0.00	0.0025	2.77	2.80	4.0	1.8	9.8	17.8	10.4	17.5	8.9	11.9	0.72	2.72	0.90	2.68	0.54	1.28
20	OU	33.19	1.89	0.00	0.0019	2.73	2.74	4.0	1.8	7.2	15.2	8.0	15.1	6.6	9.6	0.02	2.02	0.25	2.03	-0.11	0.64
21	OU	33.21	1.95	0.00	0.0020	2.87	2.74	4.0	1.8	7.5	15.5	8.3	15.4	6.8	9.8	0.24	2.24	0.32	2.10	-0.04	0.70
22	OU	33.25	1.93	0.00	0.0019	2.76	2.62	4.0	1.8	7.4	15.4	8.2	15.3	6.8	9.7	0.11	2.11	0.18	1.96	-0.19	0.56
23	OU	33.27	2.05	0.00	0.0021	2.74	2.62	4.0	1.8	8.0	16.0	8.7	15.9	7.3	10.3	0.23	2.23	0.31	2.09	-0.05	0.69
24	OU	33.29	2.77	0.00	0.0028	2.74	2.62	4.0	1.8	10.9	18.9	11.4	18.5	9.9	12.9	0.98	2.98	0.97	2.75	0.61	1.35
25	OU	33.32	1.99	0.00	0.0020	2.85	2.60	4.0	1.8	7.7	15.7	8.5	15.6	7.0	10.0	0.27	2.27	0.23	2.00	-0.14	0.61
26	OU	33.35	2.17	0.00	0.0022	2.79	2.59	4.0	1.8	8.5	16.5	9.2	16.4	7.8	10.8	0.42	2.42	0.41	2.18	0.04	0.79
27	OU	33.36	2.19	0.00	0.0022	2.79	2.59	4.0	1.8	8.6	16.6	9.3	16.4	7.9	10.9	0.45	2.45	0.43	2.20	0.06	0.81
28	OU	33.38	2.00	0.00	0.0020	2.77	2.58	4.0	1.8	7.7	15.7	8.5	15.6	7.1	10.1	0.20	2.20	0.22	1.99	-0.15	0.60
29	OU	33.40	2.16	0.00	0.0022	2.80	2.37	4.0	1.8	8.5	16.5	9.2	16.3	7.7	10.7	0.42	2.42	0.18	1.95	-0.19	0.56
30	OU	33.41	2.33	0.00	0.0023	2.80	2.37	4.0	1.8	9.2	17.2	9.9	17.0	8.4	11.4	0.61	2.61	0.34	2.12	-0.02	0.72
31	OU	33.57	2.06	0.00	0.0021	1.99	2.12	4.0	1.8	8.1	16.0	8.9	15.9	7.4	10.3	-0.48	1.50	-0.16	1.60	-0.54	0.20
32	OU	33.58	1.77	0.00	0.0018	1.91	2.12	4.0	1.8	6.6	14.5	7.5	14.6	6.0	9.0	-0.94	1.04	-0.49	1.27	-0.87	-0.13

A	B	C	D	E	F	G	H	I	J	K	L	M	N	O	P	Q	R	S	T	U	V
33	OU	33.61	1.87	0.00	0.0019	2.20	2.11	4.0	1.8	7.1	15.0	8.0	15.0	6.5	9.5	-0.51	1.47	-0.38	1.38	-0.76	-0.02
34	OU	33.67	1.63	0.00	0.0016	2.16	2.10	4.0	1.8	5.8	13.7	6.8	13.8	5.3	8.3	-0.89	1.09	-0.69	1.07	-1.07	-0.33
35	OU	33.75	1.95	0.00	0.0020	1.98	1.85	4.0	1.7	7.5	15.7	8.4	15.6	6.9	9.9	-0.63	1.41	-0.55	1.26	-0.93	-0.17
36	OU	33.78	1.98	0.00	0.0020	2.01	1.85	4.0	1.7	7.7	15.8	8.5	15.8	7.0	10.1	-0.56	1.47	-0.52	1.29	-0.89	-0.13
37	OU	33.81	1.57	0.00	0.0016	1.89	1.84	4.0	1.7	5.4	13.5	6.5	13.7	5.0	8.0	-1.26	0.78	-1.04	0.77	-1.41	-0.65
38	OU	33.84	1.75	0.00	0.0018	2.19	1.84	4.0	1.7	6.5	14.6	7.4	14.7	5.9	9.0	-0.69	1.35	-0.80	1.01	-1.17	-0.41
39	OU	33.87	1.83	0.00	0.0018	1.89	1.84	4.0	1.7	6.9	15.1	7.8	15.1	6.3	9.4	-0.88	1.16	-0.70	1.11	-1.07	-0.31
40	OU	33.90	1.51	0.00	0.0015	1.89	1.78	4.0	1.7	5.0	13.2	6.1	13.4	4.6	7.7	-1.35	0.69	-1.18	0.63	-1.56	-0.80
41	OU	33.93	2.36	0.00	0.0024	1.80	1.78	4.0	1.7	9.4	17.6	10.0	17.3	8.6	11.6	-0.34	1.70	-0.20	1.61	-0.58	0.18
42	OU	33.96	2.00	0.00	0.0020	1.78	1.76	4.0	1.7	7.8	15.9	8.6	15.8	7.1	10.1	-0.77	1.27	-0.59	1.22	-0.96	-0.20
43	OU	33.99	1.91	0.00	0.0019	1.78	1.76	4.0	1.7	7.3	15.5	8.2	15.4	6.7	9.7	-0.88	1.16	-0.69	1.12	-1.06	-0.30
44	OU	34.02	2.28	0.00	0.0023	1.71	1.76	3.9	1.7	9.1	17.2	9.8	17.0	8.3	11.3	-0.50	1.52	-0.29	1.51	-0.67	0.09
45	OU	34.05	1.88	0.00	0.0019	1.64	1.76	3.9	1.7	7.2	15.3	8.1	15.3	6.6	9.6	-1.05	0.98	-0.71	1.09	-1.09	-0.34
46	OU	34.08	2.21	0.00	0.0022	1.66	1.74	3.9	1.7	8.8	16.9	9.5	16.7	8.0	11.0	-0.63	1.40	-0.38	1.42	-0.76	0.00
47	OU	34.21	1.74	0.00	0.0017	1.63	1.73	3.9	1.7	6.5	14.6	7.4	14.6	5.9	8.9	-1.25	0.78	-0.91	0.89	-1.29	-0.54
48	OU	34.36	1.89	0.00	0.0019	1.67	1.72	3.9	1.7	7.3	15.4	8.1	15.3	6.6	9.6	-1.00	1.02	-0.74	1.06	-1.12	-0.36
49	OU	34.43	1.99	0.00	0.0020	1.52	1.71	3.9	1.7	7.8	15.9	8.6	15.8	7.1	10.1	-1.03	1.00	-0.64	1.16	-1.02	-0.26
50	OU	34.13	1.86	0.00	0.0019	1.68	1.74	3.9	1.7	7.1	15.2	8.0	15.2	6.5	9.5	-1.03	0.99	-0.75	1.05	-1.13	-0.38
51	CP	31.96	1.92	0.10	0.0020	2.26	2.48	4.0	1.8	7.7	15.5	8.5	15.4	7.1	10.0	-0.31	1.64	0.12	1.84	-0.23	0.49
52	CP	32.40	2.05	0.10	0.0022	2.51	2.51	4.0	1.8	8.4	16.4	9.1	16.3	7.7	10.7	0.11	2.12	0.30	2.08	-0.06	0.69
53	CP	32.69	2.18	0.10	0.0023	2.69	2.60	4.0	1.8	9.0	17.0	9.6	16.8	8.2	11.2	0.43	2.45	0.51	2.30	0.16	0.91
54	CP	32.74	1.84	0.10	0.0019	2.33	2.60	4.0	1.8	7.4	15.4	8.2	15.4	6.8	9.8	-0.32	1.69	0.16	1.95	-0.20	0.55
55	CP	32.78	2.09	0.10	0.0022	2.47	2.66	4.0	1.8	8.6	16.6	9.3	16.4	7.8	10.9	0.12	2.13	0.49	2.27	0.13	0.88
56	CP	32.82	1.94	0.10	0.0020	2.51	2.66	4.0	1.8	7.9	15.9	8.7	15.8	7.2	10.2	-0.02	1.99	0.33	2.12	-0.03	0.72
57	CP	32.92	1.84	0.10	0.0019	2.60	2.67	4.0	1.8	7.4	15.4	8.3	15.4	6.8	9.8	-0.04	1.96	0.24	2.02	-0.12	0.62
58	CP	33.00	1.95	0.10	0.0021	2.46	2.72	4.0	1.8	8.0	16.0	8.7	15.9	7.3	10.3	-0.05	1.95	0.41	2.19	0.05	0.79
59	CP	33.27	1.76	0.10	0.0019	2.74	2.62	4.0	1.8	7.0	15.0	7.9	15.0	6.4	9.4	-0.01	1.99	0.10	1.88	-0.27	0.48
60	CP	33.30	1.88	0.10	0.0020	2.87	2.62	4.0	1.8	7.6	15.6	8.4	15.6	7.0	10.0	0.28	2.28	0.24	2.01	-0.13	0.62
61	CP	33.42	2.05	0.10	0.0022	2.80	2.37	4.0	1.8	8.4	16.4	9.2	16.3	7.7	10.7	0.41	2.41	0.17	1.94	-0.20	0.55
62	CP	33.48	1.79	0.10	0.0019	2.78	2.36	4.0	1.8	7.2	15.2	8.1	15.1	6.6	9.6	0.09	2.07	-0.11	1.65	-0.48	0.26
63	CP	33.75	2.20	0.10	0.0023	1.98	1.85	4.0	1.7	9.2	17.3	9.8	17.1	8.3	11.4	-0.22	1.81	-0.19	1.62	-0.56	0.20
64	CP	33.84	1.87	0.10	0.0020	2.19	1.84	4.0	1.7	7.6	15.8	8.5	15.7	7.0	10.0	-0.40	1.64	-0.54	1.27	-0.91	-0.15
65	CP	33.97	1.71	0.10	0.0018	1.78	1.76	4.0	1.7	6.8	15.0	7.7	15.0	6.2	9.3	-1.01	1.02	-0.80	1.01	-1.18	-0.42
66	CP	34.21	1.94	0.10	0.0020	1.63	1.73	3.9	1.7	8.0	16.1	8.8	16.0	7.3	10.3	-0.86	1.17	-0.56	1.24	-0.94	-0.19

A	B	**C**	D	**E**	**F**	**G**	**H**	**I**	J	K	**L**	**M**	**N**	**O**	**P**	**Q**	**R**	**S**	**T**	**U**	**V**
67	CP	34.36	1.80	0.10	0.0019	1.67	1.72	3.9	1.7	7.3	15.4	8.2	15.4	6.7	9.7	-0.99	1.03	-0.73	1.07	-1.11	-0.35
68	CP	34.43	1.74	0.10	0.0018	1.52	1.71	3.9	1.7	7.0	15.1	7.9	15.1	6.4	9.4	-1.22	0.80	-0.81	0.99	-1.19	-0.43
69	CP	32.65	2.09	0.10	0.0022	2.67	2.59	4.0	1.8	8.6	16.6	9.3	16.4	7.8	10.9	0.32	2.33	0.42	2.20	0.06	0.81
70	CP	33.26	2.02	0.10	0.0021	2.76	2.62	4.0	1.8	8.3	16.3	9.0	16.2	7.6	10.6	0.34	2.34	0.39	2.16	0.02	0.77
71	CP	34.09	1.84	0.10	0.0019	1.66	1.74	3.9	1.7	7.5	15.6	8.4	15.6	6.9	9.9	-0.95	1.07	-0.66	1.14	-1.04	-0.29
72	CP	34.13	1.89	0.10	0.0020	1.68	1.74	3.9	1.7	7.8	15.9	8.6	15.8	7.1	10.1	-0.87	1.16	-0.61	1.19	-0.99	-0.23
73	CP	33.43	1.80	0.10	0.0019	2.83	2.37	4.0	1.8	7.2	15.2	8.1	15.2	6.6	9.6	0.14	2.14	-0.10	1.67	-0.47	0.28
74	NU	31.96	1.59	0.75	0.0023	2.26	2.48	4.0	1.8	9.2	16.9	9.8	16.7	8.4	11.3	0.06	2.00	0.44	2.17	0.09	0.81
75	NU	32.27	1.67	0.75	0.0024	2.45	2.51	4.0	1.8	9.5	17.6	10.1	17.3	8.7	11.7	0.33	2.35	0.54	2.34	0.19	0.95
76	NU	33.20	1.46	0.75	0.0022	2.87	2.74	4.0	1.8	8.7	16.7	9.4	16.5	7.9	10.9	0.55	2.55	0.60	2.37	0.23	0.98
77	NU	33.32	1.65	0.75	0.0024	2.85	2.60	4.0	1.8	9.5	17.5	10.1	17.2	8.7	11.7	0.73	2.73	0.64	2.41	0.27	1.02
78	NU	33.78	1.04	0.75	0.0018	2.01	1.85	4.0	1.7	6.7	14.8	7.6	14.9	6.1	9.2	-0.81	1.23	-0.74	1.07	-1.11	-0.35
79	NU	34.21	1.22	0.75	0.0020	1.63	1.73	3.9	1.7	7.7	15.8	8.5	15.7	7.0	10.0	-0.94	1.08	-0.64	1.16	-1.02	-0.26

Appendix 5: Benthic foraminiferal Mg/Ca and $\delta^{18}O$ data for the Cenozoic used in Chapters 4 and 5.

	Title	Units	Method	Reference
A	Age	(Ma)		*Per reference*
B	Mg/Ca, Normalized	(mmol/mol)		Lear et al. (2000)
C	Calcite $\delta^{18}O$	(‰ PDB)		Zachos et al. 1993
D	Calcite $\delta^{18}O$	(‰ PDB)		Zachos et al. 2001
E	Seawater Mg/Ca	(mol/mol)		Wilkinson and Algeo (1989)
F	Seawater Mg/Ca	(mol/mol)		Hardie (1996)
G	Temperature	(°C)	Lear00	(J)
H	Temperature	(°C)	Lear00	(K)
I	Temperature	(°C)	Lear02	(J)
J	Temperature	(°C)	Lear02	(K)
K	Temperature	(°C)	Diss	(J)
L	Temperature	(°C)	Diss	(K)
M	Seawater $\delta^{18}O$	(‰ SMOW)	Lear00	(J)
N	Seawater $\delta^{18}O$	(‰ SMOW)	Lear00	(K)
O	Seawater $\delta^{18}O$	(‰ SMOW)	Lear02	(J)
P	Seawater $\delta^{18}O$	(‰ SMOW)	Lear02	(K)
Q	Seawater $\delta^{18}O$	(‰ SMOW)	Diss	(J)
R	Seawater $\delta^{18}O$	(‰ SMOW)	Diss	(K)

A	B	**C**	D	**E**	**F**	**G**	**H**	**I**	J	K	**L**	**M**	**N**	**O**	**P**	**Q**	**R**
0.43	1.07	3.6	4.3	5.2	5.2	-1.1	-1.1	0.7	0.7	0.6	0.6	-0.27	-0.27	-0.07	-0.07	-0.10	-0.10
0.75	1.21	3.5	4.2	5.2	5.2	0.1	0.1	1.8	1.8	1.7	1.7	-0.05	-0.04	0.13	0.14	0.11	0.11
1.50	1.23	3.4	3.8	5.1	4.9	0.4	0.8	2.1	2.4	1.9	2.0	-0.10	0.00	-0.23	-0.14	-0.28	-0.24
2.08	1.33	3.1	3.6	5.1	4.6	1.2	2.2	2.7	3.7	2.5	2.9	-0.21	0.06	-0.24	0.00	-0.28	-0.18
3.71	1.43	2.4	3.1	5.0	4.3	2.1	3.5	3.5	4.8	3.3	3.8	-0.69	-0.33	-0.47	-0.15	-0.54	-0.40
4.20	1.25	2.2	3.1	5.0	4.3	0.8	2.2	2.4	3.7	2.1	2.6	-1.13	-0.78	-0.81	-0.50	-0.89	-0.75
4.75	1.38	2.2	3.0	5.0	4.3	1.8	3.2	3.3	4.5	3.0	3.5	-0.92	-0.58	-0.65	-0.35	-0.73	-0.60
6.10	1.36	2.2	2.9	4.9	4.0	1.8	3.8	3.3	5.0	2.9	3.6	-0.92	-0.44	-0.80	-0.37	-0.90	-0.72
6.31	1.42	2.2	2.8	4.9	3.8	2.3	4.8	3.7	6.0	3.3	4.3	-0.78	-0.15	-0.75	-0.19	-0.86	-0.62
6.50	1.71	2.2	2.8	4.9	3.8	4.2	6.7	5.4	7.6	5.0	5.9	-0.31	0.32	-0.37	0.19	-0.47	-0.24
6.57	1.43	2.2	2.8	4.9	3.8	2.4	4.9	3.8	6.0	3.3	4.3	-0.77	-0.14	-0.78	-0.22	-0.89	-0.65
6.80	1.72	2.3	2.7	4.8	3.8	4.3	6.7	5.5	7.6	5.0	5.9	-0.26	0.35	-0.43	0.12	-0.54	-0.31
7.26	1.63	2.3	2.6	4.8	3.8	3.7	6.2	5.0	7.2	4.5	5.4	-0.39	0.22	-0.62	-0.07	-0.73	-0.50
7.30	1.60	2.3	2.6	4.8	3.8	3.6	6.0	4.9	7.0	4.4	5.3	-0.43	0.18	-0.65	-0.10	-0.76	-0.53
7.89	1.56	2.3	2.8	4.8	3.5	3.4	6.5	4.7	7.5	4.2	5.4	-0.47	0.31	-0.52	0.17	-0.65	-0.35
9.94	1.50	2.2	2.6	4.7	3.3	3.3	6.7	4.6	7.6	3.9	5.2	-0.58	0.28	-0.72	0.04	-0.88	-0.56
11.11	1.26	2.1	2.6	4.6	3.1	1.7	5.6	3.2	6.7	2.5	3.9	-1.03	-0.04	-1.14	-0.26	-1.32	-0.95
11.43	1.60	2.1	2.5	4.6	3.1	4.1	8.0	5.3	8.8	4.6	6.0	-0.43	0.55	-0.65	0.22	-0.84	-0.48
11.65	1.57	2.1	2.5	4.6	3.1	3.9	7.8	5.2	8.7	4.4	5.9	-0.46	0.52	-0.72	0.15	-0.91	-0.54
12.14	1.62	2.2	2.4	4.6	2.9	4.3	8.7	5.5	9.4	4.7	6.4	-0.36	0.74	-0.71	0.26	-0.90	-0.49
12.30	1.99	2.2	2.4	4.6	2.9	6.4	10.7	7.3	11.2	6.5	8.2	0.15	1.25	-0.24	0.73	-0.44	-0.03
13.30	1.55	2.0	2.2	4.5	2.9	3.9	8.2	5.2	9.0	4.4	6.0	-0.61	0.46	-1.02	-0.06	-1.23	-0.82
14.18	1.84	1.7	1.8	4.5	2.8	5.8	10.5	6.8	11.0	5.9	7.7	-0.49	0.69	-0.98	0.06	-1.20	-0.77
19.79	1.96	1.4	2.0	4.3	2.3	6.7	12.8	7.6	13.0	6.6	8.9	-0.50	1.02	-0.57	0.78	-0.82	-0.26
21.82	1.61	1.5	1.9	4.3	2.3	4.8	11.2	6.0	11.6	4.9	7.3	-0.92	0.67	-1.07	0.34	-1.34	-0.75
22.33	1.87	1.4	1.8	4.3	2.2	6.3	13.0	7.3	13.3	6.2	8.7	-0.58	1.10	-0.86	0.64	-1.12	-0.50
24.49	1.81	1.5	1.6	4.3	2.1	6.0	13.0	7.0	13.2	5.9	8.5	-0.56	1.17	-1.11	0.42	-1.39	-0.74
24.78	1.95	1.5	1.6	4.3	2.1	6.8	13.7	7.7	13.8	6.6	9.2	-0.44	1.29	-0.95	0.58	-1.23	-0.58
25.79	1.71	1.3	2.3	4.3	2.0	5.5	12.8	6.6	13.0	5.5	8.2	-0.91	0.91	-0.54	1.08	-0.82	-0.14
27.91	1.99	1.7	2.7	4.2	2.0	7.1	14.5	8.0	14.5	6.8	9.6	-0.07	1.78	0.15	1.79	-0.15	0.54
29.23	1.84	1.8	2.6	4.2	1.9	6.5	14.0	7.4	14.1	6.2	9.0	-0.20	1.69	-0.02	1.66	-0.33	0.37
30.05	1.69	1.6	2.6	4.1	1.9	5.8	13.5	6.8	13.7	5.5	8.4	-0.49	1.44	-0.19	1.53	-0.52	0.20

A	B	**C**	D	**E**	**F**	**G**	**H**	**I**	J	K	**L**	**M**	**N**	**O**	**P**	**Q**	**R**
30.23	1.36	1.6	2.6	4.1	1.9	3.6	11.4	4.9	11.8	3.6	6.5	-1.10	0.83	-0.68	1.04	-1.01	-0.29
30.42	1.65	1.6	2.6	4.1	1.9	5.5	13.3	6.6	13.5	5.3	8.2	-0.62	1.31	-0.29	1.43	-0.62	0.11
30.73	1.75	1.5	2.5	4.1	1.9	6.2	13.9	7.2	14.0	5.8	8.7	-0.50	1.41	-0.15	1.54	-0.50	0.22
31.21	1.70	1.6	2.5	4.1	1.8	6.0	13.8	7.0	13.9	5.6	8.5	-0.51	1.45	-0.27	1.47	-0.61	0.12
31.47	2.03	1.6	2.5	4.1	1.8	7.7	15.5	8.5	15.5	7.1	10.0	-0.09	1.87	0.11	1.85	-0.24	0.50
31.65	1.92	1.6	2.5	4.1	1.8	7.1	15.0	8.0	15.0	6.6	9.6	-0.17	1.79	-0.01	1.73	-0.36	0.37
32.17	1.84	1.7	2.5	4.0	1.8	6.8	14.5	7.7	14.6	6.3	9.2	-0.20	1.74	-0.07	1.65	-0.42	0.30
32.18	1.76	1.7	2.5	4.0	1.8	6.3	14.1	7.3	14.2	5.9	8.8	-0.30	1.64	-0.17	1.56	-0.52	0.21
32.54	1.95	1.7	2.5	4.0	1.8	7.4	15.5	8.3	15.4	6.8	9.9	0.00	2.02	0.11	1.89	-0.25	0.50
32.80	1.80	1.7	2.7	4.0	1.8	6.6	14.7	7.5	14.7	6.1	9.1	-0.20	1.81	0.05	1.84	-0.31	0.44
34.00	1.89	0.9	1.8	4.0	1.7	7.2	15.4	8.1	15.3	6.6	9.6	-0.84	1.19	-0.71	1.10	-1.09	-0.33
34.87	2.51	0.7	1.7	3.9	1.7	10.1	18.2	10.7	17.8	9.1	12.1	-0.38	1.63	-0.11	1.68	-0.50	0.25
36.72	2.22	0.7	1.7	3.8	1.7	9.1	17.4	9.8	17.1	8.1	11.2	-0.63	1.43	-0.39	1.45	-0.80	-0.03
36.73	2.08	0.7	1.7	3.8	1.7	8.5	16.7	9.2	16.5	7.5	10.6	-0.81	1.26	-0.54	1.30	-0.95	-0.18
37.03	1.93	0.7	1.6	3.8	1.7	7.8	16.0	8.6	15.9	6.9	10.0	-0.96	1.10	-0.72	1.11	-1.14	-0.37
37.47	2.51	0.6	1.6	3.8	1.7	10.5	18.6	11.0	18.2	9.3	12.3	-0.33	1.71	-0.18	1.63	-0.61	0.15
37.95	3.09	0.6	1.5	3.8	1.7	12.5	20.6	12.8	20.0	11.1	14.1	0.14	2.17	0.20	2.01	-0.23	0.53
38.59	2.27	0.6	1.4	3.7	1.6	9.6	17.8	10.2	17.5	8.4	11.5	-0.63	1.43	-0.53	1.31	-0.97	-0.20
39.27	2.07	0.4	1.3	3.7	1.6	8.7	16.9	9.4	16.7	7.6	10.7	-0.99	1.08	-0.82	1.01	-1.27	-0.50
39.47	2.37	0.4	1.3	3.7	1.6	10.0	18.2	10.5	17.9	8.8	11.9	-0.72	1.34	-0.55	1.29	-0.99	-0.22
39.78	2.48	0.4	1.3	3.7	1.6	10.5	19.0	11.0	18.5	9.2	12.4	-0.59	1.53	-0.47	1.41	-0.92	-0.13
41.37	2.30	0.2	1.0	3.7	1.6	9.8	18.4	10.4	18.0	8.6	11.8	-0.91	1.25	-0.86	1.05	-1.31	-0.51
41.92	2.18	0.2	1.0	3.7	1.6	9.3	17.9	9.9	17.5	8.1	11.3	-1.07	1.07	-1.02	0.88	-1.48	-0.68
42.55	2.29	0.2	0.9	3.7	1.5	9.9	18.6	10.5	18.2	8.6	11.8	-0.96	1.23	-0.94	1.00	-1.41	-0.60
43.39	2.39	0.1	0.9	3.7	1.5	10.3	19.0	10.8	18.6	8.9	12.2	-0.90	1.29	-0.86	1.08	-1.33	-0.52
43.72	2.41	0.0	0.9	3.6	1.5	10.4	19.1	10.9	18.7	9.0	12.3	-0.96	1.21	-0.83	1.10	-1.31	-0.50
44.34	2.59	0.0	0.9	3.6	1.5	11.2	20.0	11.6	19.4	9.7	13.0	-0.74	1.45	-0.67	1.27	-1.16	-0.34
44.65	2.24	0.0	0.9	3.6	1.5	9.8	18.5	10.4	18.1	8.4	11.7	-1.10	1.09	-1.02	0.92	-1.51	-0.69
44.96	2.33	0.1	0.8	3.6	1.5	10.1	18.9	10.7	18.5	8.7	12.0	-0.97	1.22	-0.99	0.95	-1.48	-0.66
45.38	2.30	0.0	0.8	3.6	1.5	10.1	19.0	10.6	18.6	8.7	12.0	-1.03	1.20	-1.08	0.90	-1.57	-0.74
45.46	2.72	0.0	0.7	3.6	1.5	11.7	20.6	12.1	20.0	10.1	13.5	-0.62	1.61	-0.75	1.24	-1.23	-0.40
45.69	2.47	0.0	0.7	3.6	1.5	10.7	19.7	11.2	19.2	9.3	12.6	-0.92	1.31	-1.00	0.99	-1.49	-0.66
46.00	2.32	-0.1	0.6	3.6	1.5	10.2	19.1	10.7	18.6	8.7	12.1	-1.12	1.11	-1.20	0.79	-1.69	-0.85
47.08	2.69	-0.3	0.4	3.6	1.4	11.7	20.7	12.0	20.1	10.1	13.4	-0.96	1.31	-1.09	0.93	-1.58	-0.73

A	B	**C**	D	**E**	**F**	**G**	**H**	**I**	J	K	**L**	**M**	**N**	**O**	**P**	**Q**	**R**
47.20	2.66	-0.4	0.4	3.6	1.4	11.5	20.6	11.9	20.0	9.9	13.3	-1.05	1.22	-1.14	0.88	-1.64	-0.79
48.23	3.24	-0.5	0.2	3.6	1.4	13.5	22.7	13.7	21.9	11.7	15.1	-0.75	1.55	-0.88	1.17	-1.37	-0.51
48.39	2.78	-0.5	0.2	3.6	1.4	12.0	21.2	12.3	20.5	10.3	13.8	-1.13	1.17	-1.25	0.80	-1.75	-0.89
48.61	2.90	-0.5	0.1	3.6	1.4	12.4	21.6	12.7	20.9	10.7	14.2	-1.03	1.28	-1.18	0.87	-1.67	-0.81
53.89	2.73	-0.6	0.2	3.5	1.4	12.1	21.4	12.4	20.7	10.3	13.8	-1.11	1.22	-1.18	0.90	-1.71	-0.84
54.85	2.62	-0.4	0.3	3.5	1.3	11.7	21.3	12.1	20.6	10.0	13.5	-1.08	1.31	-1.21	0.91	-1.75	-0.86
55.07	2.70	-0.4	0.3	3.5	1.3	12.1	21.6	12	21	10	14	-0.94	1.43	-1.09	1.01	-1.64	-0.76

Appendix 6: Planktonic foraminiferal data used in Chapter 5.

Column	*Description*
A	Core, Section, Interval Top (cm)–Interval Bottom (cm)
B	Species of *Morozovella*
C	Depth (mbsf)
D	Age (Ma)
E	Normalized Mg/Ca (mol/mol)
F	Foraminiferal carbonate $\delta^{18}O$ (‰ PDB) from Bralower (1995)
G	Seawater Mg/Ca (mol/mol) from Hardie (1996)
H	Seawater Mg/Ca (mol/mol) from Wilkinson and Algeo (1989)
I	Mg-paleotemperature calculated using the method of Tripati et al. (2003) and (G)
J	Mg-paleotemperature calculated using the method of Tripati et al. (2003) and (H)
K	Mg-paleotemperature calculated using the method of Chapter 5 and (G)
L	Mg-paleotemperature calculated using the method of Chapter 5 and (H)
M	Seawater $\delta^{18}O$ calculated using the method of Tripati et al. (2003) and (I)
N	Seawater $\delta^{18}O$ calculated using the method of Tripati et al. (2003) and (J)
O	Seawater $\delta^{18}O$ calculated using the method of Chapter 5 and (K)
P	Seawater $\delta^{18}O$ calculated using the method of Chapter 5 and (L)

A	B	C	D	E	F	G	H	I	J	K	L	M	N	O	P
4, 6, 20-22	spinulosa	35.20	39.76	0.00353	-0.6	3.7	1.6	28.1	37.6	26.3	30.3	1.8	3.9	1.4	2.3
4, 6, 20-22	spinulosa	35.20	39.76	0.00373	-0.6	3.7	1.6	28.7	38.2	26.9	30.9	1.9	4.0	1.5	2.4
4, 6, 20-22	lehneri	35.20	39.76	0.00402	-0.6	3.7	1.6	29.6	39.0	27.8	31.8	2.1	4.2	1.7	2.6
5, 2, 70-72	lehneri	39.20	40.62	0.00415	-0.5	3.7	1.6	30.0	39.4	28.1	32.1	2.4	4.4	2.0	2.8
5, 4, 70-72	lehneri	42.20	41.27	0.00433	-0.6	3.7	1.6	30.4	40.0	28.6	32.7	2.3	4.4	1.9	2.8
5, 5, 70-72	spinulosa	43.70	41.60	0.00459	-0.7	3.7	1.6	31.1	40.7	29.3	33.3	2.4	4.4	2.0	2.8
5, 5, 70-72	spinulosa	43.70	41.60	0.00451	-0.7	3.7	1.6	31.0	40.5	29.1	33.1	2.3	4.4	1.9	2.8
5, 5, 70-72	lehneri	43.70	41.60	0.00436	-0.7	3.7	1.6	30.6	40.1	28.7	32.8	2.2	4.3	1.8	2.7
5, 5, 70-72	lehneri	43.70	41.60	0.00443	-0.7	3.7	1.6	30.8	40.3	28.9	32.9	2.3	4.4	1.9	2.8
6, 1, 81-83	spinulosa	47.31	42.38	0.00443	-0.7	3.7	1.5	30.8	40.6	28.9	33.1	2.3	4.4	1.9	2.8
6, 1, 81-83	lehneri	47.31	42.38	0.00413	-0.7	3.7	1.5	30.0	39.8	28.1	32.3	2.1	4.3	1.7	2.6
6, 1, 81-83	lehneri	47.31	42.38	0.00424	-0.7	3.7	1.5	30.3	40.1	28.4	32.6	2.2	4.3	1.8	2.7
6, 4, 70-72	aragonensis	51.70	42.96	0.00417	-0.8	3.7	1.5	30.2	39.9	28.3	32.4	2.1	4.2	1.7	2.6
6, 4, 70-72	spinulosa	51.70	42.96	0.00402	-0.8	3.7	1.5	29.8	39.5	27.9	32.0	2.0	4.1	1.6	2.5
7, 1, 118-120	aragonensis	57.18	43.69	0.00368	-0.8	3.6	1.5	28.9	38.5	26.9	31.0	1.8	3.9	1.4	2.3
7, 1, 118-120	aragonensis	57.18	43.69	0.00396	-0.8	3.6	1.5	29.7	39.3	27.7	31.8	2.0	4.1	1.5	2.4
7, 1, 118-120	aragonensis	57.18	43.69	0.00370	-0.8	3.6	1.5	28.9	38.6	27.0	31.1	1.8	3.9	1.4	2.3
7, 1, 118-120	spinulosa	57.18	43.69	0.00388	-0.8	3.6	1.5	29.4	39.1	27.5	31.6	1.9	4.0	1.5	2.4
7, 4, 66-68	aragonensis	61.18	44.22	0.00392	-1.0	3.6	1.5	29.6	39.4	27.6	31.8	1.7	3.9	1.3	2.2
7, 4, 66-68	spinulosa	61.18	44.22	0.00399	-1.0	3.6	1.5	29.8	39.6	27.8	32.0	1.8	3.9	1.3	2.2
7, 4, 66-68	spinulosa	61.18	44.22	0.00388	-1.0	3.6	1.5	29.5	39.3	27.5	31.7	1.7	3.8	1.3	2.2
7, 4, 66-68	spinulosa	61.18	44.22	0.00403	-1.0	3.6	1.5	29.9	39.7	27.9	32.1	1.8	3.9	1.4	2.3
7, 4, 68-70	aragonensis	61.20	44.22	0.00374	-1.0	3.6	1.5	29.1	38.9	27.1	31.2	1.6	3.8	1.2	2.1
8, 1, 89-91	spinulosa	66.39	44.91	0.00417	-1.5	3.6	1.5	30.3	40.1	28.3	32.5	1.4	3.5	0.9	1.8
8, 3, 70-72	aragonensis	69.20	45.65	0.00377	-1.3	3.6	1.5	29.2	39.2	27.2	31.4	1.3	3.5	0.9	1.8
8, 4, 67-69	aragonensis	70.67	46.21	0.00391	-1.4	3.6	1.5	29.6	39.6	27.6	31.8	1.4	3.5	0.9	1.8
8, 5, 70-72	aragonensis	72.20	46.79	0.00388	-1.5	3.6	1.4	29.6	39.7	27.6	31.8	1.2	3.4	0.8	1.7
8, 5, 70-72	aragonensis	72.20	46.79	0.00411	-1.5	3.6	1.4	30.2	40.3	28.2	32.5	1.3	3.6	0.9	1.8
8, 5, 70-72	aragonensis	72.20	46.79	0.00380	-1.5	3.6	1.4	29.4	39.5	27.3	31.6	1.2	3.4	0.7	1.7
8, 5, 70-72	aragonensis	72.20	46.79	0.00393	-1.5	3.6	1.4	29.7	39.9	27.7	32.0	1.2	3.4	0.8	1.7
8, 5, 70-72	aragonensis	72.20	46.79	0.00381	-1.5	3.6	1.4	29.4	39.5	27.4	31.6	1.2	3.4	0.7	1.7

A	B	C	D	E	F	G	H	I	J	K	L	M	N	O	P
8, 6, 70-72	aragonensis	73.70	47.36	0.00436	-1.5	3.6	1.4	30.9	41.0	28.8	33.1	1.5	3.7	1.1	2.0
9, 1, 13-15	aragonensis	75.13	47.90	0.00505	-1.5	3.6	1.4	32.5	42.6	30.5	34.8	1.9	4.1	1.4	2.4
9, 2, 20-22	aragonensis	76.70	48.50	0.00516	-1.8	3.6	1.4	32.7	43.0	30.7	35.1	1.7	3.9	1.2	2.2
9, 2, 20-22	aragonensis	76.70	48.50	0.00488	-1.8	3.6	1.4	32.1	42.4	30.1	34.5	1.5	3.8	1.1	2.1
9, 2, 20-22	aragonensis	76.70	48.50	0.00493	-1.8	3.6	1.4	32.2	42.5	30.2	34.6	1.6	3.8	1.1	2.1
9, 2, 20-22	aragonensis	76.70	48.50	0.00512	-1.8	3.6	1.4	32.6	42.9	30.6	35.0	1.7	3.9	1.2	2.2
9, 3, 20-22	aragonensis	78.20	49.07	0.00506	-1.7	3.6	1.4	32.6	42.8	30.5	34.9	1.7	3.9	1.3	2.2
9, 3, 120-125	aragonensis	79.20	49.46	0.00499	-1.5	3.6	1.4	32.5	42.6	30.4	34.7	1.8	4.0	1.4	2.3
9, 4, 10-12	aragonensis	79.60	49.60	0.00506	-1.7	3.6	1.4	32.6	42.8	30.6	34.9	1.7	4.0	1.3	2.2
9, 5, 120-122	aragonensis	82.20	51.16	0.00527	-1.4	3.5	1.4	33.1	43.6	31.0	35.5	2.1	4.4	1.6	2.6
9, 5, 120-122	aragonensis	82.20	51.16	0.00514	-1.4	3.5	1.4	32.8	43.4	30.7	35.2	2.0	4.3	1.5	2.5
9, 5, 120-125	aragonensis	82.20	51.16	0.00521	-1.4	3.5	1.4	33.0	43.5	30.9	35.4	2.0	4.3	1.6	2.6
10, 1, 83-85	aragonensis	85.33	51.68	0.00446	-2.1	3.5	1.4	31.3	41.8	29.2	33.6	1.0	3.3	0.6	1.5
10, 2, 120-122	aragonensis	87.20	51.99	0.00455	-1.8	3.5	1.4	31.6	42.0	29.4	33.9	1.3	3.6	0.9	1.8
10, 2, 120-122	aragonensis	87.20	51.99	0.00469	-1.8	3.5	1.4	31.9	42.4	29.8	34.2	1.4	3.7	0.9	1.9
10, 2, 120-125	aragonensis	87.20	51.99	0.00439	-1.8	3.5	1.4	31.2	41.6	29.0	33.5	1.3	3.5	0.8	1.8
10, 2, 120-125	subbotinae	87.20	51.99	0.00444	-1.8	3.5	1.4	31.3	41.7	29.1	33.6	1.3	3.6	0.8	1.8
10, 3, 4-6	subbotinae	87.54	52.05	0.00432	-2.1	3.5	1.4	31.0	41.4	28.8	33.3	1.0	3.3	0.5	1.5
10, 3, 4-6	aragonensis	87.54	52.05	0.00421	-2.1	3.5	1.4	30.7	41.2	28.6	33.0	0.9	3.2	0.5	1.4
10, 3, 60-62	subbotinae	88.10	52.14	0.00485	-1.9	3.5	1.4	32.3	42.7	30.1	34.6	1.5	3.7	1.0	2.0
10, 4, 60-62	velazcoensis	89.60	52.39	0.00441	-2.0	3.5	1.4	31.2	41.7	29.1	33.5	1.1	3.4	0.6	1.6
10, 4, 60-62	velazcoensis	89.60	52.39	0.00431	-2.0	3.5	1.4	31.0	41.4	28.8	33.3	1.0	3.3	0.5	1.5
10, 4, 60-62	velazcoensis	89.60	52.39	0.00439	-2.0	3.5	1.4	31.2	41.6	29.0	33.5	1.1	3.3	0.6	1.6
10, 4, 60-62	velazcoensis	89.60	52.39	0.00457	-2.0	3.5	1.4	31.6	42.1	29.5	33.9	1.2	3.4	0.7	1.7
10, 5, 60-62	subbotinae	91.10	52.74	0.00440	-1.9	3.5	1.4	31.3	41.7	29.1	33.5	1.2	3.5	0.7	1.7
11, 2, 20-22	subbotinae	95.70	53.80	0.00406	-1.9	3.5	1.4	30.4	40.8	28.2	32.6	1.0	3.3	0.5	1.5
11, 2, 20-22	velazcoensis	95.70	53.80	0.00410	-1.9	3.5	1.4	30.5	41.0	28.3	32.7	1.1	3.3	0.6	1.5
11, 2, 20-22	velazcoensis	95.70	53.80	0.00405	-1.9	3.5	1.4	30.4	40.8	28.2	32.6	1.0	3.3	0.5	1.5
11, 2, 20-22	velazcoensis	95.70	53.80	0.00404	-1.9	3.5	1.4	30.4	40.8	28.1	32.6	1.0	3.3	0.5	1.5
11, 2, 85-87	subbotinae	96.35	53.95	0.00403	-2.1	3.5	1.3	30.4	41.0	28.1	32.6	0.8	3.1	0.3	1.3
11, 5, 85-87	subbotinae	100.85	54.99	0.00427	-2.1	3.5	1.3	31.1	41.6	28.8	33.3	1.0	3.3	0.5	1.4

A	B	C	D	E	F	G	H	I	J	K	L	M	N	O	P
11, 5, 85-87	velazcoensis	100.85	54.99	0.00422	-2.1	3.5	1.3	31.0	41.5	28.7	33.2	0.9	3.2	0.4	1.4
11, 6, 85-87	subbotinae	102.35	55.27	0.00418	-2.1	3.5	1.3	30.9	41.4	28.6	33.0	0.9	3.2	0.4	1.4
11, 6, 85-87	velazcoensis	102.35	55.27	0.00414	-2.1	3.5	1.3	30.7	41.3	28.5	32.9	0.9	3.2	0.4	1.4
12, 1, 0-2	velazcoensis	103.50	55.49	0.00426	-2.1	3.5	1.3	31.1	41.8	28.8	33.3	1.0	3.3	0.5	1.5
12, 1, 10-12	velazcoensis	103.60	55.50	0.00489	-1.7	3.5	1.3	32.6	43.3	30.3	34.9	1.7	4.1	1.2	2.2
12, 1, 10-12	velazcoensis	103.60	55.50	0.00427	-1.7	3.5	1.3	31.1	41.8	28.8	33.4	1.4	3.7	0.9	1.9
12, 1, 10-12	velazcoensis	103.60	55.50	0.00421	-1.7	3.5	1.3	30.9	41.7	28.6	33.2	1.4	3.7	0.9	1.9
12, 1, 20-22	velazcoensis	103.70	55.51	0.00394	-1.9	3.5	1.3	30.2	40.9	27.9	32.5	1.0	3.3	0.5	1.5
12, 1, 40-42	velazcoensis	103.90	55.52	0.00394	-1.8	3.5	1.3	30.2	40.9	27.9	32.5	1.1	3.4	0.6	1.6
12, 1, 70-72	subbotinae	104.20	55.54	0.00359	-1.8	3.5	1.3	29.2	39.9	26.9	31.4	0.9	3.2	0.4	1.4
12, 1, 70-72	velazcoensis	104.20	55.54	0.00366	-1.8	3.5	1.3	29.4	40.1	27.1	31.6	0.9	3.3	0.4	1.4
12, 1, 70-72	velazcoensis	104.20	55.54	0.00383	-1.8	3.5	1.3	29.9	40.6	27.6	32.1	1.0	3.4	0.5	1.5
12, 1, 70-72	velazcoensis	104.20	55.54	0.00378	-1.8	3.5	1.3	29.8	40.5	27.4	32.0	1.0	3.3	0.5	1.5
12, 2, 20-22	velazcoensis	105.20	55.60	0.00405	-1.8	3.5	1.3	30.5	41.2	28.2	32.8	1.2	3.5	0.7	1.7
12, 2, 70-72	velazcoensis	105.70	55.63	0.00410	-1.8	3.5	1.3	30.6	41.4	28.4	32.9	1.2	3.5	0.7	1.7
12, 3, 20-22	velazcoensis	106.70	55.69	0.00400	-1.8	3.5	1.3	30.4	41.1	28.1	32.6	1.1	3.5	0.6	1.6
12, 5, 20-22	velazcoensis	109.70	55.87	0.00416	-1.8	3.5	1.3	30.8	41.5	28.5	33.1	1.2	3.6	0.7	1.7
12, 6, 70-72	velazcoensis	111.70	55.99	0.00392	-1.8	3.5	1.3	30.1	40.9	27.9	32.4	1.1	3.4	0.6	1.6
13, 1, 70-72	velazcoensis	113.70	56.11	0.00426	-1.8	3.5	1.3	31.1	41.8	28.8	33.3	1.3	3.6	0.8	1.8
13, 2, 70-72	velazcoensis	115.20	56.20	0.00403	-1.8	3.4	1.3	30.5	41.2	28.2	32.7	1.2	3.5	0.7	1.7
13, 3, 70-72	velazcoensis	116.70	56.36	0.00361	-1.8	3.4	1.3	29.3	40.0	27.0	31.5	0.9	3.2	0.4	1.4
13, 3, 70-72	velazcoensis	116.70	56.36	0.00393	-1.8	3.4	1.3	30.2	40.9	27.9	32.4	1.1	3.4	0.6	1.6
13, 3, 70-72	velazcoensis	116.70	56.36	0.00387	-1.8	3.4	1.3	30.1	40.7	27.7	32.3	1.1	3.4	0.6	1.6
13, 4, 70-72	velazcoensis	118.20	56.65	0.00411	-1.8	3.4	1.3	30.7	41.4	28.4	32.9	1.2	3.5	0.7	1.7
13, 5, 70-72	velazcoensis	119.70	56.94	0.00407	-1.8	3.4	1.3	30.7	41.5	28.3	32.9	1.2	3.6	0.7	1.7
13, 6, 70-72	velazcoensis	121.20	57.23	0.00456	-1.8	3.4	1.3	32.0	42.8	29.6	34.2	1.5	3.9	1.0	2.0
13, 6, 70-72	velazcoensis	121.20	57.23	0.00455	-1.8	3.4	1.3	31.9	42.8	29.6	34.2	1.5	3.8	1.0	2.0
13, 6, 70-72	velazcoensis	121.20	57.23	0.00455	-1.8	3.4	1.3	31.9	42.8	29.6	34.2	1.5	3.8	1.0	2.0
14, 1, 20-22	velazcoensis	122.70	57.53	0.00401	-1.8	3.4	1.3	30.6	41.4	28.2	32.8	1.2	3.5	0.7	1.7
14, 2, 20-22	velazcoensis	124.20	57.82	0.00384	-1.8	3.4	1.3	30.1	40.9	27.7	32.3	1.1	3.4	0.6	1.6
14, 2, 20-22	velazcoensis	124.20	57.82	0.00374	-1.8	3.4	1.3	29.9	40.6	27.4	32.0	1.0	3.4	0.5	1.5

A	B	C	D	E	F	G	H	I	J	K	L	M	N	O	P
14, 2, 20-22	velazcoensis	124.20	57.82	0.00381	-1.8	3.4	1.3	30.1	40.8	27.6	32.2	1.1	3.4	0.5	1.5
14, 3, 76-78	velazcoensis	126.26	58.29	0.00407	-1.8	3.4	1.3	30.8	41.6	28.4	33.0	1.2	3.6	0.7	1.7
14, 4, 23-25	velazcoensis	127.23	58.60	0.00394	-1.8	3.4	1.3	30.5	41.3	28.0	32.6	1.2	3.5	0.6	1.6

References

Ahr, W.M., 1989, Sedimentary and tectonic controls on the development of an Early Mississippian carbonate ramp, Sacramento Mountains area, New Mexico; Controls on carbonate platform and basin development, *in* Crevello, P.D., Wilson, J.J., Sarg, J.F., and Read, J.F., eds., Controls on carbonate platform and basin development, Volume 44: Lo, p. 203-212.

Ahr, W.M., Stanton, R.J.J., Strogen, P., Somerville, I.D., and Jones, G.D., 1996, Constituent composition of Early Mississippian carbonate buildups and their level-bottom equivalents, Sacramento Mountains, New Mexico; Recent advances in Lower Carboniferous geology: Geological Society Special Publications, v. 107, p. 83-95.

Aissaoui, D.M., 1986, Diagénèse carbonatée en domaine récifal: Paris, University of Paris-Sud.

Alt, J.C., and Honnorez, J., 2003, Hydrothermal fluxes at mid-ocean ridges and on ridge flanks; Alterations hydrothermales de la lithosphere oceanique--Hydrothermal alterations of the oceanic lithosphere: Comptes Rendus–Academie des sciences: Geoscience, v. 335, p. 853-864.

Anand, P., Elderfield, H., and Conte, M.H., 2003, Calibration of Mg/Ca thermometry in planktonic foraminifera from a sediment trap time series: Paleoceanography, v. 18.

Arth, J.G., 1976, Behavior of trace-elements during magmatic processes—summary of theoretical models and their applications: Journal of Research of the US Geological Survey, v. 4, p. 41-47.

Arvidson, R.S., Mackenzie, F.T., and Guidry, M., 2006, MAGic: A Phanerozoic model for the geochemical cycling of major rock-forming components: American Journal of Science, v. 306, p. 135-190.

Barrett, P.J., Elston, D.P., Harwood, D.M., McKelvey, B.C., and Webb, P.N., 1987, Mid-Cenozoic record of glaciation and sea-level change on the margin of the Victoria Land basin, Antarctica: Geology (Boulder), v. 15, p. 634-637.

Bathurst, R.G.C., 1971, Carbonate sediments and their diagenesis: Amsterdam; New York, Elsevier, 620 p.

Benito, M.I., Lohmann, K.C., and Mas, R., 2005, Late Jurassic paleogeography and paleoclimate in the northern Iberian Basin of Spain: Constraints from diagenetic records in reefal and continental carbonates: Journal of Sedimentary Research, v. 75, p. 82-96.

Berner, R.A., 2004, A model for calcium, magnesium and sulfate in seawater over Phanerozoic time: American Journal of Science, v. 304, p. 438-453.

Billups, K., and Schrag, D.P., 2002, Paleotemperatures and ice volume of the past 27 Myr revisited with paired Mg/Ca and O^{18}/O^{16} measurements on benthic foraminifera: Paleoceanography, v. 17.

—, 2003, Application of benthic foraminiferal Mg/Ca ratios to questions of Cenozoic climate change: Earth and Planetary Science Letters, v. 209, p. 181-195.

Birkenmajer, K., 1998, Zlodowacenia antarktydy w kenozoiku. Cenozoic glaciation in Antarctica: Kosmos, v. 47, p. 397-407.

Bohaty, S.M., Zachos, J.C., and 2003, Significant Southern Ocean warming event in the late middle Eocene: Geology, v. 31, p. 1017-1020.

Bourque, P.A., and Raymond, L., 1994, Diagenetic alteration of early marine cements of Upper Silurian stromatactis: Sedimentology, v. 41, p. 255-269.
Bralower, T.J., Zachos, J.C., Thomas, E., Parrow, M., Paull, C.K., Kelly, D.C., Premoli Silva, I., Sliter, W.V., and Lohmann, K.C., 1995, Late Paleocene to Eocene paleoceanography of the Equatorial Pacific Ocean; stable isotopes recorded at Ocean Drilling Program Site 865, Allison Guyot: Paleoceanography, v. 10, p. 841-865.
Brand, U., 1982, The oxygen and carbon isotope composition of Carboniferous fossil components; sea-water effects: Sedimentology, v. 29, p. 139-147.
Brand, U., Logan, A., Hiller, N., and Richardson, J.R., 2003, Geochemistry of modern brachiopods; applications and implications for oceanography and paleoceanography: Chemical Geology, v. 198, p. 305-334.
Brezinski, D.K., 2000, Lower Mississippian trilobites from southern New Mexico: Journal of Paleontology, v. 74, p. 1043-1064.
Browning, J.V., Miller, K.G., and Pak, D.K., 1996, Global implications of lower to middle Eocene sequence boundaries on the New Jersey coastal plain; the icehouse cometh: Geology (Boulder), v. 24, p. 639-642.
Burton, E.A., and Walter, L.M., 1987, Relative precipitation rates of aragonite and Mg calcite from seawater; temperature or carbonate ion control?: Geology (Boulder), v. 15, p. 111-114.
Carpenter, S.J., and 1991, Isotopic and minor element chemistry of Devonian-Carboniferous abiotic marine calcite.
Carpenter, S.J., Erickson, J.M., and Holland, F.D., Jr., 2003, Migration of a Late Cretaceous fish: Nature (London), v. 423, p. 70-74.
Carpenter, S.J., and Lohmann, K.C., 1992, Sr/Mg ratios of modern marine calcite: empirical indicators of ocean chemistry and precipitation rate: Geochimica et Cosmochimica Acta, v. 56, p. 1837-1849.
Carpenter, S.J., Lohmann, K.C., Holden, P., Walter, L.M., Huston, T.J., and Halliday, A.N., 1991, $\delta^{18}O$ values, $^{87}Sr/^{86}Sr$ and Sr/Mg ratios of Late Devonian abiotic marine calcite: implications for the composition of ancient seawater: Geochimica et Cosmochimica Acta, v. 55, p. 1991-2010.
Chave, K.E., 1954, Aspects of the biogeochemistry of magnesium; Part 1, Calcareous marine organisms: Journal of Geology, v. 62, p. 266-283.
Choquette, P.W., and James, N.P., 1990, Limestones—the burial diagenetic environment, *in* McIlreath, I.A., and Morrow, D.W., eds., Diagenesis, Volume 4: St. John's, Geological Association of Canada, p. 75-111.
Cicero, A.D., and Lohmann, K.C., 2001, Sr/Mg variation during rock-water interaction; implications for secular changes in the elemental chemistry of ancient seawater: Geochimica et Cosmochimica Acta, v. 65, p. 741-761.
Comans, R.N.J., and Middelburg, J.J., 1987, Sorption of trace metals on calcite; applicability of the surface precipitation model: Geochimica et Cosmochimica Acta, v. 51, p. 2587-2591.
Davies, G.R., 1977, Former magnesian calcite and aragonite submarine cements in upper Paleozoic reefs of the Canadian Arctic; a summary: Geology, v. 5, p. 11-15.

Davis, J.A., Fuller, C.C., and Cook, A.D., 1987, A model for trace metal sorption processes at the calcite surface; adsorption of Cd2+ and subsequent solid solution formation: Geochimica et Cosmochimica Acta, v. 51, p. 1477-1490.
de Villiers, S., Dickson, J.A.D., Ellam, R.M., and 2005, The composition of the continental river weathering flux deduced from sea water Mg isotopes: Chemical Geology, v. 216, p. 133-142.
Deconto, R.M., and Pollard, D., 2003, Rapid Cenozoic glaciation of Antarctica induced by declining atmospheric CO_2: Nature, v. 421, p. 245-249.
Delaney, M.L., Be, A.W.H., and Boyle, E.A., 1985, Li, Sr, Mg, and Na in Foraminiferal Calcite Shells from Laboratory Culture, Sediment Traps, and Sediment Cores: Geochimica Et Cosmochimica Acta, v. 49, p. 1327-1341.
Demicco, R.V., 2004, Modeling seafloor-spreading rates through time: Geology (Boulder), v. 32, p. 485-488.
Demicco, R.V., Lowenstein, T.K., Hardie, L.A., and Spencer, R.J., 2005, Model of seawater composition for the Phanerozoic: Geology (Boulder), v. 33, p. 877-880.
Devore, G.W., 1955, The Role of Adsorption in the Fractionation and Distribution of Elements: Journal of Geology, v. 63, p. 159-190.
Dickson, J.A.D., 2002, Fossil echinoderms as monitor of the Mg/Ca ratio of Phanerozoic oceans: Science, v. 298, p. 1222-1224.
—, 2004, Echinoderm skeletal preservation; calcite-aragonite seas and the Mg/Ca ratio of Phanerozoic oceans: Journal of Sedimentary Research, v. 74, p. 355-365.
Doerner, H.A., and Hoskins, W.M., 1925, Co-precipitation of radium and barium sulfates: Journal of the American Chemical Society, v. 47, p. 662-675.
Douthit, T.L., 1990, A Geochemical analysis of the Irish Waulsortian Limestone: implications for the strontium isotopic composition of Lower Carboniferous seawater: Stony Brook, State University of New York, Stony Brook.
Dutton, A., Lohmann, K.C., and Leckie, R.M., 2005, Insights from the Paleogene tropical Pacific: Foraminiferal stable isotope and elemental results from Site 1209, Shatsky Rise: Paleoceanography, v. 20, p. -.
Dwyer, G.S., Cronin, T.M., Baker, P.A., Raymo, M.E., Buzas, J.S., and Correge, T., 1995, North-Atlantic Deep-Water Temperature-Change during Late Pliocene and Late Quaternary Climatic Cycles: Science, v. 270, p. 1347-1351.
Elderfield, H., Vautravers, M., and Cooper, M., 2002, The relationship between shell size and Mg/Ca, Sr/Ca, $\delta^{18}O$, and $\delta^{13}C$ of species of planktonic foraminifera: Geochemistry, Geophysics, Geosystems—G^3, v. 3, p. 13.
Elderfield, H., Yu, J., Anand, P., Kiefer, T., and Nyland, B., 2006, Calibrations for benthic foraminiferal Mg/Ca paleothermometry and the carbonate ion hypothesis: Earth and Planetary Science Letters, v. 250, p. 633-649.
Eldrett, J.S., Harding, I.C., Wilson, P.A., Butler, E., and Roberts, A.P., 2007, Continental ice in Greenland during the Eocene and Oligocene: Nature, v. 446, p. 176-179.
Epstein, S.A., Buchsbaum, R., Lowenstam, H.A., and Urey, H.C., 1951, Carbonate-water isotopic temperature scale: Geological Society of America Bulletin, v. 62, p. 417-425.
Erez, J., and Luz, B., 1983, Experimental Paleotemperature Equation for Planktonic-Foraminifera: Geochimica Et Cosmochimica Acta, v. 47, p. 1025-1031.

Farley, K.J., Dzombak, D.A., and Morel, F.M.M., 1985, A Surface Precipitation Model for the Sorption of Cations on Metal-Oxides: Journal of Colloid and Interface Science, v. 106, p. 226-242.

Frank, T.D., and Lohmann, K.C., 1995, Early cementation during marine-meteoric fluid mixing; Mississippian Lake Valley Formation, New Mexico: Journal of Sedimentary Research, v. 65, p. 263-273.

—, 1996, Diagenesis of fibrous magnesian calcite marine cement; implications for the interpretation of $\delta^{18}O$ and $\delta^{13}C$ values of ancient equivalents: Geochimica et Cosmochimica Acta, v. 60, p. 2427-2436.

Frank, T.D., Lohmann, K.C., and Meyers, W.J., 1996, Chronostratigraphic significance of cathodoluminescence zoning in syntaxial cement; Mississippian Lake Valley Formation, New Mexico: Sedimentary Geology, v. 105, p. 29-50.

Freitas, P., Clarke, L.J., Kennedy, H., Richardson, C., and Abrantes, F., 2005, Mg/Ca, Sr/Ca, and stable-isotope ($\delta^{18}O$ and $\delta^{13}C$) ratio profiles from the fan mussel *Pinna nobilis*: Seasonal records and temperature relationships: Geochemistry Geophysics Geosystems, v. 6, p. Q04D14.

Fuchtbauer, H., and Hardie, L.A., 1976, Experimentally determined homogeneous distribution for precipitated magnesian calcites; application to marine carbonate cements, Geological Society of America Annual Meeting, Volume 8: Denver, CO, USA, p. 877.

Füchtbauer, H., and Hardie, L.A., 1980, Comparison of experimental and natural magnesian calcites, International Association of Sedimentologists Meeting: Bochum, Germany, p. 167-169.

Gaffin, S., 1987, Ridge volume dependence on seafloor generation rate and inversion using long term sealevel change: American Journal of Science, v. 287, p. 596-611.

Given, R.K., and Lohmann, K.C., 1985, Derivation of the original isotopic composition of Permian marine cements: Journal of Sedimentary Petrology, v. 55, p. 430-439.

Given, R.K., and Wilkinson, B.H., 1987, Dolomite abundance and stratigraphic age; constraints on rates and mechanisms of Phanerozoic dolostone formation: Journal of Sedimentary Petrology, v. 57, p. 1068-1078.

Goldstein, R.H., 1990, Petrographic and geochemical evidence for origin of paleospeleothems, New Mexico; implications for the application of fluid inclusions to studies of diagenesis: Journal of Sedimentary Petrology, v. 60, p. 282-292.

Gonzalez, L.A., and Lohmann, K.C., 1985, Carbon and oxygen isotopic composition of Holocene reefal carbonates: Geology, v. 13, p. 811-814.

Hardie, L.A., 1996, Secular variation in seawater chemistry; an explanation for the coupled secular variation in the mineralogies of marine limestones and potash evaporites over the past 600 m.y: Geology, v. 24, p. 279-283.

Hay, W.W., Migdisov, A., Balukhovsky, A.N., Wold, C.N., Floegel, S., Soding, E., Buggisch, W., and 2006, Evaporites and the salinity of the ocean during the Phanerozoic; implications for climate, ocean circulation and life; Evolution of the system Earth in the late Palaeozoic; clues from sedimentary geochemistry: Palaeogeography, Palaeoclimatology, Palaeoecology, v. 240, p. 3-46.

Henderson, L.M., and Kracek, F.C., 1927, The fractional precipitation of barium and radium chromates: Journal of the American Chemical Society, v. 49, p. 738-749.
Hendry, J.P., Trewin, N.H., and Fallick, A.E., 1996, Low-Mg calcite marine cement in Cretaceous turbidites; origin, spatial distribution and relationship to seawater chemistry: Sedimentology, v. 43, p. 877-900.
Holland, H.D., Horita, J., and Seyfried, W.E., 1996, On the secular variations in the composition of Phanerozoic marine potash evaporites: Geology (Boulder), v. 24, p. 993-996.
Horita, J.A.B., Friedman, T.J., Lazar, B., and Holland, H.D., 1991, The composition of Permian seawater: Geochimica et Cosmochimica Acta, v. 55, p. 417-432.
Horita, J.A.B., Zimmermann, H., Holland, H.D., and Candela, P.A., 2002, Chemical evolution of seawater during the Phanerozoic; implications from the record of marine evaporites: Geochimica et Cosmochimica Acta, v. 66, p. 3733-3756.
Hut, G., 1987, Consultants group meeting on stable isotope reference samples for geochemical and hydrological investigations, Report to the Director General: Vienna, International Atomic Energy Agency, p. 42.
Ivany, L.C., Lohmann, K.C., Hasiuk, F., Blake, D.B., Glass, A., Aronson, R.B., and Moody, R.M., 2008, Eocene climate record of a high southern latitude continental shelf: Seymour Island, Antarctica: Geological Society of America Bulletin, v. 120, p. 659-678.
Ivany, L.C., Wilkinson, B.H., Lohmann, K.C., Johnson, E.R., McElroy, B.J., and Cohen, G.J., 2004, Intra-annual isotopic variation in Venericardia bivalves; implications for early Eocene temperature, seasonality, and salinity on the U.S. Gulf Coast: Journal of Sedimentary Research, v. 74, p. 7-19.
James, N.P., and Choquette, P.W., 1990, Limestones—the meteoric diagenetic environment, *in* McIlreath, I.A., and Morrow, D.W., eds., Diagenesis, Volume 4: St. John's, Geological Association of Canada, p. 35-74.
Kasting, J.F., Howard, M.T., Wallmann, K., Veizer, J., Shields, G., and Jaffres, J., 2006, Paleoclimates, ocean depth, and the oxygen isotopic composition of seawater: Earth and Planetary Science Letters, v. 252, p. 82-93.
Katz, A., 1973, The interaction of magnesium with calcite during crystal growth at 25-90°C and one atmosphere: Geochimica et Cosmochimica Acta, v. 37, p. 1563-1586.
Katz, A., Sass, E., Starinsky, A., and Holland, H.D., 1972, Strontium behavior in the aragonite-calcite transformation; an experimental study at 40-98°C: Geochimica et Cosmochimica Acta, v. 36, p. 481-496.
Kendall, A.C., Schneidermann, N., and Harris, P.M., 1985, Radiaxial fibrous calcite; a reappraisal: SEPM Special Publication, v. 36, p. 59-77.
Kennett, J.P., Barker, P.F., O'Connell, S.B., Berkowitz, S., Bryant, W.R., Burckle, L.H., Egeberg, P.K., Fuetterer, D.K., Gersonde, R.E., Golovchenko, X., Hamilton, N., Lawver, L., Lazarus, D.B., Lonsdale, M.J., Mohr, B.A.R., Nagao, T., Pereira, C.P.G., Pudsey, C.J., Robert, C.M., Schandl, E.S., Spiess, V., Stott, L.D., Thomas, E., Thompson, K.F.M., and Wise, S.W., Jr., 1990, Latest Cretaceous to Cenozoic climate and oceanographic developments in the Weddell Sea, Antarctica; an ocean-drilling perspective: Proceedings of the Ocean Drilling Program, Scientific Results, v. 113, p. 937-960.

Kennett, J.P., and Brunner, C.A., 1973, Antarctic Late Cenozoic Glaciation; evidence for Initiation of Ice Rafting and Inferred Increased Bottom-Water Activity: Geological Society of America Bulletin, v. 84, p. 2043-2052.

Kennett, J.P., and von der Borch, C.C., 1986, Southwest Pacific Cenozoic paleoceanography: Initial Reports of the Deep Sea Drilling Project, v. 90, p. 1493-1517.

Kim, S.-T., and O'Neil, J.R., 1997, Equilibrium and nonequilibrium oxygen isotope effects in synthetic carbonates: Geochimica et Cosmochimica Acta, v. 61, p. 3461-3475.

Kirkby, K.C., Hunt, D., Strogen, P., Somerville, I.D., and Jones, G.D., 1996, Episodic growth of a Waulsortian buildup; the Lower Carboniferous Muleshoe Mound, Sacramento Mountains, New Mexico, USA; Recent advances in Lower Carboniferous geology: Geological Society Special Publications, v. 107, p. 97-110.

Klein, R.T., Lohmann, K.C., and Thayer, C.W., 1996, Sr/Ca and $^{13}C/^{12}C$ ratios in skeletal calcite of *Mytilus trossulus*; covariation with metabolic rate, salinity, and carbon isotopic composition of seawater: Geochimica et Cosmochimica Acta, v. 60, p. 4207-4221.

Kovalevich, V.M., Peryt, T.M., and Petrichenko, O.I., 1998, Secular variation in seawater chemistry during the Phanerozoic as indicated by brine inclusions in halite: Journal of Geology, v. 106, p. 695-712.

Langer, G., Gussone, N., Nehrke, G., Riebesell, U., Eisenhauer, A., Kuhnert, H., Rost, B., Trimborn, S., and Thoms, S., 2006, Coccolith strontium to calcium ratios in Emiliania huxleyi: The dependence on seawater strontium and calcium concentrations: Limnology and Oceanography, v. 51, p. 310-320.

Larson, R.L., 1991, Latest pulse of Earth; evidence for a Mid-Cretaceous super plume: Geology (Boulder), v. 19, p. 547-550.

Lawrence, J.R., Gieskes, J.M., and Anderson, T.F., 1976, Oxygen isotope material balance calculations, Leg 35: Initial Reports of the Deep Sea Drilling Project, v. 35, p. 507-512.

Lea, D.W., Mashiotta, T.A., and Spero, H.J., 1999, Controls on magnesium and strontium uptake in planktonic foraminifera determined by live culturing: Geochimica Et Cosmochimica Acta, v. 63, p. 2369-2379.

Lear, C.H., Elderfield, H., and Wilson, P.A., 2000, Cenozoic deep-sea temperatures and global ice volumes from Mg/Ca in benthic foraminiferal calcite: Science, v. 287, p. 269-272.

—, 2003a, A Cenozoic seawater Sr/Ca record from benthic foraminiferal calcite and its application in determining global weathering fluxes: Earth and Planetary Science Letters, v. 208, p. 69-84.

Lear, C.H., Rosenthal, Y., Coxall, H.K., and Wilson, P.A., 2004, Late Eocene to early Miocene ice sheet dynamics and the global carbon cycle: Paleoceanography, v. 19, p. 11.

Lear, C.H., Rosenthal, Y., and Slowey, N.C., 2002, Benthic foraminiferal Mg/Ca-paleothermometry; a revised core-top calibration: Geochimica et Cosmochimica Acta, v. 66, p. 3375-3387.

Lear, C.H., Rosenthal, Y., and Wright, J.D., 2003b, The closing of a seaway: ocean water masses and global climate change: Earth and Planetary Science Letters, v. 210, p. 425-436.
Lewis, A.R., Marchant, D.R., Ashworth, A.C., Hemming, S.R., and Machlus, M.L., 2007, Major middle Miocene global climate change; evidence from East Antarctica and the Transantarctic Mountains: Geological Society of America Bulletin, v. 119, p. 1449-1461.
Lohmann, K.C., 1988, Geochemical patterns of meteoric diagenetic systems and their application to studies of paleokarst, *in* James, N.P., and Choquette, P.W., eds., Paleokarst: New York, Springer, p. 58-80.
Lohmann, K.C., and Meyers, W.J., 1977, Microdolomite inclusions in cloudy prismatic calcites; a proposed criterion for former high-magnesium calcites: Journal of Sedimentary Petrology, v. 47, p. 1078-1088.
Lohmann, K.C., and Walker, J.C.G., 1989, The $\delta^{18}O$ record of Phanerozoic abiotic marine calcite cements: Geophysical Research Letters, v. 16, p. 319-322.
Lowenstein, T.K., Hardie, L.A., Timofeeff, M.N., and Demicco, R.V., 2003, Secular variation in seawater chemistry and the origin of calcium chloride basinal brines: Geology, v. 31, p. 857-860.
Lowenstein, T.K., Timofeeff, M.N., Brennan, S.T., Hardie, L.A., and Demicco, R.V., 2001, Oscillations in Phanerozoic seawater chemistry; evidence from fluid inclusions: Science, v. 294, p. 1086-1088.
Lowenstein, T.K., Timofeeff, M.N., Kovalevych, V.M., and Horita, J., 2005, The major-ion composition of Permian sea water: Geochimica et Cosmochimica Acta, v. 69, p. 1701-1719.
Mackensen, A., and Ehrmann, W.U., 1992, Middle Eocene through early Oligocene climate history and paleoceanography in the Southern Ocean; stable oxygen and carbon isotopes from ODP Sites on Maud Rise and Kerguelen Plateau: Marine Geology, v. 108, p. 1-27.
Mackenzie, F.T., and Pigott, J.D., 1981, Tectonic controls of Phanerozoic sedimentary rock cycling: Journal of the Geological Society of London, v. 138, Part 2, p. 183-196.
Major, R.P., and Wilber, R.J., 1991, Crystal habit, geochemistry, and cathodoluminescence of magnesian calcite marine cements from the lower slope of Little Bahama Bank; with Suppl. Data 91-07: Geological Society of America Bulletin, v. 103, p. 461-471.
Malone, M.J., and Baker, P.A., 1999, Temperature dependence of the strontium distribution coefficient in calcite: An experimental study from 40º degrees to 200ºC and application to natural diagenetic calcites: Journal of Sedimentary Research, v. 69, p. 216-223.
Margolis, S., and Kennett, J.P., 1970, Antarctic glaciation during the Tertiary recorded in sub-Antarctic deep-sea cores: Science, v. 170, p. 1085-1087.
Marshall, J.D., and Ashton, M., 1980, Isotopic and trace element evidence for submarine lithification of hardgrounds in the Jurassic of eastern England: Sedimentology, v. 27, p. 271-289.

Martin, P.A., Lea, D.W., Rosenthal, Y., Shackleton, N.J., Sarnthein, M., and Papenfuss, T., 2002, Quaternary deep sea temperature histories derived from benthic foraminiferal Mg/Ca: Earth and Planetary Science Letters, v. 198, p. 193-209.
Matthews, R.K., and Poore, R.Z., 1980, Tertiary $\delta^{18}O$ record and glacio-eustatic sea-level fluctuations: Geology (Boulder), v. 8, p. 501-504.
Mazzullo, S.J., Bischoff, W.D., and Lobitzer, H., 1990, Diagenesis of radiaxial fibrous calcites in a subunconformity, shallow-burial setting—Upper Triassic and Liassic, Northern Calcareous Alps, Austria: Sedimentology, v. 37, p. 407-425.
McArthur, J.M., Howarth, R.J., and Bailey, T.R., 2001, Strontium isotope stratigraphy; LOWESS Version 3; best fit to the marine Sr-isotope curve for 0-509 Ma and accompanying look-up table for deriving numerical age: Journal of Geology, v. 109, p. 155-170.
McIntire, W.L., 1963, Trace element partition coefficients; a review of theory and applications to geology: Geochimica et Cosmochimica Acta, v. 27, p. 1209-1264.
Meyers, W.J., 1974, Carbonate cement stratigraphy of the Lake Valley Formation (Mississippian) Sacramento Mountains, New Mexico: Journal of Sedimentary Petrology, v. 44, p. 837-861.
Meyers, W.J., and Lohmann, K.C., 1978, Microdolomite-rich syntaxial cements: proposed meteoric-marine mixing zone phreatic cements from Mississippian limestones, New Mexico: Journal of Sedimentary Petrology, v. 48, p. 475-488.
—, 1985, Isotope geochemistry of regionally extensive calcite cement zones and marine components in Mississippian limestones, New Mexico: SEPM Special Publication, v. 36, p. 223-239.
Mii, H.S., Grossman, E.L., Yancey, T.E., and 1999, Carboniferous isotope stratigraphies of North America; implications for Carboniferous paleoceanography and Mississippian glaciation: GSA Bulletin, v. 111, p. 960-973.
Miller, K.G., Fairbanks, R.G., and Mountain, G.S., 1987, Tertiary oxygen isotope synthesis, sea level history, and continental margin erosion: Paleoceanography, v. 2, p. 1-19.
Miller, K.G., Kominz, M.A., Browning, J.V., Wright, J.D., Mountain, G.S., Katz, M.E., Sugarman, P.J., Cramer, B.S., Christie-Blick, N., and Pekar, S.F., 2005, The phanerozoic record of global sea-level change: Science, v. 310, p. 1293-1298.
Milliken, K.L.a.P., J. D., 1977, Variation of oceanic Mg/Ca ratio through time—implications of the calcite sea: Geological Society of America, Abstracts with Programs, South-Central Section, p. 64.
Milliman, J.D., 1974, Marine Carbonates: Berlin, Springer-Verlag, 375 p.
Mitsuguchi, T., Uchida, T., Matsumoto, E., Isdale, P.J., and Kawana, T., 2001, Variations in Mg/Ca, Na/Ca, and Sr/Ca ratios of coral skeletons with chemical treatments; implications for carbonate geochemistry: Geochimica et Cosmochimica Acta, v. 65, p. 2865-2874.
Moran, K., Backman, J., Brinkhuis, H., Clemens, S.C., Cronin, T., Dickens, G.R., Eynaud, F., Gattacceca, J., Jakobsson, M., Jordan, R.W., Kaminski, M., King, J., Koc, N., Krylov, A., Martinez, N., Matthiessen, J., McInroy, D., Moore, T.C., Onodera, J., O'Regan, M., Palike, H., Rea, B., Rio, D., Sakamoto, T., Smith, D.C., Stein, R., St John, K., Suto, I., Suzuki, N., Takahashi, K., Watanabe, M., Yamamoto, M., Farrell, J., Frank, M., Kubik, P., Jokat, W., and Kristoffersen, Y.,

2006, The Cenozoic palaeoenvironment of the Arctic Ocean: Nature, v. 441, p. 601-605.
Moriya, K., Wilson, P.A., Friedrich, O., Erbacher, J., and Kawahata, H., 2007, Testing for ice sheets during the mid-Cretaceous greenhouse using glassy foraminiferal calcite from the mid-Cenomanian tropics on Demerara Rise: Geology (Boulder), v. 35, p. 615-618.
Morrison, J.O., and Brand, U., 1986, Paleoscene Geochemistry of Recent marine invertebrates: Geoscience Canada, v. 13, p. 237-254.
Morse, J.W., and Bender, M.L., 1990, Partition coefficients in calcite; examination of factors influencing the validity of experimental results and their application to natural systems: Chemical Geology, v. 82, p. 265-277.
Mucci, A., 1987, Influence of temperature on the composition of magnesian calcite overgrowths precipitated from seawater: Geochimica et Cosmochimica Acta, v. 51, p. 1977-1984.
Mucci, A., and Morse, J.W., 1983, The incorporation of Mg^{2+} and Sr^{2+} into calcite overgrowths: Influences of growth rate and solution composition: Geochimica et Cosmochimica Acta, v. 47, p. 217-233.
Nürnberg, D., Bijma, J., and Hemleben, C., 1996, Assessing the reliability of magnesium in foraminiferal calcite as a proxy for water mass temperatures: Geochimica et Cosmochimica Acta, v. 60, p. 803-814.
Pagani, M., Lemarchand, D., Spivack, A., and Gaillardet, J., 2005, A critical evaluation of the boron isotope-pH proxy; the accuracy of ancient ocean pH estimates: Geochimica et Cosmochimica Acta, v. 69, p. 953-961.
Petrychenko, O.Y., and Peryt, T.M., 2004, Geochemical conditions of deposition in the Upper Devonian Prypiac' and Dnipro-Donets evaporite basins (Belarus and Ukraine): Journal of Geology, v. 112, p. 577-592.
Porter, S.M., 2007, Seawater chemistry and early carbonate biomineralization: Science, v. 316, p. 1302-1302.
Pray, L.C., and 1961, Geology of the Sacramento Mountains escarpment, Otero County, New Mexico: Bulletin - New Mexico Bureau of Mines & Mineral Resources, p. 144-144.
Rahnis, M.A., 1995, Calcite in the Capitan Formation, Texas and New Mexico, University of Texas at Austin, Austin, TX, United States (USA).
Rasbury, E.T., Ward, W.B., Hemming, N.G., Li, H., Dickson, J.A.D., Hanson, G.N., Major, R.P., and 2004, Concurrent U/Pb age and sea water 87Sr/ 86Sr value of a marine cement: Earth and Planetary Science Letters, v. 221, p. 355-371.
Rathburn, A.E., and De Deckker, P., 1997, Magnesium and strontium compositions of Recent benthic Foraminifera from the Coral Sea, Australia and Prydz Bay, Antarctica: Marine Micropaleontology, v. 32, p. 231-248.
Rathmann, S., and Kuhnert, H., 2008, Carbonate ion effect on Mg/Ca, Sr/Ca and stable isotopes on the benthic foraminifera Oridorsalis umbonatus off Namibia: Marine Micropaleontology, v. 66, p. 120-133.
Ries, J.B., 2004, Effect of ambient Mg/Ca ratio on Mg fractionation in calcareous marine invertebrates; a record of the oceanic Mg/Ca ratio over the Phanerozoic: Geology, v. 32, p. 981-984.

—, 2005, Aragonite production in calcite seas; effect of seawater Mg/Ca ratio on the calcification and growth of the calcareous alga *Penicillus capitatus*: Paleobiol., v. 31, p. 445-458.
—, 2006a, Aragonitic algae in calcite seas; effect of seawater Mg/Ca ratio on algal sediment production: Journal of Sedimentary Research, v. 76, p. 515-523.
—, 2006b, Mg fractionation in crustose coralline algae: Geochemical, biological, and sedimentological implications of secular variation in the Mg/Ca ratio of seawater: Geochimica Et Cosmochimica Acta, v. 70, p. 891-900.
Rimstidt, J.D., Balog, A., and Webb, J., 1998, Distribution of trace elements between carbonate minerals and aqueous solutions: Geochimica et Cosmochimica Acta, v. 62, p. 1851-1863.
Rohde, R.A., 2005, GeoWhen.org, International Commission on Stratigraphy.
Rosenthal, Y., Boyle, E.A., and Slowey, N.C., 1997, Temperature control on the incorporation of magnesium, strontium, fluorine, and cadmium into benthic foraminiferal shells from Little Bahama Bank; prospects for thermocline paleoceanography: Geochimica et Cosmochimica Acta, v. 61, p. 3633-3643.
Rosenthal, Y., Field, M.P., and Sherrell, R.M., 1999, Precise determination of element/calcium ratios in calcareous samples using sector field inductively coupled plasma mass spectrometry: Analytical Chemistry, v. 71, p. 3248-3253.
Rosenthal, Y., Lear, C.H., Oppo, D.W., and Linsley, B.K., 2006, Temperature and carbonate ion effects on Mg/Ca and Sr/Ca ratios in benthic Foraminifera; aragonitic species *Hoeglundina elegans*: Paleoceanography, v. 21, p. 14.
Rosenthal, Y., and Lohmann, G.P., 2002, Accurate estimation of sea surface temperatures using dissolution-corrected calibrations for Mg/Ca paleothermometry: Paleoceanography, v. 17, p. 16-1 - 16-6.
Rowley, D.B., 2002, Rate of plate creation and destruction: 180 Ma to present: Geological Society of America Bulletin, v. 114, p. 927-933.
Russell, A.D., Hosnisch, B., Spero, H.J., and Lea, D.W., 2004, Effects of seawater carbonate ion concentration and temperature on shell U, Mg, and Sr in cultured planktonic Foraminifera: Geochimica et Cosmochimica Acta, v. 68, p. 4347-4361.
Saller, A.H., 1986, Radiaxial calcite in lower Miocene strata, subsurface Enewetak Atoll: Journal of Sedimentary Petrology, v. 56, p. 743-762.
Sandberg, P.A., 1975, New interpretations of Great Salt Lake ooids and of ancient non-skeletal carbonate mineralogy: Sedimentology, v. 22, p. 497-537.
—, 1983, An oscillating trend in Phanerozoic non-skeletal carbonate mineralogy: Nature, v. 305, p. 19-22.
Schlager, W., Reijmer, J.J.G., Betzler, C., and Mutti, M., 2003, Benthic carbonate factories of the Phanerozoic; New perspectives in carbonate sedimentology: International Journal of Earth Sciences, v. 92, p. 445-464.
Schlanger, S.O., 1988, Strontium storage and release during deposition and diagenesis of marine carbonates related to sea-level variations: NATO ASI Series Series C: Mathematical and Physical Sciences, v. 251, p. 323-340.
Segev, E., and Erez, J., 2006, Effect of Mg/Ca ratio in seawater on shell composition in shallow benthic Foraminifera: Geochemistry, Geophysics, Geosystems—G^3, v. 7, p. 8.

Shackleton, N.J., 1974, Attainment of isotopic equilibrium between ocean water and the benthonic foraminifera genus Uvigerina; isotopic changes in the ocean during the last glacial, Colloques Internationaux du CNRS: Les Methodes quantitative d'etude variation climat au cours de Pleistocene, Volume 219, p. 203-209.
Shevenell, A.E., Kennett, J.P., and Lea, D.W., 2004, Middle Miocene Southern Ocean cooling and Antarctic cryosphere expansion: Science, v. 305, p. 1766-1770.
Smith, E.A., 2005, Permian seawater chemistry from marine cements and echinoderms, Capitan Reef, West Texas, USA: Ann Arbor, University of Michigan.
Spencer, R.J., and Hardie, L.A., 1990, Control of seawater composition by mixing of river waters and mid-ocean ridge hydrothermal brines: Special Publication - Geochemical Society, v. 2, p. 409-419.
Stanley, S.M., and Hardie, L.A., 1998, Secular oscillations in the carbonate mineralogy of reef-building and sediment-producing organisms driven by tectonically forced shifts in seawater chemistry: Palaeogeography, Palaeoclimatology, Palaeoecology, v. 144, p. 3-19.
Stanley, S.M., Ries, J.B., and Hardie, L.A., 2002, Low-magnesium calcite produced by coralline algae in seawater of Late Cretaceous composition: Proceedings of the National Academy of Sciences of the United States of America, v. 99, p. 15323-15326.
—, 2005, Seawater chemistry, coccolithophore population growth, and the origin of Cretaceous chalk: Geology, v. 33, p. 593-596.
Stanton, R.J.J., Jeffery, D.L., and Ahr, W.M., 2002, Early Mississippian climate based on oxygen isotope compositions of brachiopods, Alamogordo Member of the Lake Valley Formation, south-central New Mexico: Geological Society of America Bulletin, v. 114, p. 4-11.
Steuber, T., and Veizer, J., 2002, Phanerozoic record of plate tectonic control of seawater chemistry and carbonate sedimentation: Geology, v. 30, p. 1123-1126.
Stoll, H.M., and Schrag, D.P., 1996, Evidence for glacial control of rapid sea level changes in the early Cretaceous: Science, v. 272, p. 1771-1774.
Takesue, R.K., and van Geen, A., 2004, Mg/Ca, Sr/Ca, and stable isotopes in modern and Holocene *Protothaca staminea* shells from a Northern California coastal upwelling region: Geochimica et Cosmochimica Acta, v. 68, p. 3845-3861.
Tesoriero, A.J., and Pankow, J.F., 1996, Solid solution partitioning of Sr^{2+} , Ba^{2+} , and Cd^{2+} to calcite: Geochimica et Cosmochimica Acta, v. 60, p. 1053-1063.
Thompson, T.G., Chow, T.J., 1955, The strontium-calcium atomic ratio in carbonate-secreting marine organism, Papers in Marine Biology and Oceanography, Volume 3, Pergamon Press, p. 20-30.
Tobin, K.J., and Bergstrom, S.M., 2002, Implications of Ordovician (nearly equal 460 Myr) marine cement for constraining seawater temperature and atmospheric pCO_2: Palaeogeography, Palaeoclimatology, Palaeoecology, v. 181, p. 399-417.
Tobin, K.J., and Walker, K.R., 1996, Ordovician low- to intermediate-Mg calcite marine cements from Sweden; marine alteration and implications for oxygen isotopes in Ordovician seawater: Sedimentology, v. 43, p. 719-735.
—, 1997, Ordovician oxygen isotopes and paleotemperatures: Palaeogeography, Palaeoclimatology, Palaeoecology, v. 129, p. 269-290.

Tobin, K.J., Walker, K.R., and Goldberg, S.G., 1997, Burial diagenesis of middle Ordovician carbonate buildups (Alabama, USA): documentation of the dominance of shallow burial conditions: Sedimentary Geology, v. 114, p. 223-236.

Tobin, K.J., Walker, K.R., Steinhauff, D.M., and Mora, C.I., 1996, Fibrous calcite from the Ordovician of Tennessee; preservation of marine oxygen isotopic composition and its implications: Sedimentology, v. 43, p. 235-251.

Tripati, A., Backman, J., Elderfield, H., and Ferretti, P., 2005, Eocene bipolar glaciation associated with global carbon cycle changes: Nature, v. 436, p. 341-346.

Tripati, A.K., Delaney, M.L., Zachos, J.C., Anderson, L.D., Kelly, D.C., and Elderfield, H., 2003, Tropical sea-surface temperature reconstruction for the early Paleogene using Mg/Ca ratios of planktonic foraminifera: Paleoceanography, v. 18, p. 1-13.

Tripati, A.K., Eagle, R.A., Morton, A., Dowdeswell, J.A., Atkinson, K.L., Bahe, Y., Dawber, C.F., Khadun, E., Shaw, R.M.H., Shorttle, O., and Thanabalasundaram, L., 2008, Evidence for glaciation in the Northern Hemisphere back to 44 Ma from ice-rafted debris in the Greenland Sea: Earth and Planetary Science Letters, v. 265, p. 112-122.

Urey, H.C., 1947, The thermodynamic properties of isotopic substances: Journal of the Chemical Society, v. 1947, p. 562-581.

Vail, P.R., Mitchum, R.M., Thompson, S., and Payton, C.E., 1977, Seismic stratigraphy and global changes of sea level Part 4, Global cycles of relative changes of sea level, *in* Payton, C.E., ed., Seismic stratigraphy–applications to hydrocarbon exploration, Volume 26, p. 83-97.

Veizer, J., Ala, D., Azmy, K.K., Bruckschen, P., Buhl, D., Bruhn, F., Carden, G.A.F., Diener, A., Ebneth, S., Godderis, Y., Jasper, T., Korte, C., Pawellek, F., Podlaha, O.G., and Strauss, H., 1999, $^{87}Sr/^{86}Sr$, $\delta^{13}C$ and $\delta^{18}O$ evolution of Phanerozoic seawater: Chemical Geology, v. 161, p. 59-88.

Walker, J.C.G., and Lohmann, K.C., 1989, Why the oxygen isotopic composition of sea water changes with time: Geophysical Research Letters, v. 16, p. 323-326.

Watson, E.B., 2004, A conceptual model for near-surface kinetic controls on the trace-element and stable isotope composition of abiogenic calcite crystals: Geochimica et Cosmochimica Acta, v. 68, p. 1473-1488.

Webb, G.E., Kiessling, W., Fluegel, E., and Golonka, J., 2002, Latest Devonian and Early Carboniferous reefs; depressed reef building after the middle Paleozoic collapse, Phanerozoic reef patterns, Volume 72: SEPM Special Publication: Tulsa, OK, SEPM, p. 239-269.

Weber, J.N., 1968, Fractionation of the stable isotopes of carbon and oxygen in calcareous marine invertebrates; the Asteroidea, Ophiuroidea and Crinoidea: Geochimica et Cosmochimica Acta, v. 32, p. 33-70.

—, 1969, The incorporation of magnesium into the skeletal calcites of echinoderms: American Journal of Science, v. 267, p. 537-566.

Weber, J.N., and Raup, D.M., 1966, Fractionation of the stable isotopes of carbon and oxygen in marine calcareous organisms. The Echinoidea; Part 2, Environmental and genetic factors: Geochimica et Cosmochimica Acta, v. 30, p. 705-736.

Wei, G., Sun, M., Li, X., and Nie, B., 2000, Mg/Ca, Sr/Ca and U/Ca ratios of a *Porites* coral from Sanya Bay, Hainan Island, South China Sea and their relationships to

sea surface temperature: Palaeogeography, Palaeoclimatology, Palaeoecology, v. 162, p. 59-74.
Whittaker, S.G., James, N.P., and Kyser, T.K., 1994, Geochemistry of synsedimentary cements in Early Cambrian reefs: Geochimica et Cosmochimica Acta, v. 58, p. 5567-5577.
Wilkinson, B.H., and Algeo, T.J., 1989, Sedimentary carbonate record of calcium-magnesium cycling: American Journal of Science, v. 289, p. 1158-1194.
Wilkinson, B.H., Owen, R.M., and Carroll, A.R., 1984, Submarine hydrothermal weathering, global eustasy, and carbonate polymorphism in Phanerozoic marine oolites: Journal of Sedimentary Petrology, v. 55, p. 171-183.
Wilson, P.A., and Dickson, J.A.D., 1996, Radiaxial calcite; alteration product of and petrographic proxy for magnesian calcite marine cement: Geology (Boulder), v. 24, p. 945-948.
Wise, S.W., Jr., Breza, J.R., Harwood, D.M., Wei, W., and Zachos, J.C., 1992, Paleogene glacial history of Antarctica in light of Leg 120 drilling results: Proceedings of the Ocean Drilling Program, Scientific Results, v. 120, p. 1001-1030.
Wu, Y.Q., and Chafetz, H.S., 2002, Stable isotopic signature of a palaeoaquifer, Mississippian Alamogordo Member limestones, Sacramento Mountains, New Mexico, USA: Sedimentology, v. 49, p. 227-235.
Yu, K.F., Zhao, J.X., Wei, G.J., Cheng, X.R., Chen, T.G., Felis, T., Wang, P.X., and Liu, T.S., 2005, $\delta^{18}O$, Sr/Ca and Mg/Ca records of Porites lutea corals from Leizhou Peninsula, northern South China Sea, and their applicability as paleoclimatic indicators: Palaeogeography Palaeoclimatology Palaeoecology, v. 218, p. 57-73.
Zachara, J.M., Cowan, C.E., and Resch, C.T., 1991, Sorption of divalent metals on calcite: Geochimica et Cosmochimica Acta, v. 55, p. 1549-1562.
Zachos, J., Pagani, M., Sloan, L., Thomas, E., and Billups, K., 2001, Trends, rhythms, and aberrations in global climate 65 Ma to present: Science, v. 292, p. 686-693.
Zachos, J.C., Wara, M.W., Bohaty, S., Delaney, M.L., Petrizzo, M.R., Brill, A., Bralower, T.J., and Premoli Silva, I., 2003, A transient rise in tropical sea surface temperature during the Paleocene-Eocene thermal maximum: Science, v. 302, p. 1551-1554.
Zhong, S.J., and Mucci, A., 1989, Calcite and aragonite precipitation from seawater solutions of various salinites—precipitation rates and overgrowth compositions: Chemical Geology, v. 78, p. 283-299.
Zimmermann, H., 2000, Tertiary seawater chemistry; implications from primary fluid inclusions in marine halite: American Journal of Science, v. 300, p. 723-767.
Zimmermann, H., Holland, H.D., and Horita, J.A.B., 2000, The evolution of seawater during the Phanerozoic; record from marine evaporites and fluid inclusions in halite, Geological Society of America Annual Meeting, Volume 32: Reno, NV, USA, p. 67.
Zuddas, P., and Mucci, A., 1998, Kinetics of calcite precipitation from seawater; II, The influence of the ionic strength: Geochimica et Cosmochimica Acta, v. 62, p. 757-766.